PROTON TRANSFER REACTIONS IN PHOTOSYNTHETIC WATER OXIDATION: SECOND SPHERE LIGANDS OF THE MANGANESE CLUSTER MODULATE THE WATER OXIDATION MECHANISM OF PHOTOSYSTEM II

By

PRESTON LEE DILBECK

Bachelor of Science in Cell and Molecular Biology
Oklahoma State University
Stillwater, OK
2006

Submitted to the Faculty of the
Graduate College of the
Oklahoma State University
in partial fulfillment of
the requirements for
the Degree of
DOCTOR OF PHILOSOPHY
December 2012

PROTON TRANSFER REACTIONS IN PHOTOSYNTHETIC WATER OXIDATION: SECOND SPHERE LIGANDS OF THE MANGANESE CLUSTER MODULATE THE WATER OXIDATION MECHANISM OF PHOTOSYSTEM II

Dissertation Approved:

Robert Burnap

Dissertation Adviser

Wouter Hoff

Rolf Prade

William Henley

Changan Yu

Outside Committee Member

Dr. Sheryl A. Tucker

Dean of the Graduate College

TABLE OF CONTENTS

Chapter Page

LIST OF TABLES

Table Page

LIST OF FIGURES

Figure Page

CHAPTER I

Introduction to Photosystem II

1.1 Photosystem II

The function of a photosynthetic bacterial reaction center is to provide the cell with a source of reductant with sufficient energy to be used for the biosynthesis of compounds and/or to provide energy in the form of a proton gradient that can be used for ATP synthesis and membrane transport processes (for review see (*1, 2*)). A photosynthetic reaction center uses the energy from an absorbed photon to produce a charge separation. This charge separation results in the transfer of an electron from a special pair of chlorophyll to an electron acceptor, such as a quinone, and leaving an unbalanced electron hole at the special pair chlorophylls. This hole is filled by oxidizing a reduced substrate such as sulfide or molecular hydrogen. These substrates thereby serve as the ultimate electron donors for the reaction centers, whereas the special pair of chlorophylls serve as the primary donor. Unlike other bacterial reaction centers, the Photosystem II (PSII) complex of cyanobacteria, algae, and plants, uses water as its reaction center donor substrate and thus water serves as the ultimate source of electrons for cell biosynthesis in organisms capable of oxygenic photosynthesis (for review see (*3-11*). This provides an advantage in that PSII is not likely to be limited by the lack of an electron donor, which allows the cell to grow rapidly using only inorganic nutrients.

However, the utilization of water as the ultimate photosynthetic electron donor also presents several fundamental difficulties. The first difficulty is thermodynamic: water is more thermodynamically stable than the other possible substrates and consequently, the electron hole generated by primary photochemical charge separation must produce a very powerful oxidant that is capable of removing the tightly bound electrons of substrate water. This oxidant is potentially harmful if allowed to react with other cellular components and it presence may underlie the still poorly-understood processes of photodamage and photoinhibition that seems to be inexorably linked to oxygenic photosynthesis (*12-14*). The second fundamental difficulty of using water as the ultimate source of electrons for photosynthetic metabolism is kinetic: the conversion of two water molecules to one dioxygen molecule and four protons is a four-electron process, yet it must still be carried out using the univalent photochemistry of a chlorophyll special pair. PSII overcomes these difficulties by using a Mn_4CaO_5 cluster to act as an interface between the univalent photochemistry and the more complicated multielectron oxygen formation reaction. The Mn_4CaO_5 provides a site for the accumulation and stabilization of the four electron holes needed to complete this reaction. An important part of the process of stabilizing the formation of the electron holes and their transfer to the substrate is the ability of PSII to selectively remove protons from the environment around the active site. Neither of these two processes are fully understood and there is still a substantial amount of research that needs to be done to fully characterize the mechanism of PSII. This dissertation will focus on answering questions regarding the removal of protons from PSII and how this facilitates the stabilization of intermediates in the catalytic cycle of PSII.

1.2 The photosynthetic electron transport chain

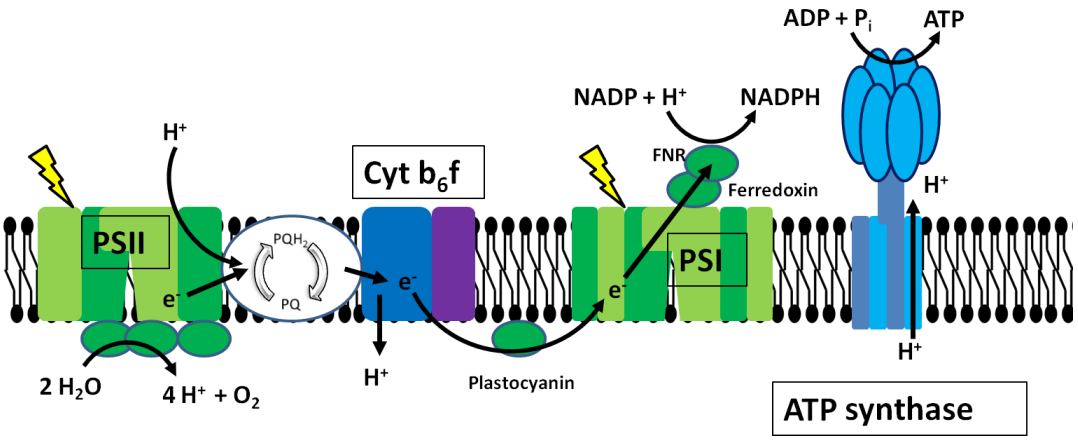

Figure 1.1 The photosynthetic electron transport chain involves the serial cooperation of two photochemical reaction centers, PSII and PSI, that are 'bioelectronically' connected by and an intervening electron transport chain. PSII is able to provide a constant source of electrons to the photosynthetic electron transport chain (PETC), because of its ability to oxidize an ubiquitous electron donor. PSI is able of further energize the electrons initially extracted from water to the level of reduced ferredoxin and NADPH, which provide the energized electrons for the needs of reductive cellular metabolism. Protons are deposited in the thylakoid membrane lumen during the water oxidation and PETC producing an electrochemical proton gradient that drives ATP synthesis giving the phosphorylation potential also required for reductive cellular metabolism. (Figure adapted from Taiz and Zeiger, 2007.

Photosystem II (PSII) is a multi-subunit protein found in plants, algae and cyanobacteria that allows these organisms to undergo oxygenic photosynthesis. Oxygenic photosynthesis is carried out by the photosynthetic electron transport chain (PETC), a group of proteins whose activities result in a series of chemical reactions that convert light energy into usable forms of chemical energy (Figure 1.1). The major components of the PETC are PSII, Cytochrome b_6f, Photosystem I (PSI) and ATP synthase. These multi-subunit proteins are embedded in the thylakoid membrane, which is located in the chloroplasts of plants and algae and are contained within (and probably derive from) the cytoplasmic membrane in cyanobacteria

(*15-17*). The role of PSII in the PETC is to contribute to the proton gradient which is used to produce ATP and provides a constant source of reductant to the rest of the PETC which will eventually be converted in to NADPH and used to fix inorganic carbon. PSII carries out this role by using a photon-induced charge separation to catalyze two reactions. The first is the oxidation of water and the release of four protons (Equation 1) thereby contributing to ATP synthesis via chemiosmotic coupling to the membrane-bound ATP synthase.

$$2\ H_2O + 4\ \text{photons} \rightarrow 4\ H^+ + O_2 + 4\ e^-$$

Equation 1

The second is the reduction of plastoquinone. Each time plastoquinone becomes oxidized by PSII it forms a semi-quinone radical which remains bound to PSII until a second electron transfer reduces the semi-quinone to plastoquinol, which is then released into the plastoquinone/plastoquinol pool (Equation 2).

$$1\ \text{plastoquinone} + 2\ H^+ + 2\ e^- + 2\ \text{photons} \rightarrow 1\ \text{plastoquinol}$$

Equation 2

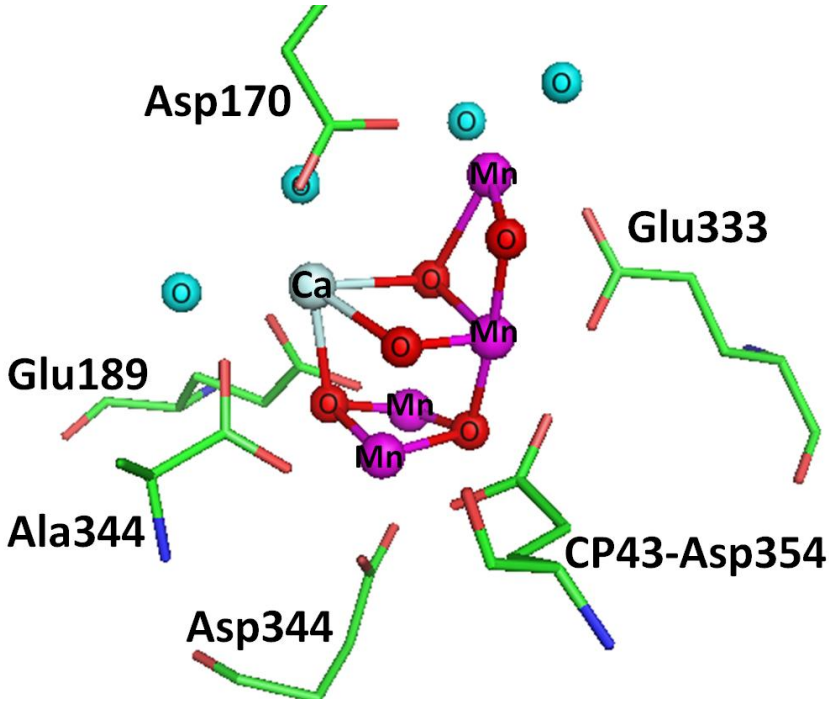

Figure 1.2 The Mn_4CaO_5 Cluster. The manganese and calcium cluster that catalyzes the oxidation of H_2O and the formation of O_2. The Mn_4CaO_5 is ligated by seven amino acids. Six of these ligands come from the D1 subunit of PSII and one, Asp354, comes from the CP43 sub-unit of PSII. The blue oxygen atoms represent four H_2O molecules that directly interact with the Mn_4CaO_5. Rendered using the program PyMOL using the coordinates (PDB 3BZ2) based upon the crystal structure from Umena et al (*18*).

1.3 The photochemistry of PSII charge separation

1.3.1 The Mn_4CaO_5 cluster.

The site of water oxidation in PSII, is the Mn_4CaO_5 cluster which is composed of four manganese and one calcium ions linked by μ-oxo bridges in a cuboidal structure with one dangling Mn (*18*) (Fig. 1.2). The Mn_4CaO_5 is ligated by several amino acid residues, which along with the Mn_4CaO_5 and the substrate H_2O molecules comprise the water oxidation complex (WOC) located near the luminal surface of PSII (Fig. 1.3).

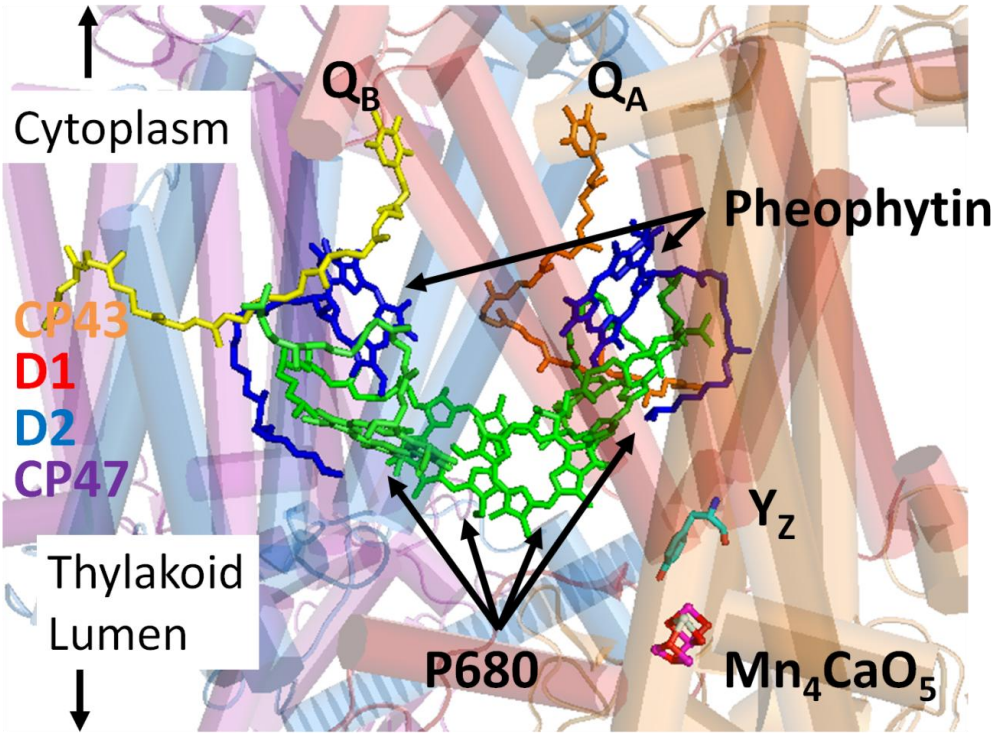

Figure 1.3 PSII cofactors involved in electron transfer. The cofactors involved in charge separation and electron transfer are labeled individually. The four major PSII subunits intrinsic to the thylakoid membrane are labeled by color: CP43 (orange), D1 (red), D2 (blue), and CP47 (purple). Rendered using the program PyMOL using the coordinates (PDB 3BZ2) based upon the crystal structure from Umena et al (*18*).

Each of the four oxidation events that lead to the release of O_2 from the Mn_4CaO_5 is initiated by the absorption of a photon by a group of four chlorophyll *a* molecules that has been labeled P680, this causes a large decrease in the redox potential of P680 and the rapid transfer of an electron to a nearby pheophytin molecule (Figure 1.3) within 3.2 ps (*19*). P680 and the two pheophytin molecules are coordinated by the D1 and D2 subunits of PSII. This reaction is followed within 200 ps by the transfer of an electron from

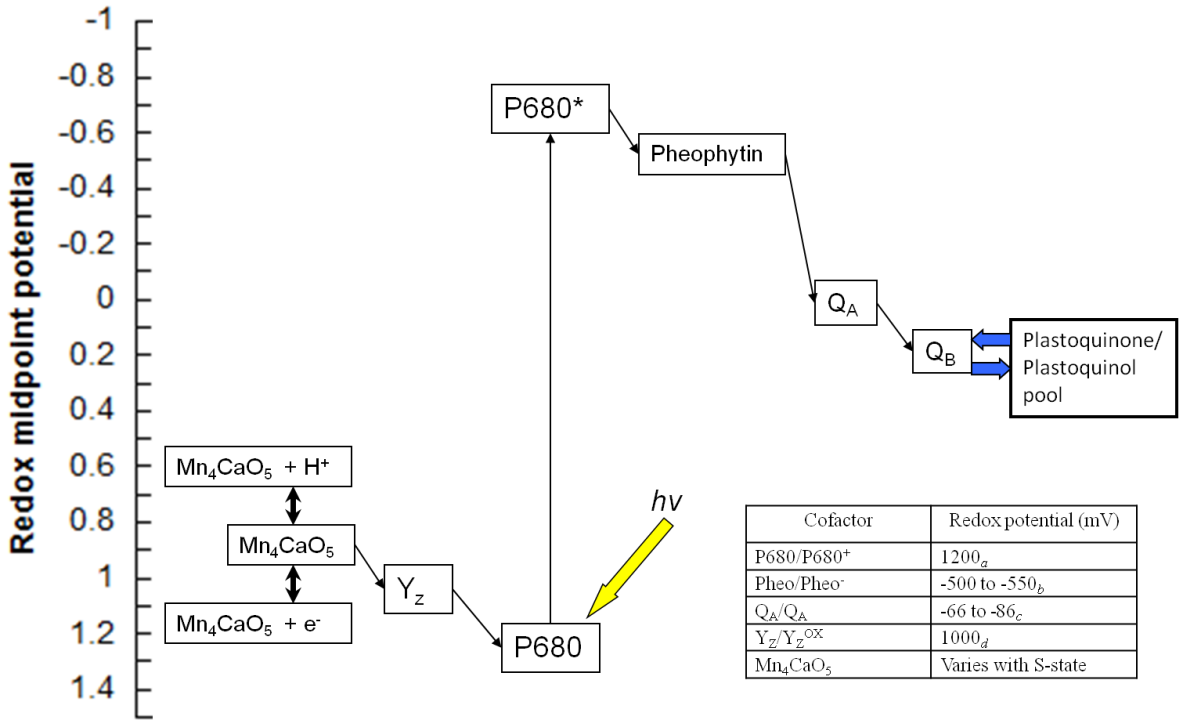

Cofactor	Redox potential (mV)
$P680/P680^+$	1200_a
$Pheo/Pheo^-$	-500 to -550_b
Q_A/Q_A^-	-66 to -86_c
Y_Z/Y_Z^{OX}	1000_d
Mn_4CaO_5	Varies with S-state

Figure 1.4 Multi-step electron transfer during PSII charge separation. Upon excitation P680 undergoes a shift in redox potential that initiates electron transfer to pheophytin. The redox potential of the Mn_4CaO_5 can be raised and lowered by the removal of electrons and protons respectively. Inset table: The redox potentials of the cofactors involved in charge separation from the following sources - *a* (*20*), *b* (*21*), *c* (*22*), *d* (*23*).

the pheophytin to Q_A, a plastoquinone molecule permanently bound to the D1 subunit. The $P680^+Q_A^-$ state is sufficiently long lived to allow for the oxidation of the tyrosine residue D1-Tyr161 (Y_Z) by $P680^+$. The newly formed tyrosine radical (Y_Z^{OX}) is then reduced by the Mn_4CaO_5 (*24*) (see figure 1.4 for the entire reaction scheme).

Two things are required of the PSII charge separation in order to successfully oxidize water. It must generate a redox potential high enough to oxidize H_2O and it must have a sufficient lifetime to allow the Mn_4CaO_5 to transition between redox states. The redox potential of $P680^+$, which is the ultimate determinate of the energetics of PSII, has not been directly measured. However, several estimates of E_m ($P680/P680^+$) have been made based on

the measured E_m(Pheo/Pheo$^-$) and the free energy of the charge separation (*21, 25, 26*). The most recent estimate is +1200 mV (*20*). This value is high enough, by a 380 mV thermodynamic margin, to oxidize H_2O, which has a redox potential of +820 mV. However, this overall thermodynamic relationship does not take into account the possibilities that realistic kinetic paths to four-electron oxidation could potentially involve much smaller thermodynamic margins at individual steps of the overall reaction. For example, if proton release does not occur, then the accumulation of a positive charge on the reaction intermediates would result in a more difficult to oxidize chemical intermediate, which why efficient proton release from the water oxidation complex appears to have evolved as discussed below.

1.4 The S-state cycle

1.4.1 Oscillating O_2 yield signals are the result of repeated redox state transitions operating as a catalytic cycle.

The Mn_4CaO_5 cluster acts as an interface between the univalent photochemistry described above and the four-electron reaction required for the complete oxidation of the two substrate H_2O molecules that act as the ultimate source of electrons for oxygenic photosynthesis. Each time the Mn_4CaO_5 is oxidized by Y_Z^{OX} it stores the oxidizing potential as an electron hole on one of the individual manganese atoms. This is repeated until there are enough oxidizing equivalents to completely oxidize both substrate H_2O molecules and release one O_2 molecule. A model describing the accumulation of oxidizing equivalents by the Mn_4CaO_5 was developed by Kok et al (*27, 28*), based on the observation that under a series of brief (<10μs) saturating flashes a dark-adapted sample of PSII releases O_2 in an oscillating pattern with a periodicity of four (*29*)(see Fig. 1.5A). In this model, known as the 'S-state cycle' (see Fig. 1.5B), each charge separation at the photochemical reaction center

causes the Mn_4CaO_5 to advance through a repeating series of oxidation states, called S-states (or storage states), designated S_0 through S_4 according to the number of stored oxidizing equivalents [For reviews, see (*4, 8, 30-32*)]. Note that these states while corresponding to the progressive removal of electrons are not necessarily storing charge because of the release of proton, at least for three of the four transitions (see below).

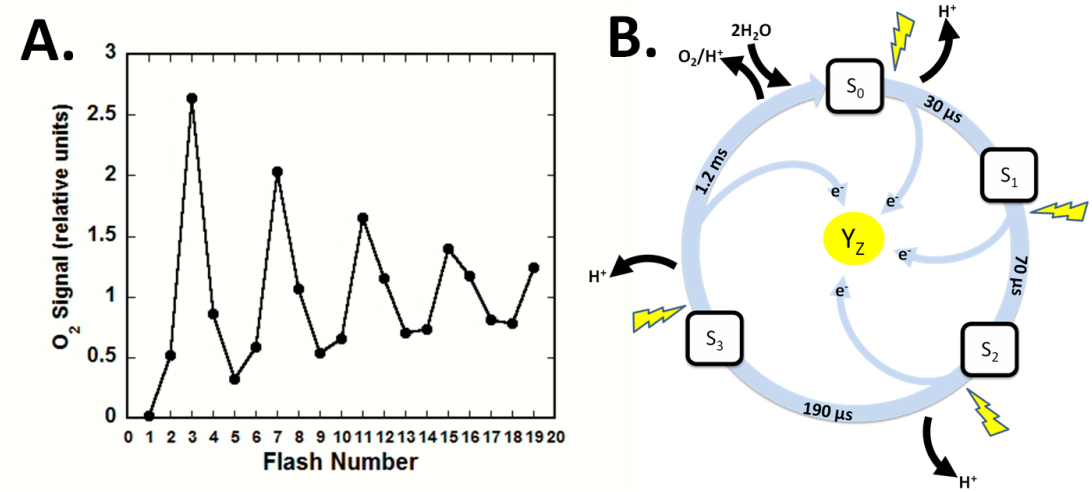

Figure 1.5 The catalytic cycle of PSII. Panel A: The yield of O_2 from PSII exposed to brief saturating pulses of light oscillates with peaks every four flashes beginning with the third flash. Panel B: Data similar to that shown in panel A was the basis for a model of the repeating series of redox state transitions that PSII undergoes that is known as the S-state cycle (*28*).

1.4.2 S-state transitions

The transition between S-states begins when Y_Z is oxidized by $P680^+$ and is complete when Y_Z^{OX} is re-reduced (Figure 4B). Because of changes in the redox state and structural arrangement of the Mn_4CaO_5, the transitions between individual pairs of S-states vary in a number of important ways. These include the rate of each transition, the number of protons released during the transition, and pH and temperature sensitivity.

Three of the four S-state transitions are accompanied by the release of protons from the WOC (Figure 4B). The release of protons from the WOC is part of the 'redox leveling' process that allows the repeated oxidation of Mn_4CaO_5 by Y_Z by preventing the buildup of a positive charge (*33*). The well coordinated removal of both protons and electrons from the metal complex and its ligand environment is, among other things, mechanistically crucial for facilitating the successive one-electron oxidation of the Mn_4CaO_5 without a prohibitive increase in its oxidation potential by appropriate redox-potential leveling (*8, 24, 34*).

The S_1 state is dark-stable, unlike the higher S_2 and S_3 states, which decay in a matter of seconds to minutes. Dark adapted PSII centers in the S_0 state can become oxidized to the S_1 state by the Y_D^{OX} radical, which like Y_Z is a redox active tyrosine, but unlike Y_Z, Y_D is not directly involved in the catalysis of water oxidation, but instead seems to serve a function of maintaining the Mn_4CaO_5 in an active redox configuration (*35*). It tends to accumulate in oxidized form in the light and then oxidize the S_0 state in the dark. This means that in dark adapted sample of PSII the S_1 state will dominate and in a typical experiment PSII will release O_2 after being exposed to three flashes of light (*28*) with a period four oscillation of O_2 release during a train of subsequent flashes (Fig. 2a).

One notable feature of the S_1 to S_2 transition is that unlike the other S-state transitions, it does include the release of a proton. This causes the accumulation of a positive charge on the Mn_4CaO_5 during the S_1 to S_2 transition. The quantum efficiency of this reaction is also not sensitive to pH (*36, 37*) and it can occur at much lower temperatures than the other S-state transitions (*38*). Another curious observation is that the reversal of this transition is sensitive to pH (*39*). The reverse of the S_1 to S_2 transition is also much more sensitive to temperature than the forward reaction. The apparent contradiction is an

overlooked piece of evidence that has not been factored in to current models into the mechanism of the S_1 to S_2 transition. The S_1 to S_2 transition may involve the transfer of a proton through a low energy barrier hydrogen bond similar to the hydrogen bond between Y_Z and His190 (i.e. the proton is not removed from PSII) (*11, 40*). This hydrogen bond should then be subjected to a rearrangement that increases the distance between the hydrogen bond partners thus increasing the energy barrier for proton transfer. Assuming that the reversal of the electron transfer from the Mn_4CaO_5 promotes the re-protonation of the original donor without reforming the low energy barrier hydrogen bond would explain why the reversal of the S_1 to S_2 state transition appears to be constrained by the transfer of protons while the forward reaction does not. The assumption of the presence and subsequent loss of a low energy hydrogen bond in the WOC during this transition could provide an important constraint for distinguishing between various models of the mechanism of water oxidation by the WOC.

Compared to the S_1 to S_2 transition the S_2 to S_3 transition is more complex and appears to involve a significant structural change based upon X-ray absorption studies of interatomic distances of the metals of the Mn_4CaO_5 (*32*). Unlike the S_1 to S_2 transition the S_2 to S_3 transition involves the removal of a proton, which accompanies the structural rearrangement of the Mn_4CaO_5 (*41-46*). The S_2 to S_3 transition is also twice as slow as the S_1 to S_2 transition (*47, 48*). This is also the first transition that takes place after the accumulation of a positive charge on the Mn_4CaO_5, which may introduce the requirement for a catalytic base to remove a proton from the WOC prior to the rereduction of Y_Z^{OX} (*33*).

The S_4 state is a hypothetical transient state, formed by the oxidation of the Mn_4CaO_5 in the S_3 state, which precedes the formation of O_2 and the reduction of the Mn_4CaO_5 by

substrate H_2O (*28*). However, X-ray absorption spectroscopy has shown that manganese is oxidized during the first three S-state transitions but this has not been demonstrated for the transition that results in the formation of O_2 (*46, 49-52*). The lack of observation of the oxidation of Mn following a flash given to samples poised in the S_3 state could be due to the transient nature of this putative state and the technical challenges of observing it. Nevertheless, it remains possible that Mn is not oxidized and instead a ligand-centered oxidation of the Mn_4CaO_5-substrate complex occurs as the precursor to dioxygen formation chemistry during this last step of the catalytic cycle Because of this the oxygen yielding S-state transition is typically referred to as the S_3-S_0 transition or alternatively, the S_3–[S_4]-S_0 transition.

1.4.3 The lag phase and O_2 release.

A lag phase occurring between the rapid exposure of PSII to a saturating light source and the onset of activity indicative of S_3-S_0 transition is the only well supported intermediate in the S_3 to S_0 transition. This post actinic flash lag phase could be due to the formation of a deprotonated intermediate between the S_3 state and the S_0 state, that has previously been designated the S_3^n state (*4*).

This lag phase has been observed in different types of PSII sample and using several different techniques. For example, a lag between the actinic flash and the onset of the re-reduction of Y_Z^{ox} by the Mn_4-Ca during the S_3-S_0 transition has been observed by UV spectroscopy at 295 nm (*53*). This lag corresponded in length to the more rapid phase of the biphasic electrochromic shift observed at 440 to 425 nm (*53*). The half decay times of the two phases of the electrochromic shift, (30 μs for the rapid phase and 1.2 ms for the slower

phase) roughly correspond to the observed rates of the release of the first and second protons from PSII in the S_3-S_0 transition (*54*). A post-actinic flash lag phase has also been observed using EPR oximetry under sub-optimal conditions for water oxidation (*55*). These lag phases had periods of 200 μs in low pH buffer (pH 6.0) and 100 μs in 0.8 M NaCl but was not observable (under 50 μs) under conditions closer to the optimum (pH 7.5 and 50 mM NaCl) nor was it observable in the rise of the Y_Z^{ox} EPR signal. Polarographic measurements of O_2 release corrected for the flash artifact have shown a lag with a period of 320 μs at 28.7°C which increased with decreasing temperature (*56*). Corresponding measurements of Y_Z reoxidation by UV spectroscopy at 360 nm did not reveal a lag at any temperature (*56*). The UV spectroscopy measurements in this work bare the same apparent paradox. Since a definitive atomic level assignment of the UV transient has not been accomplished, the UV transient measured at 360 nm may reflect the activity observed in the rapid phase of the electrochromic shift as well as some slower component of the S_3-S_0 transition. A lag in the hundreds of microseconds range (250 μs) has also been observed through the use of X-ray absorption spectroscopy (*57*).

1.4.4 Dioxygen release

The formation and release of O_2 from the Mn_4CaO_5 is the least understood component of the mechanism of PSII. It is know that the substrate H_2O molecules remains exchangeable until at least the S_3 state, so any chemistry that directly involves H_2O takes place after S_3 to S_0 transition has been initiated (*58*). The S_3 to S_0 transition concludes with a number of events, including the release of O_2, the release of a second proton and reduction of both the Mn_4CaO_5 and Y_Z^{OX}, all occur at indistinguishable rates that have typically measured at between 1.1 and 1.4 ms. It is therefore impossible to determine the order of these events.

It has been demonstrated that the O_2 reaction affected by high O_2 back pressure on the reaction (*59, 60*). Models of O-O bond formation do exist, but there is little direct evidence to confirm or reject these hypotheses.

1.5 Structure of the proton exit pathway

Crystal structures of PSII reveal a putative hydrophilic channel that could plausibly serve as a proton exit pathway from the WOC to the lumen of the thylakoid membrane (*18, 61, 62*) (Fig. 5). This pathway includes the titratable residues D1–Asp61, D1–Glu65, D2–Lys317, D2–Glu312, PsbO-Asp158, PsbO-Asp222, PsbO-Asp223, PsbO-Asp224, PsbO-His228 and PsbO-Glu229. Computational analysis (*63*) based on the crystal structure of PSII indicates that the pK_a of each of these residues, along with D1-Asp59, D1-Arg64, and PsbO-Arg152, increased with distance away from the Mn_4CaO_5 and towards the lumenal surface of the protein. Several of these residues (D1–Asp61, D1–Glu65, D1-Asp59, D2–Lys317 and D2–Glu312) also come into contact with the putative water channels that connect the Mn_4CaO_5 with the proteins surface, which presents the possibility that ordered H_2O molecules also play a role in the proposed proton exit pathways (*61, 64-66*). More recent work has shown that water can flow to one of the more commonly accepted substrate biding sites through this tunnel (*67*).

So far this pathway has not been verified by experimentation, although it has been shown that several of the amino acids in this pathway contribute to the same peak in the PSII FTIR spectrum, despite being separated by significant distances (*68*).

1.6 Proton release from PSII

1.6.1 Stoichiometry of proton release per S-state transition.

The overall chemical equation of photosynthetic water oxidation calls for four protons to be produced for each completed S-state cycle. This is an obvious consequence of the oxidation of the two substrate H_2O molecules. However, rather than being released during the formation of O_2 in the S_3 to S_0 transition, the release of the four protons are distributed unevenly among the four S-state transitions (*41-44, 69*) .

The stoichiometry of proton release per S-state transition was a long standing controversy in the PSII community. Several studies found proton release from PSII to have non-integer stoichiometries which approached 1 (S_0-S_1), 0 (S_2-S_2), 1 (S_2-S_3) and 2 (S_3-S_0) protons released per S-state transition at neutral pH, using different techniques to measure proton release and using several types of PSII preparation (*41-44*). In PSII core complexes that have not been stabilized by glycerol, the stoichiometry becomes 1:1:1:1 without affecting oxygen evolution (*41, 70*). The fraction of protons released in each S-state transition was also shown to vary with pH (*43, 44, 69*).

These studies typically used either a glass electrode or a pH sensitive dye to detect the release of protons. In a 2009 study FTIR difference spectroscopy was used to monitor proton release from PSII particles suspended in a buffer with a high concentration of isotopically labeled buffer (*45*). This allowed for the simultaneous monitoring of uptake of protons by the buffer and of the processes within PSII that can lead to the uptake or loss of protons. This study concluded that the stoichiometry of proton release per S-state transition is 1:0:1:2 and apparent non-integer stoichiometries observed by other studies were due to protons being trapped by or released from the periphery of the protein (*45*).

1.6.2 The mechanism of proton abstraction

The simplest model of proton abstraction from the Mn_4CaO_5, involves the removal of a proton by Y_Z each time it is reduced by the Mn_4CaO_5 and the release to bulk of a proton each time that Y_Z is oxidized by $P680^+$. This model was eliminated as a possibility when it was demonstrated that the thermodynamics of electron transfer between P680, Y_Z and the Mn_4CaO_5 suggest distances between the three cofactors that would prohibit efficient proton transfer between Y_Z and the Mn_4CaO_5 (*71*). Later work has supported the hypothesis that the protons lost by Y_Z upon its oxidation are shuffled back and forth between it and D1-His190 (*72*).

Another model of proton extraction calls for the formation of a catalytic base in order to compensate for charge build up due to oxidation of the Mn_4CaO_5 and to accept protons released by the oxidation of H_2O (*33*). The residue CP43-Arg357 has been proposed as a candidate for this role based on its proximity to the Mn_4CaO_5 (*8*). This hypothesis has wide acceptance and has been included in models of the Mn_4CaO_5 catalytic cycle (*73*). However, there has been no direct evidence for the deprotonation of arginine in physiological condition and it has been shown that arginine can remain protonated in a protein environment even at pH 10 (*74*). Despite this CP43-Arg357 may be critical for promoting the deprotonation of another component of the WOC, such as one of the substrate H_2O's or a protonated μ-oxo bridge.

Currently the origin of the protons released in any of the S-state transitions has not been confirmed. The fact that the substrate H_2O molecules remain labile strongly suggests that the first three protons released during the S-state cycle are the product of the

deprotonation of weak bases near the Mn_4CaO_5. Although it has been suggested that the slow rate of the proton release in the S_2 to S_3 transition is evidence that it is the product of a chemical reaction rather than an electrostatic effect (*69*). And given that the fourth proton is released at the same rate as O_2 it is reasonable to assume they are both the product of the same chemical reaction (*69*).

1.7 Questions and Goals

Photosynthetic water oxidation depends upon undefined proton transfer reactions directed by hydrogen bond networks composed of the second sphere ligands of the Mn_4CaO_5. In fact the substitution of second sphere ligands has often resulted in more severe defects in the yield and kinetics of O_2 release than substitutions to the first sphere of amino acids that directly ligate the Mn_4CaO_5 (personal communication with Richard Debus). Possibly because the first sphere ligands only participate in the assembly of the Mn_4CaO_5 and not in any of the rearrangements that take place during the S-state cycle. Despite the importance of the proton transfer reactions to the mechanism of PSII, there are many unknown details regarding the pathways taken by protons as they leave PSII, the identity of the weak acids that are deprotonated, the mechanism by which deprotonation reactions are initiated and other possible consequences of the hydrogen bond networks in the WOC.

The goal of this research project has been to test the activity of PSII under conditions that are known or suspected to perturb the efficient removal of protons from the WOC. The most effective means of doing this is to introduce point mutations into the subunits of PSII in the cyanobacterium *Synechocystis sp* PCC6803. This allows for specific and localized

changes to be made to the structure of the protein. Evaluation of the effects of point mutations can be combined with changes in the pH of measuring buffers and the use of heavy proton isotope for greater insight into the mechanism of PSII.

This research project included two studies that yielded significant results. The first, presented in Chapter 3, examined the effects of changes in proton and deuteron concentration on the *Synechocystis* mutant D1-D61N. In this mutant the first residue in the predicted proton exit pathway, D1-Asp6 (*63*), is replaced with an asparagine residue resulting in a large decrease in the rate of the final S-state transition (*75*).

The second study, presented in Chapter 4, is the basic characterization of several point mutants, where the replaced residue was positioned with its side chain facing the water cavity surrounding the Mn_4CaO_5. These mutants were originally intended to block the movement of H_2O around the Mn_4CaO_5, but newer developments in the structure of PSII (*18*) and in the energetics of H_2O movement in the WOC (*67*) make it clear that these mutants are better suited for the study of the hydrogen bond networks that include H_2O molecules that are displaced by the new side chain in each mutant.

CHAPTER II

Experimental Procedures

2.1 Growth conditions.

The naturally transformable, glucose-tolerant strain of *Synechocystis* sp. PCC6803 was maintained on solid BG-11 and in liquid BG-11 buffered with 20 mM HEPES-NaOH (pH 8.0) supplemented with 5 mM glucose and 10 µM DCMU (solid media only). Experimental cultures were illuminated with ~70 µmol $m^{-2}s^{-1}$ Cool White fluorescent lights with bubbling filter sterilized air, enriched with ~3% CO_2. A LiCor (Lincoln, NE) photometer was used to measure the light intensity.

2.2 Strains and Mutagenesis.

Each D1 mutation was constructed by introducing a point mutation into the *psbA2* gene fragment located on the plasmid pRD1031 using a QuikChange mutagenesis kit (Stratagene, La Jolla, CA). The resulting plasmids were used to transform a recipient strain of *Synechocystis* lacking the *psbA1, psbA2* and *psbA3* genes, which had been replaced with spectinomycin, erythromycin and chloramphenicol resistance cassettes respectively (*76, 77*). The transformation of the *psbA* deletion strain replaces the erythromycin resistance cassette with the mutated *psbA2* fragment and a kanamycin

resistance cassette. Therefore, these D1 mutants can be selected for using kanamycin. Because *Synechocystis* has a chromosome copy number between 8 and 12, the transformed *Synechocystis* is initially inoculated on to solid media with a low concentration of kanamycin (5 μg/ml) and then gradually moved to media with higher concentrations of antibiotic (30 μg/ml. The recipient strain also contained a hexahistidine 'tag' genetically fused to the C-terminus of the CP47 protein conferring resistance to gentamycin (*76, 77*). A hexahistidine-tagged control strain, was similarly constructed using the same *psbA*-less, recipient strain, but transformed with the wild type *psbA2* gene resulting in a strain possessing PSII activity similar to the true wild type (*77*) and is referred to as the wild type.

2.3 Determination of chlorophyll concentration.

The concentration of chlorophyll in individual samples was determined as mg of chlorophyll per ml of solution, using absorption spectroscopy. The chlorophyll concentration of whole cell suspensions is determined by diluting the sample 100 fold in liquid BG-11 growth media and measuring the absorption of the sample at 620, 678 and 750 nm in a 1 cm cuvette using a UV-Vis scanning spectrophotometer (UV-201PC, Shimadzu, Kyoto, Japan) and using the following equation (*78*).

$$[Chl] = (14.96*(A_{678} - A_{750})) - 0.607*(A_{620} - A_{750}))$$

The chlorophyll concentration in suspended thylakoid membranes is determined by dissolving a 10 μl sample in 990 μl of methanol for 5 min and then centrifuging the sample for 10 min at 14,000 rpm. The absorption of the supernatant at 665 nm is

measured in a 1 cm cuvette and the concentration was determined using an extinction coefficient of 12.5 .

2.4 Isolation of thylakoid membranes.

Two separate protocols were used to isolate thylakoid membranes from *Synechocystis.* These two protocols will be referred to as the large scale thylakoid membrane prep and the small scale thylakoid membrane prep. As the names suggest the two protocols vary mainly in the volume of the starting cultures. Large scale membrane preps are performed using either 2-3 x 10 L or 4-7 x 800 ml cultures of *Synechocystis* grown to mid-log phase. The 10 L cultures were prepared by inoculating 10 L of BG11 liquid media in a large glass carboy with 300-500 ml of *Synechocystis* grown in a shaking culture as described above. The cells were grown with filter sterilized bubbling air and are continually mixed by a magnetic stir bar while being illuminated by a bank of Cool White fluorescent lights. After 2-4 days of growth the bubbling air was supplemented with 3% CO_2 and an additional bank of lights was activated to ensure a continued high rate of growth. The 10 L cultures are typically harvested after 5 days of growth. 800 ml cultures are inoculated with 50 to 100 ml of liquid shaking culture and then grown for ~3 days while being illuminated by ~70 µmol $m^{-2}s^{-1}$ Cool White fluorescent lights with bubbling filter sterilized air, enriched with ~3% CO_2 for 3-4 days. *Synechocystis* cells were harvested by centrifugation for 10 min at 8,000 x g and then re-suspended in thylakoid membrane breaking buffer (TBB) which is composed of 50 mM MES-NaOH (pH 6.0), 10% glycerol (v/v), 1.2 M betaine, 5 mM $MgCl_2$ and 5 mM $CaCl_2$, and then

collected in to a single container, washed with ~200 ml of TBB, re-centrifuged and resuspended to a concentration of 1 mg of chlorophyll ml^{-1}. The resuspended cells were incubated in the dark and on ice for one hour. After incubation the samples were kept on ice and in the dark as much as possible. The cell suspension was then added to a breaking vessel with 25 grams of 0.1 mm diameter zirconium/silica beads soaked in TBB. Additional vessels were used when necessary. Prior to cell breakage, benzamidine, ε-amino-η-caproic acid, and phenylmethanesufonyl fluoride were added to the cell suspension to a concentration of 1 mM each. The cell breakage was performed in a 4° C room under a dim green light. The cells were broken by 5 cycles (5 s on and 5 min off) of agitation with 0.1 mm diameter zirconium/silica beads in a Bead-Beater (BioSpec Products, Bartlesville, OK) in a water-ice jacket. After breakage the supernatant was removed from the breakage vessel and the beads were washed 3 to 5 times with TBB. Unbroken cells and suspended zirconium/silica beads were removed from the supernatant by centrifugation at 3,500 x g for 10 min at 4°C. The extracted thylakoid membranes were collected by centrifugation at 40,000 rpm for 20 min at 4°C in a Beckman 70Ti rotor. The pelleted thylakoid membranes were resuspended in 50 mM MES-NaOH (pH 6.0), 10% glycerol (v/v), 1.2 M betaine, 20 mM $CaCl_2$ and 5 mM $MgCl_2$ to a Chl concentration of 1-1.5 mg ml^{-1}, before being flash-frozen in liquid nitrogen and stored at -80°C.

Small scale thylakoid membrane preps were performed using smaller cell cultures. The *Synechocystis* cultures used for small scale thylakoid membrane preps were much smaller and used either 1-2 x 800 ml BG-11 cultures or 3 x 100 ml shaking cultures. Harvesting the cells and preparing them for breakage was carried out in the

same manner as for the large scale prep. Prior to breakage 1.2 ml of cell suspension were added to 1.4 ml of 0.1 mm zirconium/silica beads in a 2 ml screw top centrifuge tube. The number of tubes used varied depending on the volume of cell suspension. For the small scale prep cells were shaken by a Mini-BeadBeater (BioSpec Products, Bartlesville, OK, USA) for four cycles of 20 sec with 5 min cool downs. After breakage the contents of each tube were added to a small beaker. The beads were allowed to settle to the bottom of the beaker and the supernatant was removed with a pipette. The beads were then washed 3 to 5 times with an equal volume of TBB. The extracted thylakoid membranes were collected by centrifugation at 14,000 rpm for 30 min at 4°C in a table top centrifuge (Eppendorf 5417R, Hauppauge, NY, USA). Because the thylakoid membrane fragments produced by this protocol are larger than those produced by the large scale protocol removing unbroken cells is difficult, however examining the broken cell/membrane suspension under a microscope showed that >90% of cells were successfully broken. The pelleted thylakoid membranes were resuspended in 50 mM MES-NaOH (pH 6.0), 10% glycerol (v/v), 1.2 M betaine, 20 mM $CaCl_2$ and 5 mM $MgCl_2$ to a Chl concentration of 1.0 to 1.5 mg ml^{-1}, before being flash-frozen in liquid nitrogen and stored at -80°C. Alternatively, the thylakoids were

2.5 Isolation of PSII core particles.

Histidine-tagged PSII core particles were extracted from thylakoid membranes using previously described procedures as described in the previous section. Thylakoid membranes were diluted to a concentration of one milligram of chlorophyll per milliliter

and solubilized by adding 1% (w/v) *n*-dodecyl β-D-maltoside (Anatrace Incorporated, Maumee, OH, USA) drop wise from a 10% (w/v) solution of *n*-dodecyl β-D-maltoside dissolved in 50 mM MES (pH 6.0), 10% (v/v) glycerol, 1.2 M betaine, 5 mM $MgCl_2$, and 20 mM $CaCl_2$ to a final concentration of 1% (w/v) to the thylakoid suspension while stirring on ice. Insoluble material was removed from the membrane extract by centrifugation at 22,300 rpm for 10 min at 4°C in a Beckman 70Ti rotor. The resulting supernatant was pumped onto a 2.6 cm diameter column of Ni-NTA Superflow (Qiagen, Inc.) affinity resin with a peristaltic pump at 1.5 mL/min in a darkened cabinet at 4°C to facilitate binding of the His-tagged PSII complexes to the affinity resin. The column was washed with 50 mM MES (pH 6.0), 10% (v/v) glycerol, 1.2 M betaine, 5 mM $MgCl_2$, 20 mM $CaCl_2$ and 0.03% *n*-dodecyl β-D-maltoside. The PSII complexes bound to the affinity column were eluted with buffer containing 50 mM L-histidine, 50 mM MES (pH 6.0), 10% (v/v) glycerol, 1.2 M betaine, 5 mM $MgCl_2$, 20 mM $CaCl_2$ and 0.03% *n*-dodecyl β-D-maltoside. The eluted solution was concentrated in two stirred ultrafiltration cells (first in a 400 mL cell, then in a 10 mL cell) (Amicon YM-100 membranes under 60 psi N_2 at 4°C) to a final Chl concentration of 1.0-1.5 mg ml^{-1}.

2.6 Polarographic measurements of O_2 evolution.

Measurement of flash number dependent O_2 yields and O_2 release kinetics was performed with isolated thylakoid membranes using a bare platinum electrode that allows for the deposition of samples by centrifugation as described previously (*79-82*). Samples for polarographic measurement were prepared in the dark. For each measurement a

sample of thylakoid membranes containing 3 µg of chlorophyll was added to 500 µL of 50 mM MES-NaOH (pH 4.0-8.0 or pD 5.0 to7.5), 1 M sucrose, 10 mM $CaCl_2$ in the detachable sensor unit of the electrode. The pD was calculated as $pD = pD_{read} + 0.4$, where pD_{read} is the pH meter reading. NaCl (40 µl of a 2.5M solution) was also added to the sample to a concentration of 200 mM for most experiments, although at other times when the rapid response of the electrode was not required 50 mM NaCl was used instead. The sample and the sensor unit are then agitated manually in order to disperse the viscous thylakoid membranes sample into the solution. Samples were centrifuged onto the electrode surface at 10,500 x g for 10 min at 25°C in a Sorvall HB-4 swing out rotor. The temperature of the electrode was regulated, by circulating thermostatted water through a copper jacket that surrounds the electrode. The temperature was set to 30° C for most experiments. Polarization of the electrode (0.73 V) was initiated twenty seconds before the start of data acquisition, and the flash sequence was initiated 333 ms after that. The response time of the polarographic amplifier is approximately 100 µs, whereas the electrode-electrolyte system responds within approximately 200-400 µs at the specified NaCl concentration in the measuring buffer. Acquisition of the data and the control of the instrumentation was implemented using a plug-in data acquisition circuitry and software (National Instruments Corp, Austin, TX) that permitted timing and coordination of the flash illumination and data acquisition in a synchronous mode with nanosecond accuracy (independent of computer motherboard and operating system). Timing of the flash points relative to the O_2 signals and instrument response time was verified in separate trials by observing the photoelectric signal resulting from exposing the silver electrode to unfiltered xenon flashes. Samples were allowed to thermally equilibrate to

the temperature of the water jacket for 10 min on the electrode receiver before the data acquisition was initiated. This proved critical in obtaining reproducible oxygen signal decay transients due to their strong temperature dependence especially seen in the rate of the decay of O_2 signal.

Measurements of O_2 release patterns for the determination of the S-state cycling parameters (hit, miss, double hit frequencies) utilized a Xenon flash lamp that provides saturating flashes with a duration of approximately 6 μs at full intensity signal width, half maximum amplitude. Prior to centrifugation, the thylakoid membrane samples were exposed to normal room light for thirty seconds to provide samples uniformly populated among the S-states and to promote homogeneity with respect to the redox state of secondary donors such as Y_D. The samples were centrifuged for 10 min in the dark. After centrifugation the samples were exposed to a single saturating flash from a xenon lamp and then dark-adapted for 10 min to increase the fraction of PSII centers in the S_1-state. Samples were given a series of 19 flashes at a frequency of 1 Hz and the resulting oscillatory pattern of O_2 release was analyzed using a four state model (*80, 83*).

For measurements of the flash induced O_2 release kinetics (rate of appearance of O_2 at the electrode), a different procedure was used. The electronic disturbance from the discharge of the xenon flash lamp proved problematic for measurements of early time points after the flash artifact. This is due to a polarographic current artifact that the discharge induced together with the photoelectric effect as described earlier (*56*). Therefore, an alternative form of flash illumination using a high intensity light-emitting diode (LED) was employed, which minimized this flash artifact. Samples were exposed to a train of 50 μs flashes from a red (nominally 627 nm) Luxeon III Emitter LED

(Philips Electronics) driven by a strobe current generator (Pulsar 710, Advanced Illumination, Rochester, Vermont, USA), placed 0.9 cm from the surface of the electrode given at 2 Hz after allowing the sample and electrode to temperature equilibrate to 30°C. Each sample was exposed to up to 600 flashes and the signals were averaged. The kinetics of the O_2 release curves were fit to a custom made numerical model which takes into account the production of O_2, diffusion of O_2 between different layers of the thylakoid membrane sample and toward the aqueous bulk, and the consumption of O_2 by the surface of the bare platinum electrode in the lowest membrane layer (see Appendix 1 for a description of the mathematical model). Varied interval double flash procedures were used to calculate the rate of PSII turnover (*81, 84*). For these measurements samples were exposed to LED flashes at 2 Hz with the exception of the 4^{th} flash, which was given after a variable time period.

2.7 Steady State Rates of Oxygen Production.

Maximal rates of oxygen evolution from whole cells under continuous saturating illumination were measured using a water jacketed Clark-type electrode (Yellow Springs Instruments, OH, USA) maintained at 30° C (*85*). Measurements were made using samples containing 10 μg of Chl taken from cells suspended in 1.6 mL of HN buffer [10 mM Hepes-NaOH and 30 mM NaCl (pH 7.0)]. The samples were exposed to a saturating light in the presence of 2 mM $K_3Fe(CN)_6$ and 750 μM DCBQ for 60 seconds. The maximal O_2 rates were calculated from the first 30 seconds corresponding to the maximal rate of O_2 concentration increase in the closed reaction vessel. Each measured O_2 rate was corrected by subtracting 45 μmol of O_2 (mg of Chl)$^{-1}$ h^{-1}, which is the artifactual

change in O_2 concentration observed due to the increase in the temperature of the sample due to the incident illumination despite the water-jacketing.

2.8 Quantification of PSII and Measurements of Fluorescence Kinetics.

Measurements of variable fluorescence yields were performed with a double-modulation kinetic chlorophyll fluorometer fitted with a second actinic flash illumination source (PSI Instruments, Brno, Czech Republic). Cells from the mid-log growth phase were harvested, resuspended in fresh BG-11 growth media to a density corresponding to 100 μg of Chl/ml and kept under dim light on a rotary shaker at 200 rpm. Samples were then diluted to 5μg of Chl/ml as needed for measurements. Under these conditions cells typically maintain >90% of their initial O_2 evolving activity for several hours. Fluorescence kinetics were assayed using variations of the standard instrument settings that sample the low-fluorescence F_0 state in dark-adapted samples by probing fluorescence yield with four measuring pulses followed 200 μs later by a 30 μs saturating actinic flash, followed by a sequence of measuring pulses beginning 50 μs after the actinic flash. PSII has a high fluorescent yield when it is in the $P680Q_A^-$ state, which is formed when P680 absorbs a photon of light and donates an electron to Q_A. Without inhibitors, the principal component of the decay of this state is due to the oxidation of Q_A^- by a plastoquinone in the Q_B site. When DCMU blocks the transfer of electrons from Q_A to Q_B, this causes $P680Q_A^-$ to persist until the electron recombines with oxidants on the donor side, which in the case of the intact enzyme is principally the S_2 sate of the Mn_4CaO_5 cluster. The total variable fluorescence was evaluated with the equation $F_v=(F_t-F_0)/F_0$, where F_t is the fluorescence at time t and F_0 is the lowest level of

Fluorescence yield obtained as the average yield of a sequence of four weak measuring flashes applied before the first saturation flash. Analysis of the kinetic components of the fluorescence decay was performed according to Allahverdiyeva et al., except that a correction for exciton sharing between centers was not applied and a three exponential decay was used for samples measured both in the presence and absence of DCMU (*26, 86*).

Estimation of the concentration of charge-separating PSII centers was performed essentially as described previously (*82, 87*). The cells were incubated in the dark for 5 min with 300 μM DCBQ and 300 μM $K_3Fe(CN)_6$ to oxidize any residual Q_A^-. DCMU was then added to a concentration of 20 μM and the mixture was allowed to incubate for 1 min, and then 10 mM hydroxylamine was added. Measurements of variable fluorescence was initiated several seconds after the hydroxylamine was added by applying 30 saturating actinic flashes (20 Hz), with the fluorescence yield being sampled after each flash. This technique assays the relative amount of PSII complexes capable of performing photochemical charge separation regardless of whether the center is capable of also assembling functional Mn_4CaO_5 clusters (*82, 87, 88*).

2.9 Measurement of absorption changes at 360 nanometers.

The electron transfer from the Mn_4CaO_5 cluster to Y_z^{OX} was monitored by time-resolved absorption measurements at 360 nm. Core particles were diluted to 10 μM (chlorophyll concentration) in a buffer with 10% glycerol, 0.03 dodecyl-β-D-maltoside, 1 M betaine, 25 mM MES (pH 6.2), 10 mM NaCl, 5 mM $CaCl_2$ and 5 mM $MgCl_2$. 100 μM DCBQ and 500 μM potassium ferricyanide were added as artificial electron acceptors.

The absorption transients induced by flash series (flash spacing 375 ms) were collected with 100 kHz electrical bandwidth and 20 traces were averaged to increase the signal to noise ratio. The monochromatic measuring light was transmitted through the sample to the surface of the photocathode of the photomultiplier (Electron tubes, 9734B). The slow excitation of the sample by measuring light was circumvented by a photoshutter operating in front of the sample. The photomultiplier was protected from the scattered laser and prompt fluorescent light by combination of interference (Asahi spectra, ASA ZBPA 360) and band pass filters (Schott, BG3). The sample was excited perpendicular to the measuring beam by frequency-doubled, Q-switched Nd-Systems, SR560 and the signal was digitized (Adlink PCI-9812). Actinic illumination was provided by a YAG laser (Quantel BrilliantB, 532 nm, 5 ns). The intensity of the laser light was adjusted by a Glan-Taylor prism to the level, which provided saturating excitation of the sample (21 mW/cm^2). The anode voltage signal of the photomultiplier was amplified and filtered by a differential low-noise preamplifier (Stanford Research by home-written software). The analysis of the absorption transients and the modeling of the four-period oscillation were carried out by MathCAD 2001 Professional and Origin 7.5.

CHAPTER III

The D61N mutation in *Synechocystis* sp PCC 6803 allows the observation of pH-sensitive intermediates in the formation and release of O_2[‡]

[‡]This chapter is reproduced with slight modification from the following publication:

Dilbeck, P. L., Hwang, H. J., Zaharieva, I., Gerencser, L., Dau, H., and Burnap, R. L. (2012) The D1-D61N Mutation in *Synechocystis* sp PCC 6803 Allows the Observation of pH-Sensitive Intermediates in the Formation and Release of O-2 from Photosystem II, *Biochemistry 51*, 1079-1091. Reprinted with permission from Biochemstry. Copy right 2012 American Chemical Society.

Abstract

The active site of photosynthetic water oxidation by Photosystem II is a manganese-calcium cluster (Mn_4CaO_5). A postulated catalytic base is assumed to be crucial. CP43-Arg357, which is a candidate for the identity of this base, is a second sphere ligand of the Mn_4-Ca, and is located near a putative proton exit pathway, which begins with the residue D1-D61. Transient absorption spectroscopy and time-resolved O_2 polarography reveal that in the D1-D61N mutant, the electron transfer from the Mn_4CaO_5 cluster to Y_Z^{OX} and O_2 release during the final step of the catalytic cycle, the S_3-S_0 transition, proceed simultaneously but are more dramatically decelerated than previously thought ($t_{1/2}$ up to ~50 ms versus 1.5 ms in wild type). Using a bare platinum electrode to record the flash dependent yields of O_2 from mutant and wild type PSII has allowed the observation of the

kinetics of O_2 release from extracted thylakoid membranes at various pH values and in the presence of deuterated water. In the mutant, it was possible to resolve a clear lag phase prior to the appearance of O_2, indicating formation of an intermediate before onset of O_2 formation. The lag phase and the photochemical miss factor were more sensitive to isotope substitution in the mutant indicating that proton efflux in the mutant proceeds via an alternative pathway. The results are discussed in comparison with earlier results obtained from the substitution of CP43-Arg357 with lysine and in regards to hypotheses concerning the nature of the final steps in photosynthetic water oxidation. These considerations lead to the conclusion that proton expulsion during the initial phase of the S_3-S_0 transition starts with the deprotonation of primary catalytic base, probably CP43-Arg357, followed by efficient proton egress involving the carboxyl group of D1-D61 in a process that constitutes the lag phase immediately prior to O_2 formation chemistry.

3.1 The residue D1-Asp61 may play a key role in the proton exit pathway of PSII

The closest residue to the Mn_4CaO_5 in any of the proposed proton exit pathways is D1-Asp61 (D1-D61), an aspartate residue in the second coordination sphere of the Mn_4CaO_5 cluster (*61, 62*) shown in Fig. 3.1. D1-D61 is positioned about 6 Å away from CP43-Arg357, which has been proposed to serve as a catalytic base in PSII water oxidation (*57, 85, 89*). Furthermore, D1-D61 is a second sphere ligand of the Mn_4CaO_5 since it coordinates two waters molecules, one of which is a ligand of the Mn4 atom and the other is within hydrogen bonding distance of an oxo bridge of the Mn_4CaO_5 (*18*). D1-D61 and CP43-Arg357 are separated by the so-called narrow channel, one of the putative water channels that connect the Mn_4CaO_5 cluster with the lumenal surface of PSII (*64, 65*). The role of D1-D61 has been examined through mutational studies, starting with

Chu et al., where mutant strains of the cyanobacterium *Synechocystis sp.* PCC 6803 were created in which D1-D61 was replaced with asparagine, alanine, and glutamate (*76*). Subsequently, the D1-D61N mutant was determined to be defective in S-state cycling, most notably having a highly retarded O_2 release kinetic coinciding with a similarly retarded electron transfer from the Mn_4CaO_5 cluster to Y_z^{OX} (*48*, *56*, *75*).

The chemical basis for the observed slowdown of H_2O oxidation reaction in the D1-D61N mutant remains to be established. Because it is proposed to be part of the proton exit pathway and because of its proximity to the Mn_4CaO_5 cluster, it is an interesting target for analysis of potential alterations in proton handling characteristics during H_2O oxidation catalysis. Here we have analyzed the O_2 producing activity of mutant and wild type membranes under a range of pH and pD values using a bare platinum electrode capable of high time resolution.

The chemical basis for the observed slowdown of H_2O oxidation reaction in the D1-D61N mutant remains to be established. Because it is proposed to be part of the proton exit pathway and because of its proximity to the Mn_4CaO_5 cluster, it is an interesting target for analysis of potential alterations in proton handling characteristics during H_2O oxidation catalysis. Here we have analyzed the O_2 producing activity of mutant and wild type membranes under a range of pH and pD values using a bare platinum electrode capable of high time resolution. Our results show that oxygen evolution in the D1-D61N mutant has an altered pattern of pH sensitivity in comparison to the wild type, and also has a larger isotope effect upon substitution with D_2O. The

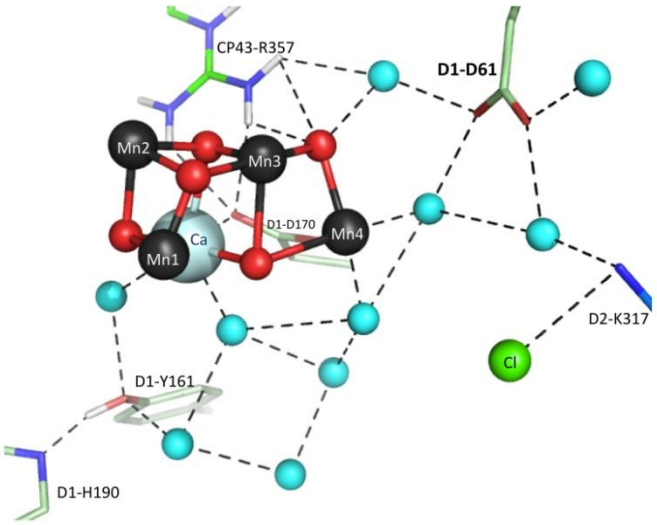

Figure 3.1 The Mn_4CaO_5 cluster and D1-Asp61. The Mn_4CaO_5 cluster of photosystem II showing the several key amino acid residues and water molecules (cyan spheres) in the environment of the metal cluster (*18*). Second sphere side chain ligands, D1-Asp61 and CP43-Arg357, are proposed to mediate proton transfer away from the active site.

relationship between the slowed O_2 release to the re-reduction of Y_z^{OX} was confirmed with UV spectroscopy. These results support a model of PSII activity where trapping of a state immediately prior to Y_z^{OX} re-reduction and dioxygen formation depends upon ejection of a proton mediated by D1-D61. However, the results also indicate that the role of D1-D61 in facilitating dioxygen formation extends beyond proton transfer alone.

3.2 RESULTS

3.2.1 pH dependence of S-state cycling.

The patterns of flash-induced O_2 production in dark-adapted thylakoid membranes were measured as a function of pH and deuterium isotope exchange to assess the proposed role of D1-Asp61 as a mediator of proton efflux from the H_2O-oxidation reaction. A period four oscillatory pattern of O_2 release, with a maximum on the third

flash, was observed in all samples upon exposure to a series of measuring flashes from a xenon discharge lamp (Figs. 3.2A and3.2C). Samples measured at pH 6.5 exhibited the most sustained oscillations for both the mutant and the wild type control (Figs. 3.2A and 3.2C, black). Assuming a four S-state model (*80, 83*) and plotting the miss factor as a function of pH shows that the miss factor is weakly sensitive to pH in the range of conditions employed (Fig. 3.3, open symbols). The D1-D61N mutant showed a higher miss factor in comparison to the wild type at each pH tested. The estimated miss factors for wild type and D1-D61N thylakoids in pH 6.5 buffer were 7% and 14%, respectively (Fig. 3.3). The general conclusion that the D1-D61N mutation results in an increased miss factor is consistent with in vivo measurements (*48*). However, the miss factors in those in vivo experiments were considerably higher for both the wild type and mutant (17% and 26%, respectively) (*48*) explainable by reduced quinone acceptors in living cells (*80, 90*). A miss factor being as low as 7% is advantageous as it implies that the acceptor side contribution to the miss factor is negligibly small. The higher miss factors in the mutant are therefore due to decreased efficiency of trapping oxidant within the WOC and support the hypothesis that D1-D61 facilitates the release of protons from the WOC as part of the oxidant-trapping mechanism.

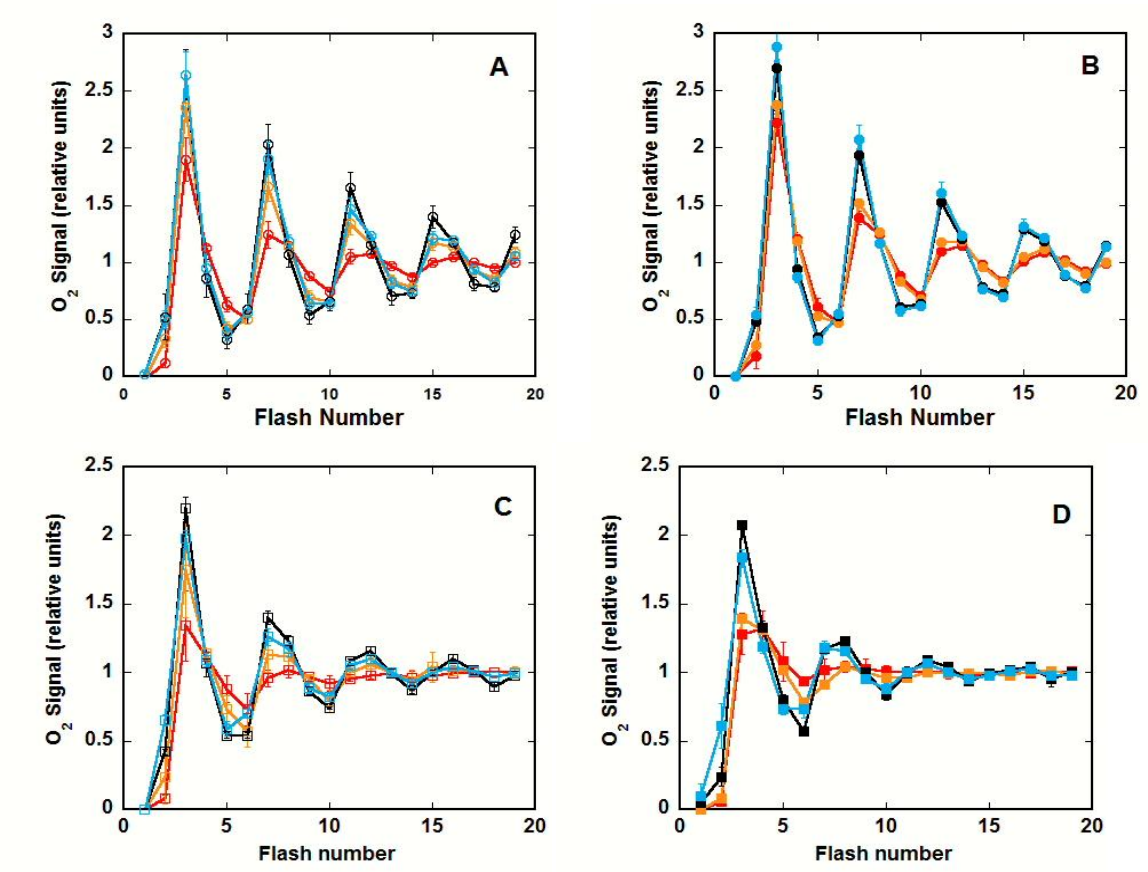

Figure 3.2 Flash dependent O_2 yields as a function of flash number. Samples of thylakoid membranes were given a single saturating flash and dark-adapted for 10 min before being exposed to 19 saturating flashes from a xenon lamp at 1 Hz while being kept at a constant temperature of 20 °C. Panel A shows the O_2 yield from wild type (open circles) at pH 5.0 (red), 5.5 (orange), 6.5 (black) and 7.5 (blue). Panels B, C, and D show the O_2 yields from wild type in D_2O buffer (closed circle), D1-D61N in H_2O buffer (open square) and D1-D61N in D_2O buffer (closed square) respectively. Each point represents the average of at least three measurements. The amplitudes from each measurement were normalized to the average amplitude of the last four flashes. Error bars represent the standard deviation of the normalized O_2 yields from 3 samples.

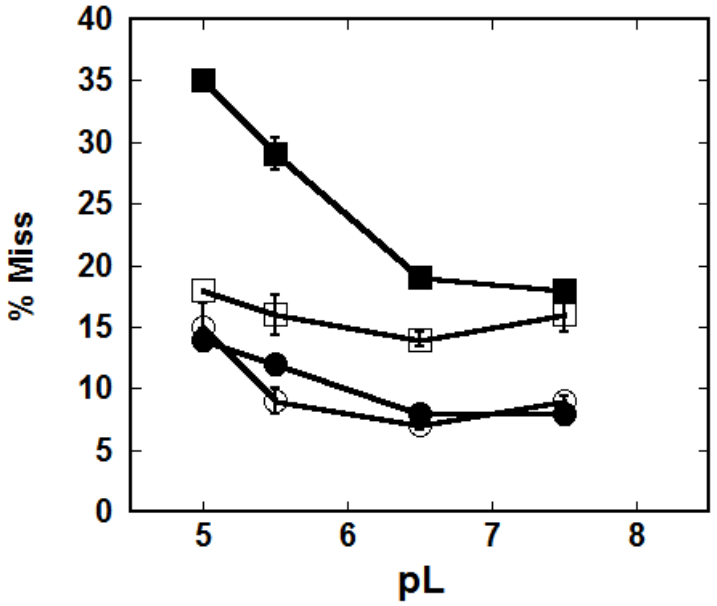

Figure 3.3 Percent of missed S-state transitions as a function of pL (pH or pD) level. Wild type (circles) and D1-D61N (squares) thylakoid membranes were dark-adapted for ten minutes after being exposed to a single saturating flash. The samples were then exposed to 19 measuring flashes. The measurements were repeated with a range of pH (open circles and open squares) and pD values (closed circles and closed squares). Each % miss was derived by analysis of the amplitudes using a four state model. Error bars represent the standard deviation of the percentage of failed S-state transitions from 3 samples for each condition.

While the miss factor for S-state advancement in D1-D61N membranes was uniformly higher than the wild type under all pH conditions, it did exhibit less sensitivity to differences in pH in the range of 5 to 7.5 than the wild type (Fig. 3.3, compare open symbols representing pH buffers). The miss factor in D1-D61N membranes increases only a few percent outside of the pH 6.5 optimum, whereas the wild type miss factor approximately doubles at pH 5.0 compared to the pH 6.5 optimum. Therefore, the wild

type PSII centers are proportionally more sensitive to changes in the concentration of external protons, although the mutant has a higher miss factor at all tested pH values. This is not unlike the effect of mutating a proton shuttle residue in the carbonic anhydrase active site, which, besides slowing the enzyme down, also has the effect of flattening its pH-dependence curve (*91, 92*).

3.2.2 H/D isotope effects on S-state cycling in D1-D61N and wild type thylakoid membranes.

To further examine how the D1-D61N mutation affects the O_2 evolving properties of PSII in relation to proton transfer characteristics, the effects of a heavy proton (^2H, alternatively, D) isotope on S-state cycling were determined (Fig. 3.2 B and D). The kinetic isotope effect (KIE) on the miss parameter, defined as (miss factor in D_2O)/(miss factor in H_2O), for the wild type was essentially negligible as shown in Fig. 3, which shows the miss factor as a function of pL (pH or pD, compare open and closed circles), consistent with previous observations in spinach (*93*). In contrast, deuterated buffer increased the miss factor in the mutant especially at acidic pLs (Fig. 3.3, compare open and closed squares). This indicates that the proton release D1-D61N mutant follows an alternate pathway compared to the wild-type. The most dramatic decrease in the efficiency of S-state transition and the largest KIE was observed at low pL values in the mutant. At pL 5.0, the KIE was approximately 2.5 in the mutant, while the KIE decreased at more alkaline pLs, with a negligible isotope effect observed at pL 7.5 (Fig. 3.3, closed versus open squares). Because the KIE in the mutant is pL-dependent, it is not likely to be a primary isotope effect involving the breaking of a bond transiently retaining the exiting proton on a titratable moiety along a single exit pathway since a

significant isotope effect would be expected at all pLs and this is not observed. Instead, the pL-dependent KIE in the mutant is more likely a secondary isotope effect involving a titratable group that controls the proton transfer process in the mutant proton conduction pathway. This titratable group appears to have a pK_a in the range of pH~5 which would be expected to rise by approximately 0.5 pH units upon binding the heavier deuteron, as is typical of amino acids in a D_2O solution (*94, 95*). The protonation of this controlling group blocks S-state advancement in the mutant, but not in the wild type since a similar KIE is not observed. We conclude that the mutation causes defect in the normal proton release mechanism and proton release instead follows an alternative path.

3.2.3 Determining O_2 release kinetics as a function of pH.

Previous analysis has shown that mutations of D1-D61 result in a large retardation of the kinetics of O_2 release during the S_3-S_0 transition (*48, 56*). To test whether the slowdown might be due to alterations in the handling of protons by the enzyme, the post-flash kinetics of O_2 appearance during the S_3-S_0 transition was recorded polarographically under a range of pH conditions (Figure 3.4). As above, thylakoid membranes from the D1-D61N mutant and the wild type were deposited in a thin layer onto the surface of a bare platinum electrode by high-speed (10,500 x g) centrifugation. Note, this is a considerably higher centrifugal force than that the 1,700 x g centrifugation in previous studies on this mutant (*56*) and, together with the higher salt concentration, likely accounts for the different signal kinetics obtained here. Illumination was provided by 50 μsec red LED flashes. This minimized flash artifacts that are more prominent using the xenon source and interfere with the observation of the onset of the O_2 signal. Furthermore, the absence of blue and ultraviolet light in the LED source avoided

significant photodamage and allowed each sample to be exposed to a larger number of flashes enabling better signal averaging.

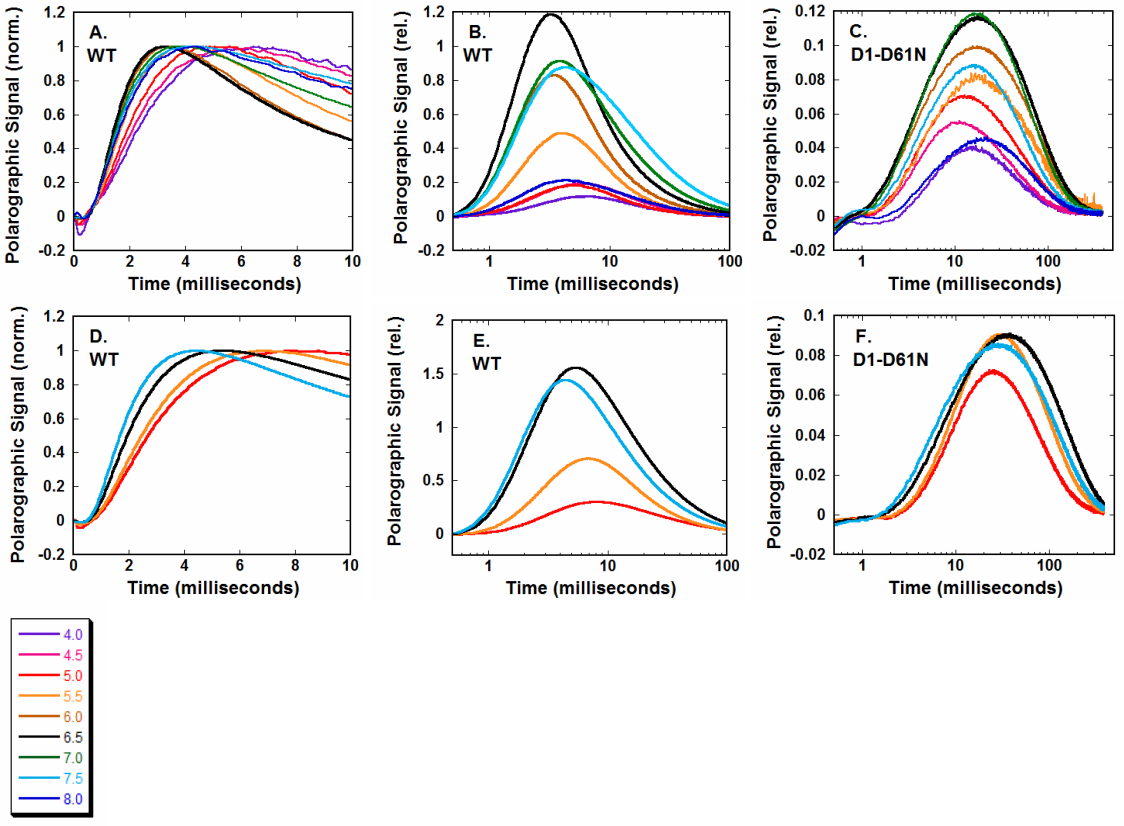

Figure 3.4 Oxygen release kinetics of wild type and D1-D161N thylakoid membranes. Membranes were measured at the pH 4.0 (purple), 4.5 (pink), 5.0 (red), 5.5 (orange), 6.0 (brown), 6.5 (black), 7.0 (green), 7.5 (light blue) and 8.0 (dark blue) (panels A,B and C) and at pD's 5.0, 5.5, 6.5, and 7.5 (panels D, E and F). The signals shown are the averaged O_2 release signals resulting from 117 to 600 individual flashes excluding the first three initial flashes in each series of flashes.

All O_2 transients feature an initial lag phase (i.e., a delayed onset of the subsequent rise) followed by a sigmoidal rise to a maximum value and a slow decay toward the pre-flash level. Lag phase duration, the rise and the signal decay are generally much slower in the D61N mutant than in WT thylakoids; and these features are sensitive

to differences in pH (pD) and to H/D exchange (Fig. 3.5). The remaining flash artifact often resulted in a negative O_2 signal within 400 µs after the LED-flash but did not create the observed lag phase behavior. The lag phase duration generally clearly exceeded the previously observed lag phase of about 200 µs detected in UV/vis and X-ray transients (*34, 53, 55, 57*). The lag phase duration and extent of sigmoidicity depended strongly on the used polarisation voltage (not shown) suggesting a contribution of the O_2-reduction reaction taking place at the bare platinum electrode. Thus the delayed rise observed in the WT presumably represented the sum of a contribution from the electrode response and a (likely minor) contribution from the reactions in PSII. Currently we cannot disentangle these two contributions. However, lag phase duration and sigmoidicity detected in the WT provide an upper limit for the influence of electrode kinetics on the O_2 transients. In the D1-D61N mutant, the lag phase was longer and the sigmoidicity was stronger than observed in the WT at the same polarization voltage and pH, implying that the delayed rise of the O_2 signal reflects reactions in the D1-D61N mutant that are strongly decelerated in comparison to the WT PSII (Fig. 3.5).

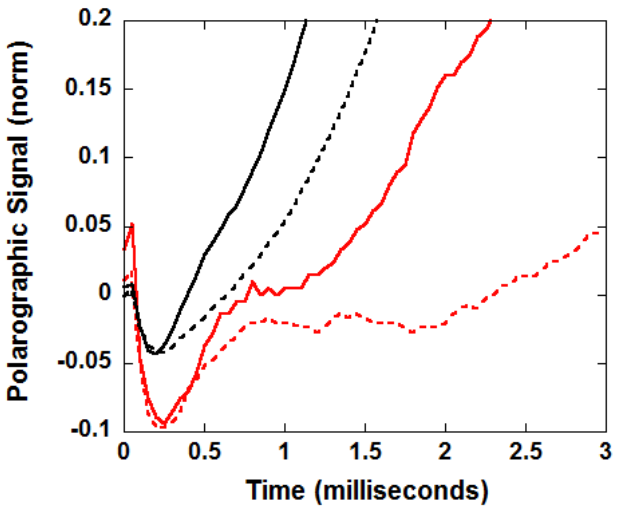

Figure 3.5 Lag in the onset of O_2 release signals from thylakoid membranes. The onset of O_2 release from a subset of the averaged O_2 release curves in Figure 4. The D1-D61N thylakoid membranes show a lag in O_2 release in both pH 5.0 buffering solution (solid red line) and in a pD 5.0 buffering solution prepared with D_2O (broken red line). The signals have been normalized to 1.0 at their respective maximums.

The wild type O_2 signal was observed to have the fastest rate of O_2 appearance at pH 6.5 (Fig.3.4A, black line) in comparison to the signals obtained at other pH levels (Fig. 3.4A, colored lines). Note that the amplitudes of these signals are normalized in Figure 3.4A and 3.4D. The results indicate that, like the maximal rate of O_2 evolution under continuous illumination (*96*) and the efficiency of S-state advancement as shown above and previously (*39*), the release of O_2 during the S_3-S_0 transition occurs most rapidly at pH 6.5 consistent with recent results using spinach membranes (*34*). The wild type O_2 signal exhibits a rise half-time of 1.3 ms, as estimated from a basic phenomenological fit of exponential functions to describe the rise and fall of the polarographic signal (*81, 97*). This value is consistent with previous polarographic

estimates of this slowest step of the wild type S-state cycle (*34, 81, 84, 98-100*) and is close to the value obtained from data fits using a physical model accounting for O_2 production, diffusion, and consumption at the electrode surface as described below. When samples were suspended in buffers adjusted to pH values on the acid and basic side of the pH 6.5 optimum, the O_2 signal exhibits a comparative slow-down (Fig. 3.4A, non-black traces). The most pronounced retardation of rise of the O_2 signal is observed at pH 4.0 (Fig. 3.4A, purple line), where the apparent half-time is about 2.2 ms, compared to the 1.3 ms half-time of the wild type trace. The rise of the signal is distinctly sigmoidal during the initial portion of the rise of the O_2 signal at lower pH indicative of a possible kinetic intermediate (pH 4.0 and pH 4.5, pink and purple curves in Fig. 3.4A). This sigmoidicity becomes especially pronounced in the wild type in D_2O (see next section). Although it is difficult to obtain reproducible amplitudes using a bare platinum electrode, there were observable patterns in the amplitudes of the polarographic signals for membranes suspended at different pH values (Fig 3.4B.). The amplitude of the O_2 signals is routinely observed to be highest at pH 6.5, as seen when representative signals are presented in un-normalized form and on a logarithmic time scale to show the entire signal compactly (Fig. 3.4B, black line). At pH 6.5 the amplitude of the peak of the wild type O_2 release curve (Fig. 3.4B, black) is about ten-fold higher than the peak of the pH 4.0 curve (Fig. 3.4B, purple). This indicates to a first approximation, that the number of PSII centers capable of O_2 evolution is greatly reduced at the extremes of pH since the decrease in the percentage of successful S-state transitions at those pH values is not large enough to account for the great decrease in the per flash O_2 yield. Therefore, we conclude that the wild type WOC functions optimally at about pH 6.5, both with respect

to the speed of the O_2-yielding S_3-S_0 transition, as well as (very approximately) the fraction of the population of PSII centers capable of O_2 evolution.

In the case of the D1-D61N mutant, the O_2 release kinetics are greatly slowed compared to the wild type as has been observed (*48, 56*) or inferred (*76*), previously. Here we have expanded upon those observations in order to test the hypothesis that the delayed release of O_2 from D1-D61N PSII centers is the result of inefficient proton transport (Fig. 3.4C). Surprisingly, values of 4-5 ms for the half-rise times of the O_2 signal were estimated using basic exponential fit of the signal (*81, 97*), which is much faster than the previously reported times for this mutant (*48, 56*). As noted above, the higher centrifugal forces presently used for depositing the membranes on the electrode surface, together with higher salt concentrations here, probably accounts for the differences. However, estimates of the half times based on the exponential fit approach greatly underestimates the O_2 release kinetics compared to when the system is physically modeled to account for delays in the decay of the signal due to O_2 diffusion and electrode consumption, as discussed in the next paragraph. In contrast to the weak dependence of the rise kinetics on pH, the lag period prior to the rise of the O_2 signal in D1-D61N exhibits a strong dependence on pH. Even with the 0.4 ms flash artifact, a clearly visible lag (estimated by inspection of the graph) was observed and ranged from 0.7 to 1.7 ms from the end of the actinic flash to the onset of O_2 release depending on the pH (Fig. 3.4). This lag was shortest (0.7 ms) at pH 6.5 (black) and increased at both higher and lower pH levels, reaching 2.0 ms at pH 4.0 (purple) and 1.7 ms at pH 8.0 (dark blue). The existence of a minimum in the duration of the lag centered at pH 6.5 suggests that the titration state of at least two protonatable residues, with pK_a values flanking the optimum,

control the rate-limiting process occurring during the lag phase prior to O_2 release in the mutant.

In the D1-D61N mutant and also in other PSII mutants with strongly decelerated O_2 evolution (*81*), the retardation of O_2 evolution affects both rise *and* decay of the O_2 signal strongly. The half-time of the O_2 rise depends strongly on the conditions of the electrode experiment, as discussed above, and thus cannot provide a meaningful estimate of the time constant of O_2 formation by PSII. Both the slow signal rise and the drastically increased half time of the signal decay in D61N (see Fig. 3.4) can be explained by the physical model outlined in the following.

Quantitative description of the kinetics of O_2 evolution was facilitated by implementation of a physical model (*101*, *102*) that takes into account the appearance of O_2 from the enzyme, the diffusive processes governing the concentration of O_2 at the platinum electrode surface, and the electrode reaction consuming O_2 at that surface. Since the occurrence of a lag phase prior to the onset of the rise of the O_2 signal has been observed, most notably in the mutant, the O_2 production terms of the kinetic model includes an intermediate, designated 'I' for the sake of generality.

$$S_3 \xrightarrow{k_1} I \xrightarrow{k_2} S_0 + O_2$$

Scheme 3.1

At each time point, the model calculates the concentration of O_2 in discrete layers of equal thickness (Δx), which contain either thylakoid membranes or only buffer. The model accounts for the effect of the thickness of the thylakoid membrane sample on the rate of O_2 diffusion away from the electrodes surface by varying the number of thylakoid

membrane containing layers above the bottom layer (x=0). The constant R_{el} refers to the rate of O_2 consumed by the electrode. Equation 3.1 is used to calculate the concentration of O_2 in the bottom layer (x=0) of the thylakoid membrane sample at each time point *t.* Aside from the bottom layer (x>0), oxygen diffusion and production (by PSII) is considered but not the oxygen consumption by the electrode. At the top layer, oxygen diffuses into the aqueous bulk. We note that Eq. 3.1 describes the delay in the rise of the electrode signal by the rate constant k_1 (k_1 is chosen to be always greater than k_2) *and* an additional time lag (t_{lag} in Eq. 3.1). The time offset (t_{lag}) and k_1 (sigmoidal rise) are used to simulate the overall delay resulting from both the O_2-reduction reaction at the electrode and delayed O_2 production in PSII. The electrode processes are ill-understood and cannot be described sufficiently well by any physicochemical model. This means that the delayed rise of the O_2-signal is described in a purely phenomenological way. Since the values of the two parameters used to describe the delay of the rise of the O_2 signal are strongly correlated, we will report the sum of t_{lag} and k_1^{-1}. (See supplementary materials for further discussion of the O_2 release model).

$$[\mathbf{O_2}]_{x=0}^{t} = [\mathbf{O_2}]_{x=0}^{t-\Delta t} + \left[\left([\mathbf{O_2}]_{x=1}^{t-\Delta t} - [\mathbf{O_2}]_{x=0}^{t-\Delta t}\right)\right] \cdot \left(\frac{\boldsymbol{D}}{\boldsymbol{\Delta x}}\right)^2$$
$$\cdot \Delta \boldsymbol{t} + \frac{\boldsymbol{k_1 \cdot k_2}}{\boldsymbol{k_1 - k_2}} \cdot \left[\boldsymbol{S_3^0}\right] \cdot \left(\boldsymbol{e}^{-\boldsymbol{k_2}\left(\boldsymbol{t}-\boldsymbol{t_{lag}}\right)} - \boldsymbol{e}^{-\boldsymbol{k_1}\left(\boldsymbol{t}-\boldsymbol{t_{lag}}\right)}\right)$$
$$\cdot \Delta \boldsymbol{t} - \boldsymbol{R_{el}} \cdot [\mathbf{O_2}]_{x=0}^{t-\Delta t} \cdot \Delta \boldsymbol{x}$$

Equation 3.1

Application of this model to O_2 transients of WT and D61N resulted in an excellent match of experimental and simulated transients (Fig. 6). To verify the diffusion

model, the two transients had been simulated using essentially identical parameter values to describe the electrode response (R_{el}) and the thickness of the PSII layer on the Pt electrode. The pronounced differences between the two transients were well reproduced by variation of the half time for O_2 formation from 1.1 ms (WT) to 31 ms. The astounding difference between the two transients can be understood as follows: In the WT, the O_2 production is clearly faster than the O_2 consumption by the electrode. Therefore, O_2 molecules can accumulate in the PSII layer and the exponential rise of the O_2 concentration results in a concomitant rise of the electrode signal. In the D61N mutant however, the rate of O_2 production ($d[O_2]^{produced}/dt$) is small and the formed O_2 is rapidly consumed by the electrode (or diffuses into the aqueous buffer). After an initial equilibration phase (rise of the D61N electrode signal), the exponentially decaying rate of O_2 production by PSII is reflected in the decay of the electrode signal.

As opposed to the D61N mutant, application of this model to the wild type signals produced fitting results (Fig. 3.6) that were comparable to the fits produced according to a purely phenomenological fit using exponentials (not shown). The half-times of the faster phase in the wild type membrane samples became incrementally slower at lower pHs. The slower phase (k_2) was fastest at pH 6.5, which harmonizes with visual inspection of the signals (Fig. 3.4B and 3.4C). These trends are more clearly illustrated by plotting the half-times of the phases as a function of pH (Fig. 3.7). The slow phase of O_2 release in wild type membranes had an optimum at pH 6.5 and became significantly slower at higher and lower pH levels. When the O_2 signals for the D1−D61N mutant were fit according to the physical model, the fast phase (k_1) of O_2 release from D1−D61N membranes, like the wild type, had an optimum at pH 6.5, but they are uniformly slower

than the wild type (Fig. 3.7C). The values for the fast phase are consistent with the estimates of the lag obtained by inspection of the graph (Fig. 3.4). The fits using the physical model indicate that the slow phase in D1−D61N membrane samples is at least an order of magnitude slower (12-31 ms) than the wild type slow phase, and qualitatively consistent with previous measurements made at pH 7.2 (*56*). However, the slow phase (k_2) of the D1-D61N mutant was paradoxically slowest at more neutral pH resulting in an 'inverted' optimum curve with respect to the fast kinetic phase.

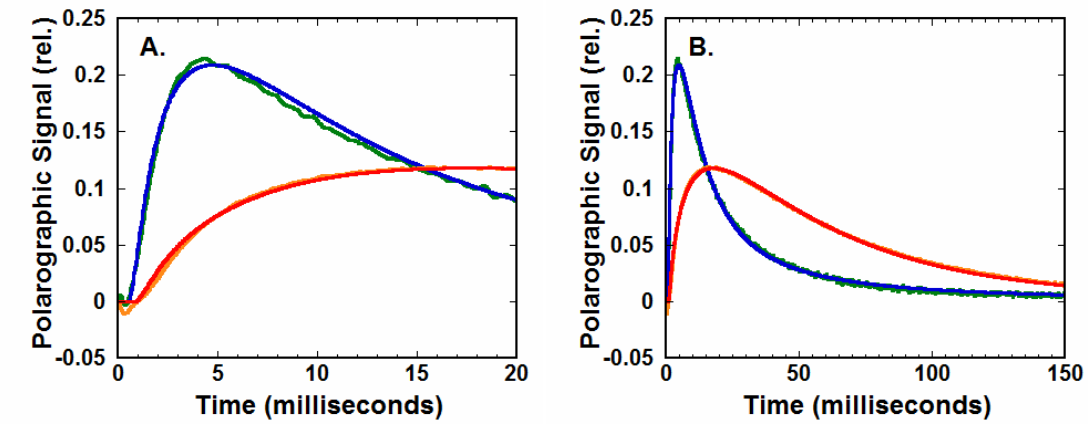

Figure 3.6 Fits of the oxygen release kinetics of wild type and D61N thylakoid membranes. Membranes from the wild type control strain (green) and the D61N mutant (orange) were measured at room temperature (30°C, pH 6.5, 200 mM NaCl). In A (0-20 ms) and B (0-150 ms), averaged transients (green and orange) and simulations (blue and red) are shown. The simulated lines were obtained by simulation on the basis of a physical model that takes into account oxygen diffusion and consumption of the electrode system used for detection of the oxygen release kinetics. The fits used a custom made program (by I. Zaharieva), which calculates two rise constants for the release of O_2 as well as the thickness of the TM layer, diffusion processes, and consumption of O_2 at the surface of the electrode. Simulation parameters were optimized by means of a least-square fit using the electrode reaction parameters for WT and D61N data. The half-time for oxygen evolution are 1.1 ms and 30.9 ms in WT and D61N mutant, respectively. (The complete sets of simulation parameters are shown in Table S1.)

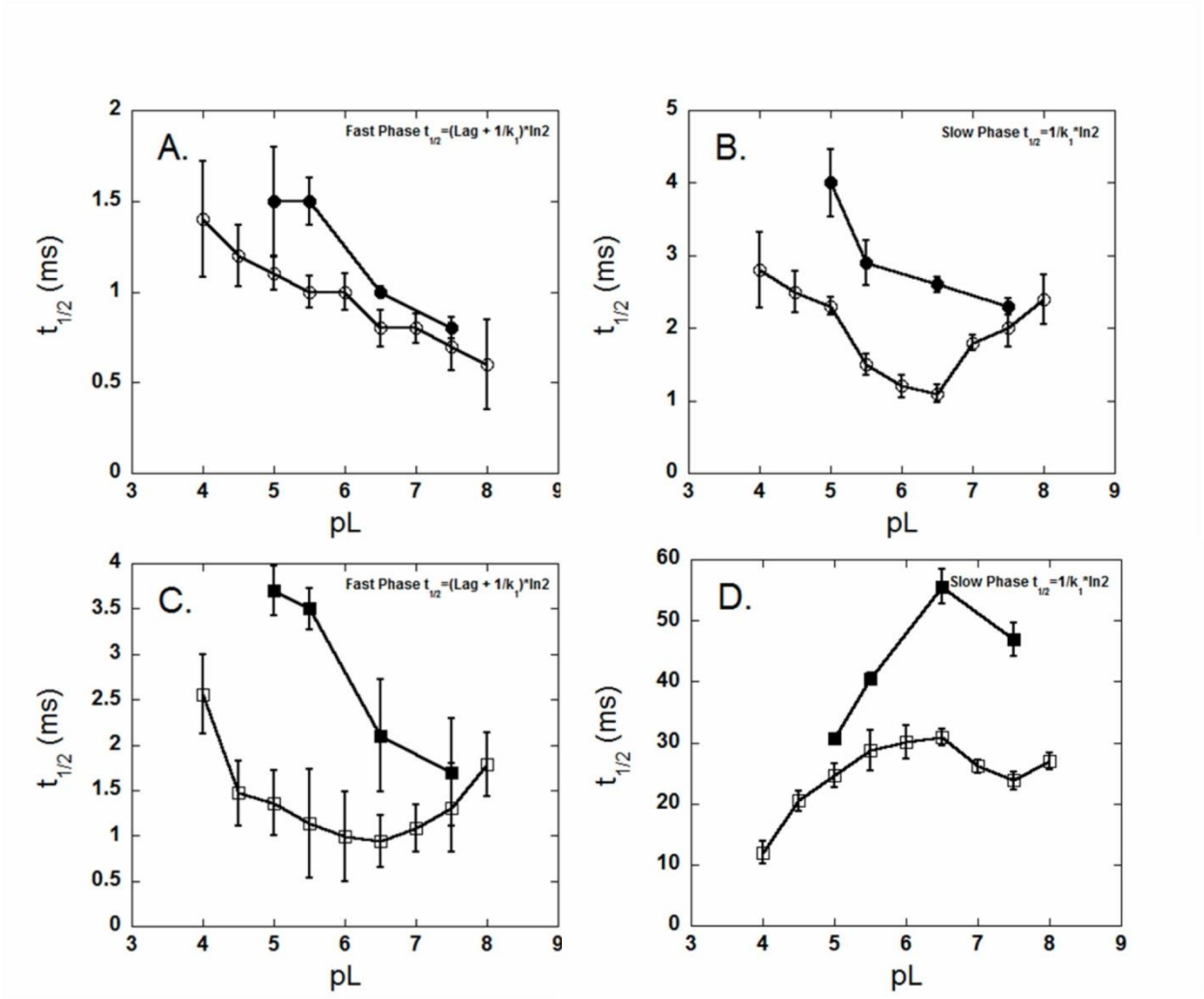

Figure 3.7 Oxygen release kinetics of wild type and D61N thylakoid membranes. Time constants of O2 release from thylakoid membranes. The O2 release traces seen in Figure 3.4 were fit using a custom made program (see text and Figure 6). For this set of data the rate of O2 consumption was held constant. Panel A shows the time constants for the fastest of the two phases (the sum of k1 and extent of the lag phase) of the O2 release curve from wild type in H2O (open circle) and D2O (closed circle) buffers as a function of pL level. Panel B shows the time constants for the slower of the two phases (k2). Panels C and D show the fast and slow phases of the D1-D61N time constants in H2O buffer (open square) and D2O buffer (closed square). Error bars represent the deviation from the given value required to double the sum of squares deviation between the experimental curve and the simulated curve; for more information see supplemental material.

3.2.4 D_2O isotope effects on O_2 release kinetics in D1-D61N and wild type thylakoid membranes.

When wild type samples are transferred to a D_2O-containing buffer and measured as above, an overall slowdown of the O_2 signal occurred at all pD values relative to the corresponding pH values (Figs. 3.5 and 3.7). However, the trends regarding the optimum were slightly different in the presence of deuterons: the fastest release is observed at alkaline values such that pD 7.5 (Fig. 3.7) is the fastest, rather than having an optimum at pH 6.5. Note that the pD 7.5 release was still slower than pH 6.5. These trends are reflected in the slower phase (k_2) of the corresponding fits of the data to the physical model (Fig. 3.7B). D1-D61N thylakoid membranes that were transferred to a D_2O-containing buffer also displayed an overall slowdown of the O_2 signal (Fig. 3.7). The faster phase of the D1-D61N O_2 signals (k_1) has a similar inverse relationship to pD as the slower phase (k_2) of the wild type O_2 signals, with the optimum at pD 7.5 and becoming slower at lower pD's (Fig. 3.7D).

The KIE of the faster phase of O_2 release (k_1) is highest at pL 5.5 and lowest at pL 7.5 in both the mutant and the wild type. However, unlike the faster phase in the wild type (k_1), which has an almost constant KIE, the KIE of the faster phase in D1-D61N increased sharply at lower pL values (Fig. 3.7C). The pD dependence of the slower phase (k_2) in the mutant O_2 signals has the same inverted pattern as the pH dependence of the signals measured in H_2O, with slower rates near neutral pD values (Fig. 3.7). The pL dependence of the KIE of the D1-D61N slow phase is also inverted in comparison to the pL dependence of the KIE in the wild type slow phase (Fig. 3.7D). The overall pattern of behavior of the mutant slow phase in relation to proton concentration and isotope appears

to be the inverse of the behavior of the mutant fast phase. This may indicate that a new rate limiting step in the formation of O_2 is introduced by the mutation of Asp61 to asparagine that requires the reversal of a proton transfer that takes place in the earlier phase, or perhaps the filling of a proton hole produced by the removal of a proton from the WOC early in the S_3 to S_0 transition.

It should be noted that the KIE with a value of 2 to 3 on the slow phase of O_2 release in the wild type appears anomalous compared to the KIE of O_2 release from PSII from spinach, which are in the range of 1.1 to 1.4 (*34, 103, 104*). Given that the our electrode system is at the margin of kinetic resolution (200-400 μs depending upon the buffer conditions) of the wild type processes, we tentatively attribute the discrepancy to measuring instrument limitations for the fastest processes of the wild type, although differences in the mechanistic characteristics of spinach versus cyanobacterial PSII cannot yet be excluded.

3.2.5 UV kinetic spectroscopy.

At pH 6.5, the description of the O_2 signal suggests that the dioxygen formation is slowed down in the mutant by a factor of about 30. To verify this dramatic deceleration and to examine whether Mn reduction in the O-O bond chemistry is slowed down to the same extent, we employed near-UV absorption spectroscopy at 360 nm (A360) for monitoring the oxidation state changes of the Mn complex, as described elsewhere (*34*). We note that in the O_2 forming S_3-S_0 transition of the WT PSII, the re-reduction Y_Z^{ox} is directly followed by reduction of Mn ions in the process of dioxygen formation. These three processes appear to proceed simultaneously and become visible as a decrease in

A360 signal (Mn reduction). The half-times of Mn reduction during the O_2 forming S_3-S_0 transition were observed to be 1.4 ms in PSII particles derived from the wild type control strain and 43 ms in PSII particles derived from the D1-D61N mutant (Fig. 3.8). The $t_{1/2}$ for D1-D61N is similar to the 54 ms $t_{1/2}$ of PSII turnover in D1-D61N thylakoid membranes measured under similar conditions with the bare platinum electrode (20°C, low salt concentration) (Table 3.1.). Differences in the type of PSII preparation (thylakoid membranes versus core particles) and slightly different buffering and temperature conditions used in each experiment are the likely causes of the difference between these two values (43 ms versus 54 ms). If an electron transfer to Y_Z^{ox} with a half-time of 43 ms preceded an O_2 formation step with a halftime of 54 ms, then a lag phase that corresponds to the 43 ms step should be present in the electrode signal. As this is not observed, we conclude that also in D61N, O_2 release parallels electron transfer to Y_Z^{ox}, Mn reduction and O-O bond formation, consistent with earlier interpretations (*105*, *106*).

	$S_1 \rightarrow S_2$, UV spectroscopy (µs)	$S_2 \rightarrow S_3$, UV spectroscopy (µs)	$S_3 \rightarrow S_0$, UV spectroscopy (ms)	$S_3 \rightarrow S_0$, Double flash polarography (ms)	$S_3 \rightarrow S_0$, O_2 diffusion model (ms)	α, UV spectroscopy	α, polarography
Wild type	65.8 ±7	114.3 ±8	1.4 ±0.5	3.7 ±0.2[c]	1.1 ±0.5[c]	NA	7%±1[c]
D1-D61N	350.0 ±21	447.0 ±55	43 ±5.1	54 ±1, (31 ±1[b]), (22 ±1[c])	56 ±1.5, (29 ±1.3[b]), (26 ±3.9 [c])	18%	14%±2[c]

Table 3.1 Comparison of time constants. The half-times of S-state transitions were measured using UV spectroscopy at 20°C in a buffer with 5 mM NaCl. The half-time of the S_3 to S_0 was also determined using double flash polarography and a mathematical fit of the O_2 signal with 10 mM NaCl. The polarographic measurements were also taken at 30°C in a buffer with 10 mM NaCl (b), and at 30°C in a buffer with 200 mM NaCl (c).

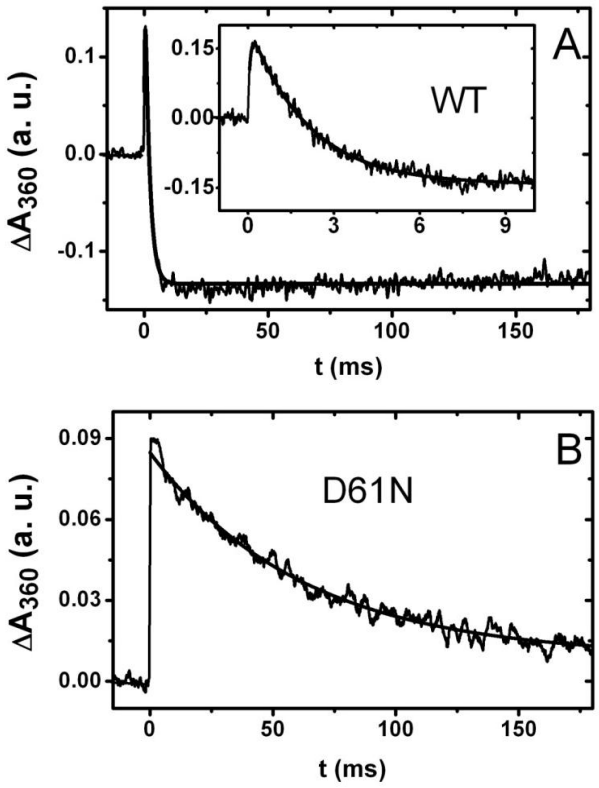

Figure 3.8 Absorption changes at 360 m monitoring reduction of Mn complex in the $S_3 \rightarrow S_0 + O_2$ transition (induced by the 3rd Laser flash applied to dark-adapted PSII core particles). The difference of the absorption change transients at 360 nm induced by the 3rd and 2nd flash was calculated for the WT (A) and D61N mutant (B). The difference signal does not show any slow acceptor side components and the decay reflects the kinetics of the $S_3 \rightarrow S_0$ transition exclusively. It is fast in the case of the wild type (τ = 2.1 ms, inset in panel A) and no further kinetic component is visible in the 100 ms time range (A). The mutation generates dramatic deceleration of the decay component (τ = 62 ms, B). The transients induced by the 1st flash ($S_1 \rightarrow S_2$) and the 2nd flash ($S_2 \rightarrow S_3$) are shown in Fig. S2.

The O_2 transients detected by the bare platinum electrode exhibited a delayed rise of the signal (lag phase of about 1 ms) pointing toward formation of a reaction intermediate. In the near-UV signal, the used background removal procedure as well as

noise contributions render the detection of a lag phase of about 1 ms before onset of the slowly rising absorption signal impossible.

The electron transfer in the D1-D61N mutant had been studied before by near-UV spectroscopy (*48, 75*). In reference (*48*), half times were reported for the $S_1 \rightarrow S_2$ and the $S_2 \rightarrow S_3$ transitions, but not for the $S_3 \rightarrow S_0$ transition. Later the same authors reported a half time also for the $S_3 \rightarrow S_0$ transition; its value was 13 ms and thus clearly smaller than the herein determined values of 43 ms. In reference (*75*) no background was subtracted whereas we corrected for a slowly decaying background by subtraction of the transient detected on the second flash (for verification of the herein used procedure, see also Fig. S3 showing period four oscillations). This background correction was essential for determination for correct determination of the half time of the extremely slow electron transfer in the $S_3 \rightarrow S_0$ transition of the D1-D61N mutant.

3.2.6 Double flash experiment measuring PSII turnover rates.

Besides the near UV-experiment, a second experiment was employed to confirm the extraordinary slow time constants derived by the O_2 release model: The rate of PSII turnover in the S_3-S_0 transition in the D1-D61N strain was measured by a double flash experiment using the bare platinum electrode (*81, 84, 107*). Under a flashing light the majority of PSII centers in a dark-adapted sample will undergo their first S_3-S_0 transition on the third flash. Four more flashes are required to reach the next S_3-S_0 transition. By gradually reducing the time interval between the third and fourth flashes the fraction of PSII centers that have completed the S_3-S_0 transition before the fourth flash occurs is also reduced. These PSII centers will be unable to complete an S-state transition during the

fourth flash and will consequently not have reached the S_3-state when the seventh flash occurs. This lowers the O_2 yield of the seventh flash relative to the yield of other flashes in the series. By fitting a curve to a normalized plot of the relative amplitude of the polarographic signal on the seventh flash versus the time period between the third and fourth flashes an estimate of the $t_{1/2}$ of PSII turnover in the S_3-S_0 transition can be obtained. With this method a $t_{1/2}$ of 22 ms was obtained for the S_3-S_0 transition turnover in D1-D61N thylakoid membranes using the same buffer and temperature used to measure O_2 release kinetics (Table 3.1.). Using the O_2 release model to fit an O_2 release curve from the same sample yielded a $t_{1/2}$ of 26 ms for the longer time constant (Table 3.1.). These values are very similar to the 30.9 ms $t_{1/2}$ from the O_2 release curve obtained during the course of the variable pH experiments (Fig. 3.7). Performing the same experiment using wild type membranes gives a time constant that is somewhat slower (3.7 ms, Table 3.1.) than the analysis of the polarographic signal. This may because the turnover of centers is limited by events on the acceptor side of the complex. Based upon fluorescence measurements (*76*), the D1-D61N mutant is not constrained by the acceptor side and thus the PSII turnover time reflects the pace of events at the WOC. Given the similarity of the estimated time constants obtained for the turn-over times and the polarographic signals in the mutant, we conclude that the analysis of the O_2 signals using the physical model (Equation 3.1) provides a reasonable approximation of the actual time constant for the S_3-S_0 transition of the WOC in the mutant. All the polarographic experiments described above were performed at the 30°C growth temperature of the cells from which the biochemical preparations were obtained. Because measurements of the UV absorbance transients associated with Y_z^{OX} re-reduction were performed at ~20°C,

additional polarographic measurements were performed at 20°C. Comparison of the polarographic measurements taken at 20°C and 30°C showed that the reaction has a very strong temperature dependence, but this was not explored further(Table 3.1).

3.3 DISCUSSION

In previous analysis, the D1-D61N mutant has been characterized as having an increased photochemical miss factor during S-state cycling and an exceptionally slow release of O_2 during the S_3-S_0 transition (*56, 75*). It has been hypothesized (*61, 64, 65*), and molecular modeling analysis supports (*63, 73, 108*), a role for the carboxyl group of D1-D61 in mediating proton release from the WOC. Nevertheless, experimental tests for this important hypothesis have not been performed. Now progress has come from characterization of the influence of pH and the impact of deuterium isotope substitution on the kinetics of S-state cycling and O_2 release in this mutant. For analysis of the O_2 release kinetics, methodological developments were required, namely the implementation of a numerical model for simulation O_2 transients and parameter determination by curve-fitting.

The D1-D61N mutation results in a very pronounced proton/deuteron-sensitive lag phase, occurring between the actinic flash and the onset of the appearance of O_2. This lag can be directly observed using a bare platinum electrode (Fig. 3.4C) and correlates with the fast phase in numerical fits of the O_2 signal. Importantly, the H/D isotope substitution effect upon lag and fast phase were different from the wild-type indicating that the proton exit pathway is different than in the wild-type. A lag phase, occurring between the actinic flash and the onset of Y_Z^{OX} re-reduction or the appearance of O_2

during the S_3-S_0 transition, has been observed in different types of PSII sample, using several different techniques (*34, 53, 57, 104, 109*), and most likely, corresponds to a deprotonation of the WOC (*34, 53, 57*). Placed in the context of these previous findings and the given fact the D1-D61N mutation results in the mechanistic recourse to an alternative proton conduction pathway, the experiments provide the first direct evidence that D1-D61 specifically facilitates proton release at this point in the reaction sequence. The results are also consistent with recent molecular dynamics simulations indicating switching of the carboxyl group of D1-D61 between different hydrogen bonding configurations relevant to the transfer process (*110*).

Although, D1-D61 is involved in mediating the release of protons, it does not appear to be the proposed catalytic base of the WOC since its mutational loss does not cause a severe impairment of S-state cycling efficiency (i.e. the miss factor is only moderately affected in the mutant). Previous analysis showed that the CP43-R357K mutation results in a very large miss factor in the higher S-state transitions (15) Although, the CP43-R357K miss factor is much larger than the D1-D61N miss factor (~46% versus 14%), each can be attributed to a reduced ability to form and stabilize a catalytic base in the de-protonated form. CP43-Arg357 has been proposed to act as the catalytic base that is deprotonated prior to electron transfer in the last two S-state transitions (*8*). There is considerable doubt that arginine can be deprotonated under physiologicaly relevant conditions (*111*), but the substitutions to CP43-Arg357 could still have an effect on the formation of a catalytic base given that arginine residues have been shown to promote the deprotonation of a group of H_2O molecules in rhodopsin (*112, 113*). CP43-Arg357 is hydrogen bonded to a similar group of H_2O molecules.

The deprotonation of catalytic base is hypothesized to occur due to the electrostatic pK_a shift caused by the net positive charge produced by the oxidation of Y_Z by $P680^+$ (*71, 114-116*). The efficiency of the transfer of the proton from catalytic base through the PSII proton exit pathway(s) to the aqueous exterior should be critical to the stability of this de-protonated intermediate state. In D1-D61N, the proton expelled from the WOC requires an alternative, less efficient and more time-consuming path to the aqueous exterior. A model system for proton transfer mediated by an amino acid shuttle is carbonic anhydrase. Mutants of the carbonic anhydrase proton shuttle residue, His64, which mediates the transfer of a proton away from a Zn-bound H_2O to bulk solvent H_2O, exhibit an order of magnitude slowing of the rate-determining proton transfer step of the CO_2 hydration mechanism that is attributable to a less efficient alternative proton conduction pathway in place of the native pathway (*91*, *92*). In the absence, of His64, the sensitivity to external pH is diminished, not unlike the reduced pH sensitivity of the miss factor in the D1-D61N. The recent crystal structure of PSII (*18*), (Fig. 3.1) identifies four H_2O potentially interacting with D1-D61, including one between D1-D61 and CP43-R357. This latter water is proposed to conduct a proton released from CP43-R357 to D1-D61N and in the absence of a carboxyl at position 61, that proton would exit via a less efficient alternative path. Another option is that the proton exit path may start from one of the water molecules coordinated to Mn4, and D1-D61 may function as the (first) proton acceptor for the released proton. In either case, the change of this residue may therefore affect the de-protonation step and/or the subsequent proton release steps. The mutation disruption of the normal proton conduction path would increase the time of residence of the proton in the vicinity of the WOC. This increase in the time of residence

would correspondingly account for the moderate elevation of the miss factor in the D1-D61N mutant owing to an increased probability for backward re-protonation of the primary catalytic base.

Interestingly, the lag phase becomes most protracted at both extremes of pH and shortest at pH 6.5 (Fig. 4C). This indicates that the presumptive proton net transfer rate depends on the titration and/or structural state of protonatable groups in the exit pathway rather than being controlled by mass action exchange of protons between the site of production and the aqueous exterior. That is, if the duration of the lag were simply determined by the mass action exchange-loss of a proton into the aqueous phase, then low pH, but not high pH, would be expected to prolong the lag. This contrasts with the behavior observed in the wild type, which did not exhibit the minimal lag at pH 6.5 and instead became progressively faster as the pH increased (Fig. 3.7A). This suggests that the wild type path is affected by mass action exchange of protons between the WOC and the aqueous exterior.

The post-lag O_2 release kinetic of the D1-D61N mutant is observed to be even slower than previously estimated [~13 milliseconds (*56*) versus more than 30 milliseconds at pH 6.5 found here]. Comparison with results obtained by UV/vis spectroscopy on various organisms indeed suggests that the pH dependence as well as the KIE on the slow phase may be smaller than reported herein, at least for the wild type. In the D61N mutant however, the extended lag phase in the O_2 signal and extremely slow O_2 formation ensure that the influence of the electrode response characteristics is comparatively small. Furthermore, the overall finding of an exceptionally slow O_2 release kinetic is corroborated by double flash techniques (Table 3.1, Fig. A.2.1) and UV-

vis spectroscopy (Fig. 3.8). Still, the pH and pD dependencies are complex and much more work will be required to understand how protons and deuterons influence the O_2 formation step. The drastic slowdown in O_2 formation may reflect the loss of a negatively charged residue near the Mn_4CaO_5 as suggested previously (*48*), however, current caluculations suggest that D1-D61 is protonated in the S_1 state (*108*) and therefore the electrostatic effect, if there is one, may be transient. The carboxyl moiety coordinates water molecules that are themselves ligands of the Mn_4CaO_5 (*18*) and therefore is in the proximity to redox active metals, the oxo bridges, and possible substrate molecules. It is likely important for maintaining an optimized hydrogen-bonding network not only for its experimentally deduced proton relay function, but also for the catalytic process of dioxygen formation occurring after the mandatory proton ejection that it facilitates.

3.4 CONCULUSIONS

Proton release throughout the S-state cycle likely functions to offset the accumulation of a positive charge on the WOC due to the sequential removal of electrons, thereby providing a redox-leveling effect on the WOC that renders the progressive oxidation steps through the higher S-states thermodynamically feasible. Although, D1-D61 is likely to be involved in mediating the release of protons, it does not appear to be the proposed primary catalytic base of the WOC since its mutational loss does not cause a severe impairment of S-state cycling efficiency (i.e. the miss factor is only moderately affected in the mutant). In this regard, D1-D61 is likely to provide a path for the exit of protons that have been extracted by the primary catalytic base. Placed in the context of previous finding on the probable catalytic base, CP43-R357 (one

alternative being the deprotonation of a substrate water), the results are consistent with a proton ejection pathway in which proton expulsion during the initial phase of the S_3-S_0 transition serves as a hole trapping function, poising the reactants and providing the time for the comparatively slow dioxygen formation chemistry to occur with high yield even under conditions where this chemistry is highly retarded. Proton removal during the S_3-S_0 transition thus serves a trapping function enabling the comparatively slow dioxygen formation chemistry to occur by minimizing competing recombinational losses and D1-D61 facilitates this process. On the other hand, the strong effect of the D1-D61N mutation on the rate of O_2 release suggests that the D1-D61 somehow functions in facilitation of dioxygen chemistry, although the mechanism of its activity remains obscure.

CHAPTER IV

Mutations perturbing the water cavity surrounding the Mn_4CaO_5 cluster have a strong effect on the water oxidation mechanism of Photosystem II[‡]

[‡]The following chapter is reproduced in a modified form from a manuscript in preparation titled "Mutations perturbing the water cavity surrounding the Mn_4CaO_5 cluster have a strong effect on the water oxidation mechanism of Photosystem II" Preston L. Dilbeck, Han Bao, Curtis L. Neveu and Robert L. Burnap

Abstract

The active site of water oxidation in Photosystem II (PSII) is a Mn_4CaO_5 cluster that is located in a cavity between the two PSII subunits by which it is coordinated. The remainder of this cavity is filled with water molecules that participate in poorly understood hydrogen bond networks that may modulate the function of the Mn_4CaO_5. These water molecules interact with the first and second spheres of amino acid ligands to the Mn_4CaO_5 and some interact with the Mn4CaO directly. These cavities also comprise portions of the tunnels that lead from the water oxidation complex to the luminal surface of PSII, allowing for the exchange for the substrates and products of the water oxidation reaction. Here we have examined mutations of amino acids that line the walls of predicted cavities in the immediate vicinity of the Mn_4CaO_5. Of these, the mutations to the residue Val185 in the D1 subunit of PSII resulted in the most interesting alterations in

the function of the Mn_4CaO_5 and are the focus of the present study. Mutations of the residue Val185 in the D1 subunit of PSII were produced in *Synechocystis* sp PCC 6803, with the intention that the substitute residue would extend in to the water cavity that includes H_2O molecules that interact with the Mn_4CaO_5, several of the amino acid ligands of the Mn_4CaO_5, Y_Z and the chloride cofactor of PSII. Three of these mutants; the asparagine, phenylalanine and threonine substitutions, were able to accumulate significant levels of charge separating PSII. These three mutant strains were characterized using polarographic and fluorescent techniques to determine their oxygen evolving capabilities and their ability to undergo light driven charge separation. Of the three substitutions the phenylalanine substitution was the most severe with a complete inability to evolve oxygen, despite being able to accumulate Photosystem II and to undergo stable charge separations. The threonine substitution had no apparent effect on oxygen evolution other than a 40% reduction in the steady state rate of O_2 production compared to type *Synechocystis*, which can be attributed to that mutants reduced ability to accumulate PSII. The asparagine substitution produced the most complex phenotype. While still able to evolve oxygen, it does so less efficiently than wild type PSII, with a miss factor 4% higher than wild type *Synechocystis*. The substitution on D1-Val185 with asparagine also decreased the $t_{1/2}$ of O_2 release from thylakoid membranes from 1.2 ms to 10.0 ms and decreased the $t_{1/2}$ lag phase prior to the onset of O_2 release to 2.8 ms. The combination of a long lag period and a decreased rate of O_2 release can also be observed in the D1-D61N mutant strains of *Synechocystis* and in PSII centers in which chloride has been replaced by iodide. The presence of this phenotype in the V185N mutant may be

due to an interaction between the substitute asparagine residue and the chloride cofactor of PSII.

4.1 Introduction

Recently, a three dimensional model of PSII based on X-ray crystallography was presented, with a resolution of 1.9 Ångstroms (*18*), a significant improvement on previous models (*61, 62, 117, 118*). As well as confirming the presence of the metal linking μ-oxo bridges within the Mn_4CaO_5, this new model also revealed the location of a number of water molecules surrounding the Mn_4CaO_5, which had previously been unresolved. This includes several apparent water ligands of the Mn_4CaO_5 and others that reside in the previously described water pathways that lead from the Mn_4CaO_5 to the surface of PSII (*64, 65*). The H_2O broad channel is connected to the narrow channel, which may provide access for substrate water to the Mn_4CaO_5 (*66*), but it is also likely to play a role in proton transfer (*63*).

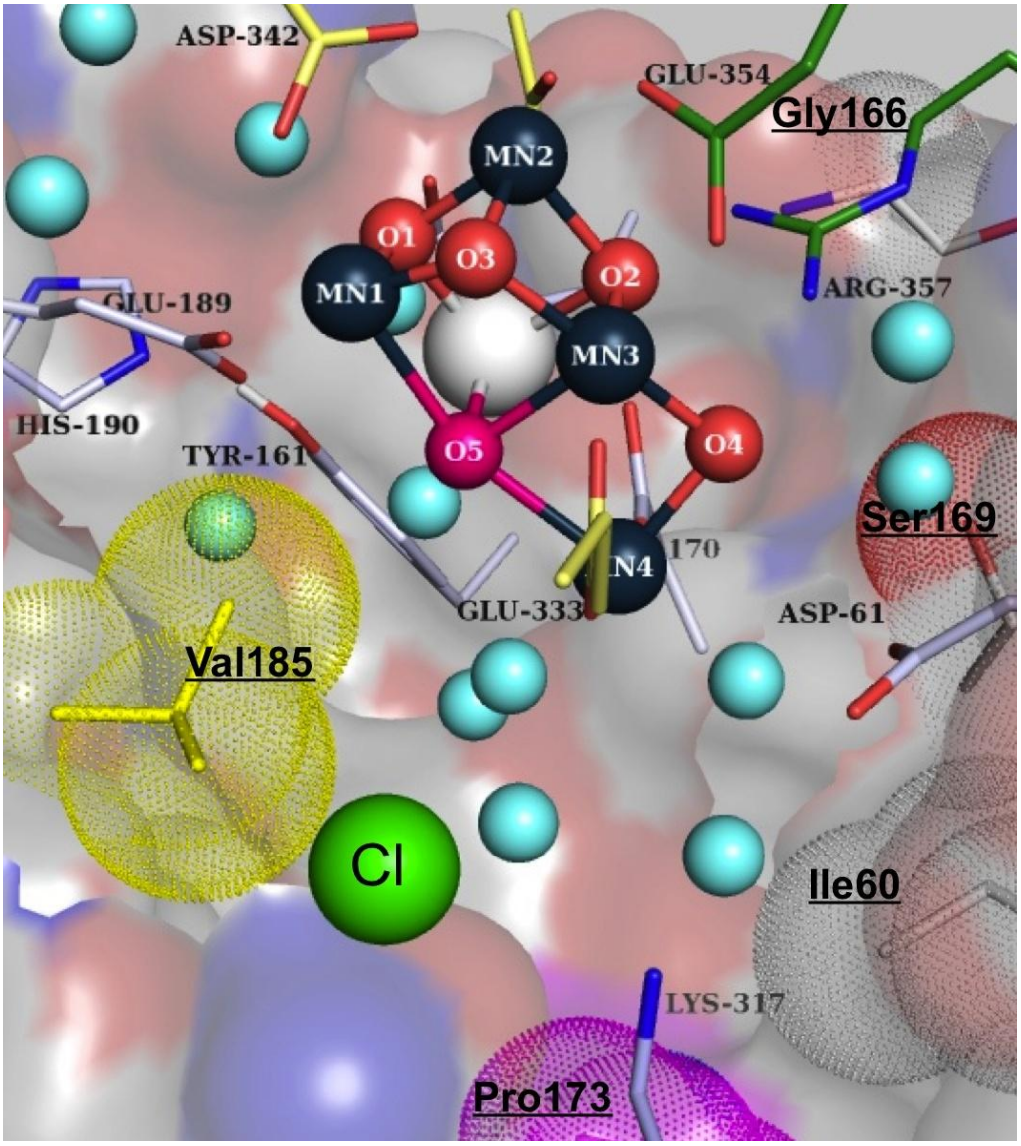

Figure 4.1 Mutations of the second sphere ligation environment of the Mn_4CaO_5. One or more single amino acid substitutions were made to the D1 residues D1-Ile60, D1-Gly166, D1-Ser169, D1-Pro173 and D1-Val185. Each of these mutations was produced with the goal of disturbing the water molecules surrounding the Mn_4CaO_5, without disturbing protein folding. The mutants with substitutions to Val185 were found to effect the water oxidation activity of PSII to varying degrees.

In order to help determine the role these water channels a set of point mutations were generated in segments of the water channels that interface with the Mn_4CaO_5 (Fig. 4.1). There are the first mutations constructed to intentionally alter the waters surrounding the

manganese cluster. These mutants where then characterized in regards to their oxygen evolving and chlorophyll fluorescence properties. Because the selected residues do not act as ligands to the Mn_4CaO_5, nor do they play a role in the exchange of substrate or products of the PSII water oxidation reaction, any phenotypes present in these mutants can be presumed to be due to either structural deformation to PSII or to the disruption of the H_2O/hydrogen bond network. Although significant phenotypes were observed in the mutants with substitutions to the positions D1-Ile60, D1-Gly166, D1-Ser169 and D1-Pro173; the mutants with substitutions to the residue D1-Val185 were observed to have the most interesting results and were subjected to further characterization.

The side chain of D1-Val185, which located is 3.7 Å from the Mn_4CaO_5, faces the broad channel as it passes the Mn_4CaO_5. One of these channels the so called broad channel, which comes into contact with Y_Z, D1-Asp170, D1-Asp61, D2-K317 and one of the chloride binding sites, and also contains many of the H_2O molecules present in the Shen structure that interact with the Mn_4CaO_5 or its ligands, including the H_2O molecules that participate in the hydrogen bond network that is proposed to facilitate the low energy hydrogen bond between Y_Z and D1-His190 (*40*). Although D1-V185 is not positioned to block the access of substrate water to the Mn_4CaO_5, mutation of D1-V185 has the potential to alter the interactions of water around the Mn_4CaO_5 notably the essential Cl^- co-factor, around the Mn_4CaO_5. Thus it is not suprising that mutations at this location can produce dramatic changes in the reactivation kinetics of the Mn_4CaO_5 as described below.

4.2 Results

4.2.1 Mutagenesis

Several amino acids on the D1 subunit of PSII were targeted for mutagenesis on the basis that their side chains face the water cavity surrounding the Mn_4CaO_5 (Fig 4.1). Sites for possible mutation were discovered by analyzing the crystal structure of PSII for unoccupied spaces in the crystal structure that are large enough to accommodate water molecules. This was accomplished using the PyMOL in conjunction with the cavity finding algorithm Caver (*119*) to identify channels in the 2AXT PSII structure (*62*). These cavities were largely in agreement with the channels previously described by Ho and Styring, (*65*) and to a lesser extent to those described by Murray and Barber (*64*). Indeed, after the initial design and construction of the mutants the high-resolution structure of the PSII complex with water molecules was determined (*18*) and these cavities in the proteins structure are shown to be occupied by water. The amino acid residues chosen for mutagenesis were D1-Ile60, D1-Gly166, D1-Ser169, D1-Pro173, and D1-Val185. One or more point mutations were constructed in *Synechocystis* at each of these amino acid sites with the goal of occupying space inside PSII that is normally occupied by water or to change the interaction between the cavity surface with that water so as to allow, for example, aberrant hydrogen bond interactions (Fig. 4.1).

Strain	photoautotrophic growth	relative PSII content (% of wt) [a]	F_v (% of wt) [b]	oxygen evolution (% of wt) [c]
wild type	+	100	100	100
D1-V185F	-	96	56	0
D1-V185D	-	NA	NA	NA
D1-V185N	+	83	71	41
D1-V185T	+	76	61	60
D1-V185W	-	16	10	0

Table 4.1 Characterization of wild type and D1-V185 mutant strains of *Synechocystis* sp. PCC6803. [a]The relative PSII content of each strain was estimated from the yield of variable chlorophyll *a* fluorescence (Fmax - F_0)/F_0 after 40 flashes. Measurements were taken by in the presence of 20 mM hydroxylamine and 20 μM DCMU, according to previously described methods (*82, 87*). [b]The ability of each strain to undergo a stable charge separation was assessed by recording the yield of variable fluorescence (F_{max} - F_0)/F_0 after a single actinic flash in the presence of 20 μM DCMU. [c]Steady state rates of oxygen evolution were measured with a Clark type electrode using a chlorophyll concentration of 6.35 μg in HN buffer [10 mM Hepes-NaOH and 30 mM NaCl (pH 6.5)] with the addition of 750 μM DCBQ and 2 mM $K_3Fe(CN)$. Each value represents the average of three or more samples. Standard deviations were less than 20%.

Each mutant was assayed for its ability to 1) grow photoautotrophically, 2) to accumulate PSII, 3) to undergo stable charge separation and 4) to produce O_2. The purpose of these tests was to determine whether each point mutation was detrimental to photosynthetic water oxidation and if so whether this was due to a defect in the water-oxidation mechanism or due to an inability to assemble stable PSII complexes. Because the aim is to help provide an understanding of the role of the surrounding water in facilitating the water-oxidation mechanism, the most interesting mutants will allow assembly of PSII complexes, yet alter the catalytic properties of the Mn_4CaO_5. Photoautotrophic growth was assayed by inoculation onto solid BG11 growth media and incubation in standard growth conditions (Table 4.1 and Table A3.1). Steady state rates of O_2 production were measured using a Clark-type electrode (Table 4.1 and Table A3.1). The ability of each strain to accumulate PSII and to undergo a stable charge separation

was assayed using a dual modulation kinetic fluorometer. The change in the yield of chlorophyll fluorescence [$(F_t-F_0)/F_0$] induced by a single saturating flash in the presence of DCMU is proportional to the to the fraction of PSII centers present in each sample that are able to form the $P680Q_A^-$ state (which has a higher fluorescence yield than the $P680Q_A$ state) in response to the saturating flash. As discussed below, the decay the high fluorescence state, in part, reflects the characteristics of the donor side of the PSII complex including whether it is capable of forming the S_2 state of the Mn_4CaO_5. Thus, it is a good indicator of whether mutant PSII centers are capable of assembling a functional Mn_4CaO_5. A similar technique was also used to estimate the amount charge-separating PSII in each mutant culture relative to the wild type. This was done by exposing samples to multiple saturating flashes in the presence of hydroxyl-amine (HA), a reductant capable of removing the Mn_4CaO_5 and then acting as the electron donor to Y_Z^+ (*82*, *87*, *88*). The presence of DCMU blocking forward electron transfer from Q_A to Q_B, the presence of HA as a donor-side reductant, and multiple saturating flashes ensure that each PSII center is able to reach the high fluorescence yield state, regardless of defects to the water oxidation complex, and therefore it provides a good biophysical measure of PSII concentration that compares well with biochemical methods *(87)*.

Using these fluorescence techniques, strains shown to accumulate PSII to concentrations that approach the concentration of PSII in wild type *Synechocystis*, while having defects in oxygen evolution were subjected to further analysis. Since three of the strains that shared these traits had substitutions to D1-Val185, mutations of this amino acid were made the focus of this study. The initial characterization of the strains

possessing substitutions to D1-Ile60, D1-Gly1166, D1-Ser169 and D1-Pro173 can be found in appendix 3 (Table A.3.1).

4.2.2 Photosystem II accumulation and activity in D1-Val185 mutant strains.

Five mutant strains were created with single amino acid substitutions of the residue D1-Val185, which faces the broad channel (*65*). Two of these, the aspartate (V185D) and tryptophan (V185W) substitutions did not accumulate significant levels of PSII as evidenced by the lack of a variable fluorescence signal. The mutants with phenylalanine (V185F), asparagine (V185N) and threonine (V185T) substitutions to D1-Val185 were able to accumulate PSII at 96, 83 and 76% of the wild type level, respectively. Of the three V185 mutants that were able to accumulate PSII only the V185N and V185T were able to grow photoautotrophically. The lack of autotrophic growth in the V185F mutant is likely due to an inability to evolve oxygen, as only negligible rates of O_2 evolving activity were detected by the Clarke-type electrode (Table 4.1). The V185N and V185T strains were, on the other hand, able to produce significant maximal rates of O_2 evolving activity, at 41 and 60% of the wild type value respectively.

4.2.3 Fluorescence Decay Kinetics.

The kinetics of the relaxation of the chlorophyll fluorescence yield were examined using a dual modulation kinetic fluorometer. In particular these techniques were used to examine the properties of the donor and acceptor side electron transfer reactions in PSII. The measurements were taken from dark adapted samples that had been grown to mid-log phase conditions that ensure maximal PSII activity in these mutants (data not shown). Samples were exposed to a single saturating flash and then a

series of weaker measuring flashes. Comparing the fluorescence yield after each measuring flash to a base line measured before the actinic flash is given allows the calculation of the fraction of PSII centers in the high fluorescence yield state ($P680Q_A^-$) to fraction in the low yield fluorescent states ($P680Q_A$ and $P680^+Q_A^-$) to be monitored as the high fluorescent state decays. These decay kinetics give information about the electron transfer processes in each strain.

The kinetics of Q_A reoxidation were measured in the wild type, V185F, V185N and V185T strains of *Synechocystis* in both the presence and absence of DCMU, which is an electron transport inhibitor that blocks the forward movement of electrons from Q_A to Q_B. In both cases the decay of the high fluorescence yield signal can be fit using three exponential components, which each correspond to a different acceptor for the electron on Q_A^- (*86*). In the absence of DCMU, the reoxidation of Q_A^- dominated by the transfer of electrons to the plastoquinone in the Q_B site in the 100's of μs time scale ($S_2Q_A^-Q_B \rightarrow S_2Q_AQ_B^-$). The next fastest component is transfer of electrons to Q_B in PSII centers that have yet bound plastoquinone into the Q_B site ($S_2Q_A^- + Q_B \rightarrow S_2Q_A^-Q_B \rightarrow S_2Q_AQ_B^-$), which occurs in about 3 milliseconds. The slowest phase which takes place in the hundreds of milliseconds time scale is the recombination between Q_A^- and the Mn_4CaO_5 cluster in the S_2 state ($S_2Q_A^-Q_B \rightarrow S_1Q_AQ_B$), which occurs if Q_A^- is long-lived, for example when reoxidation of plastoquinol is inhibited. Indeed, the presence of DCMU causes the decay of the high chlorophyll fluorescence yield signal to be dominated by the much slower transfer of an electron back to the Mn_4CaO_5, which again takes place on a hundreds of milliseconds time scale because forward electron transfer is blocked and the recombination reaction reforming the S_1 state ($S_2Q_A^-Q_B \rightarrow S_1Q_AQ_B$) is the only option

(*26, 86*). However, this assumes the presence of an intact Mn_4CaO_5, whereas in some mutants (e.g. V185W) assembly of the Mn_4CaO_5 is abolished in most PSII complexes in the thylakoid membrane and therefore the recombination of the electron on Q_A^- occurs with Y_z^{OX}, which occurs much more rapidly (~10 milliseconds).

Out of the three mutants that were examined extensively the Q_A reoxidation kinetics of the V185N mutant were the most similar to the wild type. Forward electron transfer from Q_A^- to Q_B appears largely unaffected in the V185N mutant as indicated by the similar fluorescence decay kinetics in the absence of DCMU compare to the wild type. In the presence of DCMU the S_2 state and Q_A^- recombined with a $t_{1/2}$ of 580 ms. This is slightly slower than the 421 ms $t_{1/2}$ observed in the wild type strain (Fig 4.2). This may indicate that the S_2 state of the Mn_4CaO_5 clusters in the V185N mutant have a slightly lower redox potential than in wild type PSII. Recombination between Q_A^- and alternate electron acceptors donors was also slower in the V185N mutant, with a $_{t1/2}$ of 945 ms compared to 863 ms in the wild type.

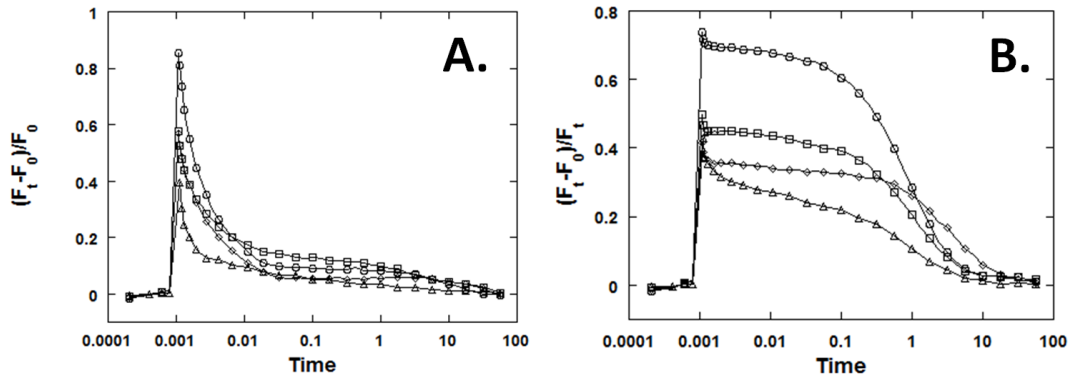

Figure 4.2 Q_A reoxidation kinetics. The decay kinetics of the flash induced variable chlorophyll *a* fluorescence $(F_t\text{-}F_0)/F_0$ for wild type (circles), V185F (triangles), V185T (diamonds) and V185N (squares) strains of *Synechocystis* were measured in both the absence (panel A.) and presence (panel B.) of 20μM DCMU. F_0 was defied as the average fluorescence yield from four weak measuring pulses given to the samples at 200 μs intervals before the exposure of the samples to a 30 μs actinic flash. The actinic flash is followed by a series of weak measuring flashes that monitor the decay of the high fluorescence yield state.

In the V185T mutant there were more substantial differences in the kinetics of Q_A^- reoxidation (Fig. 4.2). The rate of S_2 to Q_A^- charge recombination between S_2 and Q_A^- was reduced to a $t_{1.2}$ of 2.86 s in the presence of DCMU and 2.57 s in the absence of DCMU (Fig 4.2). This again can be interpreted to indicate that the S_2 state of the Mn_4CaO_5 clusters in the V185T mutant have a significantly lower redox potential than in wild type PSII. The V185T strain also differed from the wild type in the relative contributions of the various charge recombination pathways. This can be determined by comparing the relative amplitudes of each component of the fluorescence decay curve (*86*). In this case 58.5 % of Q_A^- charge recombination can be attributed to recombination with the Mn_4CaO_5 in the S_2 state and 41.5 % can be attributed other pathways (Fig. 4.2). For comparison recombination between Q_A^- and the S_2 state only accounts for 49.8 % total charge recombination in wild type *Synechocystis* and 48.2 % in the V185N mutant (Fig. 4.2).

Based on their rates of charge recombination between S_2 and Q_A^-, both the V185T and V185N substitutions appear to lower the redox potential of the Mn_4CaO_5 cluster to a degree that is roughly proportional to the electronegativity of each side chain. This is not an entirely unsuspected consequence of replacing a hydrophobic residue with polar residues in close proximity to a redox active cofactor. The Mn_4CaO_5 cluster in particular depends on several negatively charged ligands to neutralize the positive charges of the metal ions. In other cases where a second sphere ligand has been replaced by a less electronegative side chain, such as the substation of D1-Asp61 with asparagine, the rate of charge recombination between S_2 and Q_A^- has been observed to be more rapid than the wild type (*76*). This generalization does not hold true for every amino acid substitution

made near the Mn_4CaO_5 cluster (*76, 87, 120, 121*). Other means of affecting the rate of charge recombination between S_2 and Q_A^- should also be considered, especially for substitutions like the V185 substitutions which may affect the environment around Y_Z. Altering the hydrogen bond network around Y_Z should be expected to alter its redox potential, which also plays a role in the rate of charge recombination between S_2 and Q_A^-. What effect if any this should have on the catalytic properties of the Mn_4CaO_5, in terms of its ability to oxidize H_2O, are unclear.

There were also differences in the amplitudes of the maximum variable fluorescence signals of each mutant (Fig. 4.2). This indicates that the V185 mutants are unable to form stable charge separations as efficiently as wild type PSII. This may be due to less efficient formation of the S_2 state, which is required to stabilize the $Y_ZP680Q_A^-$ state, but the lower levels of PSII content is likely to also play a role, especially in the V185T mutant.

The V185F mutant has substantially altered Q_A reoxidation properties compared to wild type. It appears to allow very rapid rates of charge recombination even in the presence of DCMU (Fig 4.2). The very rapid rate of the first decay component in the absence of DCMU indicates a lack of stable charge separation; this may contribute to the lack of O_2 production by the V185F mutant.

4.3.4 S-state cycling and O_2 release kinetics.

Thylakoid membranes were prepared from each of the V185 mutant strains of *Synechocystis* in order to further characterize their oxygen evolving activity. The oxygen

evolving characteristics of these membranes were analyzed using a bare platinum electrode to determine their S-state cycling parameters and rates of O_2 release (*81, 122*).

Measurements taken with the bare platinum electrode confirmed the absence of oxygen evolving activity in V185F PSII centers. The only kinetic feature revealed by exposing centrifugally deposited samples of V185F thylakoid membranes to flashing light was the photoelectric artifact caused by the exposure of the polarized electrode surface to LED pulses. This evidence confirms that V185F mutant strain is unable to evolve oxygen.

The flash dependent O_2 yields of both the V185N and the V185T thylakoid membranes displayed period four oscillation with a peak on the third flash in dark adapted samples exposed to a series of saturating xenon flashes (Fig. 4.3). The S-state parameters of the V185T mutant were similar to those of wild type with only a 13% in the miss factor (Table 4.2, α). The V185N mutant displayed a slightly increased miss factor of 18% compared to the 14% miss factor in the wild type thylakoid membranes (Table 4.2, α).

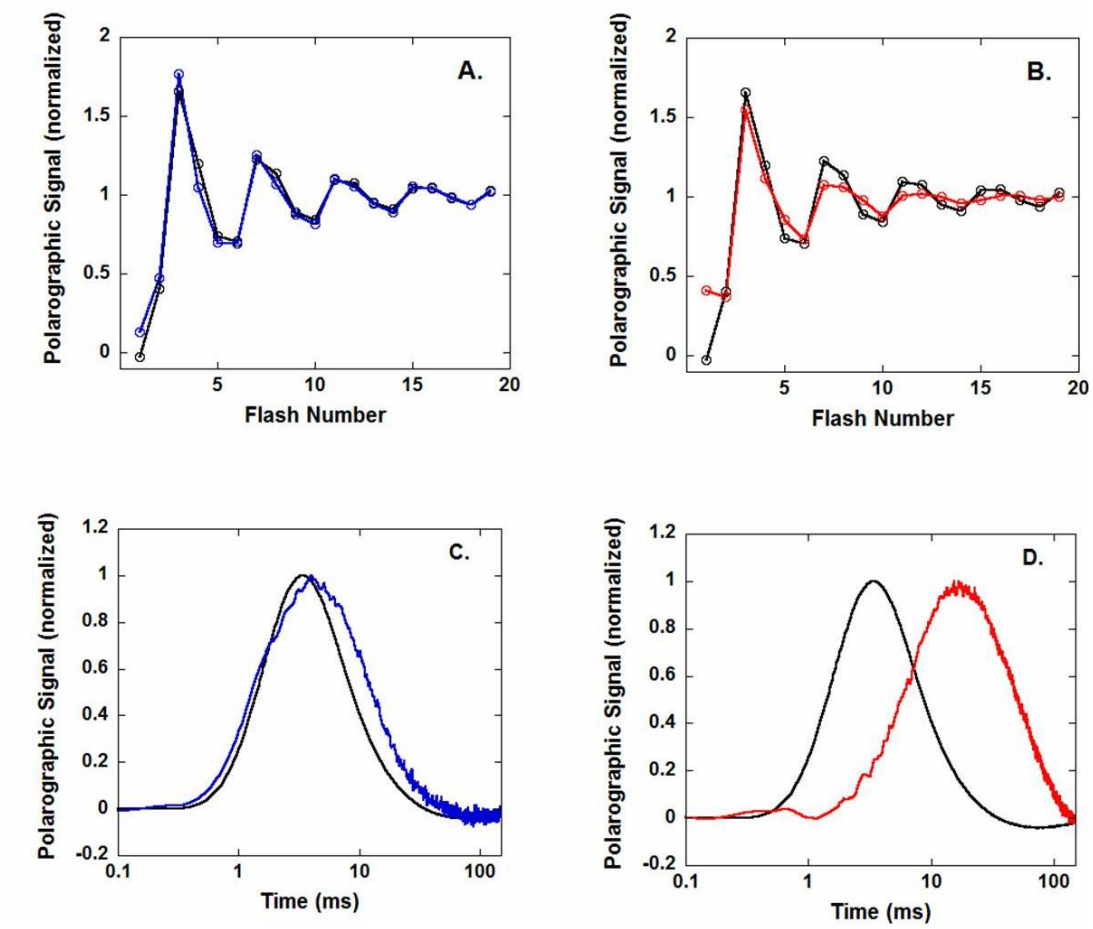

Figure 4.3 Flash dependent O_2 yields (panels A and B) from wild type (black), V185T (blue) and V185N (red) thylakoid membranes. Thylakoid membrane samples containing 3 µg of Chl exposed to a constant light source for 30 sec and then centrifugally deposited on to a bare platinum electrode. The samples were then exposed to a single actinic flash and then dark adapted for 10 min. The flash dependent O_2 yields were then measured from a series of 20 actinic flashes from a xenon flash lamp given at 2 Hz. The signals were normalized to the average amplitude of the last four flashes. Each trace represents the averaged amplitudes from 3 samples with error bars representing the standard deviation. Panels C and D show the O_2 release signals from wild type (black), V185T (blue) and V185N (red) thylakoid membranes. For O_2 release measurements thylakoid membrane samples containing 3 µg of Chl were centrifugally deposited on to a bare platinum electrode and exposed to a series of measuring flashes from a red LED at 4 Hz. Each trace represents the average of 720 (wild type and V185T) or 1200 (V185N) flashes. For the measurement of the mutant samples the gain of the polarographic amplifier was set to double the sensitivity used to measure the wild type sample.

Strain	S-state distribution [$S_0/S_1/S_2/S_3$(%)]	misses, α	hits, β	double hits, γ	O_2 signal rise $t_{1/2}$
wild type	24/64/12/0	14%	84%	2%	1.2 ms[b]
V185N	16/80/0/4	18%	80%	2%	10.0 ms[c]
V185T	17/69/13/1	13%	85%	2%	1.5 ms[b]

Table 4.2 S-state cycling parameters. [a]Thylakoid membranes samples containing 3 μg of Chl exposed to a constant light source for 30 sec and then centrifugally deposited on to a bare platinum electrode. The samples were then exposed to a single actinic flash and then dark adapted for 10 min. The flash dependent O_2 yields were then measured from a series of 20 actinic flashes from a xenon flash lamp given at 2 Hz. Estimation of S-state parameters was performed using a four state model as previously described (*80, 83*). [b]The rise kinetics of the O_2 release signals were estimated from the rising portion of the averaged O_2 release traces (Fig. 5) as previously described (*123*). [c]The rate of O_2 release as determined by a previously described mathematical model (*122*).

The O_2 release kinetics observed from V185T thylakoid membranes with the bare platinum electrode were only slightly slower than the O_2 release kinetics of the wild type. The rise kinetics of the V185T O_2 release had a $t_{1/2}$ of 1.5 ms (Table 4.2), which is only slightly slower than the 1.2 ms $t_{1/2}$ which is characteristic of wild type PSII in optimal conditions.

Unlike the V185T thylakoid membranes, V185N thylakoid membranes released O_2 at a substantially slower rate than wild type thylakoid membranes (Fig 4.4D). These thylakoid membranes also displayed a delayed the onset in the release of O_2 after each actinic flash. The combination of a decreased rate of O_2 release and a longer lag phase has also been observed in PSII samples derived from the D61N (*48, 56, 122*) mutant strain of *Synechocystis* and in PSII samples where the chloride ion had been replaced by iodide (*124*). The V185N mutant also shares a slightly increased miss factor (Fig. 4.4B, Table 4.2) with the D61N and iodide substituted PSII samples (*122, 124*). The role of the chloride ion has been hypothesized to include the modulation of the hydrogen bond

network around D1-Asp61 (*108*). Since the substitute asparagine residue in the V185N mutant is sufficiently long to interact with the chloride ion, it is possible that the phenotype of these three types of PSII center share a common mechanistic explanation involving D1-Asp61 and its role in the removal of protons from PSII.

In order to more accurately compare the kinetics of O_2 release from the V185N and D61N mutants, The O_2 release signal collected from the V185N mutant was fit according to a mathematical model of O_2 release that had previously been used to analyze the D61N mutant (*122*). This model, developed by Ivelina Zaharieva and Holger Dau, includes components that take in to account the processes that cause the decay of the polarographic O_2 signal, as well as two rise components, in order to more accurately reflect the phenomena that underlie the observed O_2 release signal (*122*). The rate of O_2 release estimated by the model for the V185N mutant was 10.0 ms, which is considerably faster than the 26 ms $t_{1/2}$ observed in the D61N mutant under similar conditions (*122*). On the other had the lag phase of observed in the V185N signal was substantially slower than the lag phase observed in the D61N mutant (2.8 ms vs .65 ms). One explanation for this discrepancy is that Asp61 interacts with H_2O directly bound to the Mn_4CaO_5 (*125*), which may have consequences for oxygen-oxygen bond formation, while Val185 does not.

4.3 Discussion

The substitutions to D1-Val185 that were generated for this work represent the first time that point mutations to PSII designed to interfere with the water cavities surrounding the Mn_4CaO_5 cluster. These substitutions have been shown to have a deleterious effect on the ability of PSII to evolve oxygen.

Of the three D1-Val185 mutants that have been characterized in detail, the V185T mutant has the least severe phenotype. This is not surprising given the similarity in the shapes of valine and threonine. Analysis of O_2 release by V185T thylakoid membranes with a bare platinum electrode revealed O_2 release kinetics and S-state cycling parameters that were nearly identical to wild type thylakoid membranes. The steady state rate of O_2 production by the V185T strain of *Synechocystis* is reduced compared to wild type *Synechocystis*, but because this rate is roughly proportional to the number of charge separating PSII centers by the V185T mutant. It is there for reasonable to assume that the reduced rate of O_2 release from V185T *Synechocystis* is attributable to a reduced ability to assemble active PSII centers.

Like the V185T mutant, the V185N mutant retained its ability to evolve oxygen (Table 4.1). However, while there is only a small discrepancy between the ability of V185T to assemble PSII and its ability to evolve oxygen, the V185N mutant can only evolve O_2 at 41% of the rate of wild type while being able to accumulate 83% as much PSII. While the V185T mutant is nearly identical to the wild type in terms of its O_2 release kinetics and S-state cycling parameters, the V185N strain displayed clear differences in both (Fig. 4.4B and D). The kinetics of O_2 release from V185N thylakoid membranes were substantially delayed compared to O_2 release from wild type thylakoid membranes (Fig. 4.4D). The V185N mutant also displayed a substantial lag period prior to the onset of O_2 release (Fig. 4.4D). This lag phase is believed to represent the formation of an intermediate in the S_3 to S_0 transition due to the release of a proton triggered by the oxidation of the $Y_Z^{\bullet}$ (*34, 53, 57*). The length of this lag phase in wild type PSII has typically been observed to be between 150 and 250 μs using various

techniques (*34, 53, 57, 104, 109*). Currently, our observation of the lag phase in wild type thylakoid membranes is limited by the response time of our electrode and the onset of O_2 release is not observed until 350 μs after the actinic flash. In V185N thylakoid membranes this lag phase is extended to ~1.4 ms, making it clearly observable by the bare platinum electrode (Fig. 4.4D).

The phenotype of the V185N mutant is similar to the phenotype of the D1-D61N mutant, another PSII point mutation that has been well characterized (*48, 56, 75, 122*). D1-Asp61 is a second sphere ligand of the Mn_4CaO_5 that interacts with substrate water (*18, 108, 125*) and acts as the first proton acceptor in the proton exit pathway (*61, 63-65, 73, 108*). The D1-D61N mutation retards the rates of S-state transitions which leads to slower O_2 release kinetics during the S_3 to S_0 transition (*48, 75*). The D1-D61N mutant also displays an extended lag phase and increased miss factor, both to an extent similar to the V185N mutation (*48, 56, 122*).

D1-Val185 is not located near D1-Asp61 and it has not been predicted to take part in the proton exit pathway; however the substituted asparagine in the V185N mutant appears to be able to interact with the chloride ion ligated by D1-E333 and D2-K317 (Fig. 1B). A recent hypothesis concerning the function of this chloride ion argues that the ion prevents the formation of a salt bridge between D1-Asp61 and D2-K317, thus modulating the interactions between D1-Asp61 and both the Mn_4CaO_5 substrate and the proton exit pathway (*108*). It should be noted that the replacement of this chloride ion with iodine results in a decreased rate of O_2 release, and extended lag phase and a moderately increased miss factor, all to roughly the same extent as the D1-D61N and V185N mutations (*124, 126*). It is there for reasonable to assume that the phenotypes of

both mutants and the ion replacement are due to a similar interference in the interactions between D1-Asp61, the Mn_4CaO_5 and the chloride ion. It should also be noted that the H_2O molecules displaced by the V185N mutation have been predicted to participate in proton transfer reactions in the S_2 to S_3 and S_3 to S_0 transitions in a model based on DFT calculations (*127*). Unlike the V185T mutant, the V185F mutant does not appear to have difficulty assembling PSII (Table 4.1). But despite being able to assemble PSII at levels commensurate with wild type *Synechocystis*, the V185F strain is unable to evolve O_2. The Q_A reoxidation kinetics displayed in Fig. 4.2 show that V185F is able to form a stable charge separation, although with only 56% of the yield seen in wild type *Synechocystis*. This demonstrates that the V185F mutant is able to assemble at least some Mn_4CaO_5 clusters. It also provides evidence that V185F can reach the S_2 state. Assuming that at least a fraction of the V185F PSII centers contain a fully assembled Mn_4CaO_5 the most likely explanation for the inability of the V185F mutant to evolve oxygen is an inability to complete either the S_2 to S_3 or the S_3 to S_0 transition.

The ability of the V185F mutant to assemble PSII at near wild type levels despite the large size difference between valine and phenylalanine suggests that the replaced residue occupies space previously occupied by H_2O rather than by other amino acids. In fact basic modeling with PyMOL suggests that the least sterically hindered isomer of the substitute phenylalanine residue causes it to displace the H_2O molecules near Y_Z (Fig. 4.1A). One recent model of the WOC based on the 1.9 Å structure suggests that these H_2O molecules are part of a hydrogen bond network that facilitates the short hydrogen bond (2.46 Å) between Y_Z and His190 (*40*). The disruption of this hydrogen bond could have consequences for proton coupled electron transport, which is vital for the efficiency

of S-state transitions particularly in the higher S-states. Other isomers of the substitute phenylalanine residue are of course possible and may lead to structural changes that affect first sphere ligands of the Mn_4CaO_5, especially D1-Gllu189. This does not rule out the possibility that the V185F substitution interferes with the binding of the chloride co-factor, which is also known to prevent water oxidation.

For both the V185N and V185F mutants, a definitive link between amino acid substitution and the resulting phenotype cannot be assigned based on the experiments presented here. Further experimentation will be needed to more clearly establish the cause of the defective oxygen evolution in these mutants, which may provide clues into the activity of the WOC.

CHAPTER V

CONCLUSIONS

The last few years have seen rapid progress in research into the mechanism of the water oxidation reaction catalyzed by PSII. This has been due to the combined use of advance spectroscopic techniques such as EPR, FTIR, and XAFS, biochemistry, and structural biology techniques that have culminated with a structural model based with a resolution of 1.9 Å (*18*). The improved resolution of this model has been combined with biophysical and biochemical insights and has allowed for improved mechanistic models of PSII. The combination of structural and kinetics data makes feasible the application computational methods to modeling the mechanism of PSII.

One of the recent developments in the study of PSII has been the improved use of EPR spectroscopy to monitor the transitions between S-states (*128*). EPR has frequently been used to study PSII, but in this case EPR was used to estimate the miss factors (percentage of failed S-state transitions per actinic flash) for individual S-state transitions. Prior to this experiment, miss factors could only be used to represent the aggregate of failed S-state transitions based on the yield of the S_3 to S_0 transition after several flashes.

This experiment showed that the majority of failed S-state transitions occurred during the S_2 to S_3 transition rather than during the slower and more complex S_3 to S_0 transition (*128*). This was attributed to the lack of back pressure from the product of the water oxidation reaction, O_2, and to the relaxation processes involved in resetting the Mn_4CaO_5 to its ground state (*128*).

Another of the important recent advancements in the study of PSII was an attempt to determine the rate of the exchange of an oxygen atom that form one of the μ-oxo bridges , labeled O(5) (Figure 5.1), in and out of the Mn_4CaO_5 (*129*). This oxygen atom is weakly defined in the x-ray structure compared to the other μ-oxo bridges (*18*) and is suspected that the pair of metal ions connected by this oxygen atom can vary, allowing the Mn_4CaO_5 to adopt multiple configurations for the same S-state (*130*). Models of the S_2 state based on an optimized version of the Shen structure (*18*) show that two iso-energetic forms of the S_2 state were possible (*130*). This provided an explanation for the two distinct EPR spectra associated with the S_2 state, whose ratios vary depending on experimental conditions (*131, 132*). Most importantly O(5) may be the identity of one of the two oxygen atoms that take part in the formation O_2. Some researchers have argued that a μ-oxo bridge linking two manganese would exchangewith solution to slowly to match the known rates of exchange of the two substrate water molecules (*133, 134*). However, this experiment, which studied the binding of O(5) using isotopically labeled water and both EPR and ENDOR techniques, showed that the exchange of O(5) could take place within the established parameters for substrate water(*129*).

Despite the growing body of knowledge pertaining to PSII, there are still significant details regarding the vital proton transfer reactions that remain poorly

understood. This lack of clarity includes uncertainty regarding origin of each of the protons released during the individual S-state transitions and the pathways that allow protons to be efficiently released from the enzyme active site. Given the complexity of these reactions, there are likely many proton transfer/hydrogen bond rearrangement processes that take place during the S-state cycle, given that each S-state transition has a different rate and stoichiometry of proton release and that the protons must be release rapidly and then prevented from returning`. Elucidating these processes will likely play an important role solving the mechanism of water-oxidation in PSII because they are necessary to coordinate the deprotonation of the Mn_4CaO_5 with each of its oxidation reactions. Luckily there are have also been advancements in experimental techniques used to study hydrogen bonds and proton transfer. One example would be the multiple phases of the FTIR signal kinetics that have been assigned to the proton release and the 1747 cm^{-1} FTIR signal assigned to a critical hydrogen bond network that releases protons from PSII (*68*, *135*).

One notable feature of the S_1 to S_2 transition is that unlike the other S-state transitions it does not involve the release of a proton. The quantum efficiency of this reaction is also not sensitive to pH within the range of protein stability and does not of have a kinetic isotope effect using H_2O to D_2O solvent exchange. The reversal of this transition, which would be regarded as any process that reduced the Mn_4CaO_5 to the S_1 state, is sensitive to pH and also displays a kinetic isotope effect. The reverse of the S_1 to S_2 transition is also much more sensitive to temperature than the forward reaction. The apparent contradiction is an overlooked piece of evidence that has not been factored in to current models into the mechanism of the S_1 to S_2 transition. It seems likely that the S_1 to

S_2 transition involves the transfer of a proton through a low energy barrier hydrogen bond similar to the hydrogen bond between Y_Z and His190. This hydrogen bond should then be subject to a structural rearrangement that increases the distance between the hydrogen bond partners thus increasing the energy barrier for proton transfer. Assuming that the reversal of the electron transfer from the Mn_4CaO_5 promotes the re-protonation of the original donor without reforming the low energy barrier hydrogen bond would explain why the reversal of the S_1 to S_2 state transition appears to be constrained by the transfer of protons while the forward reaction does not. The assumption of the presence and subsequent loss of a low energy hydrogen bond in the WOC during this transition could provide an important constraint for distinguishing between various models of the mechanism of water oxidation by the WOC.

One of the recent improvements in modeling the activity of the WOC that is mentioned above is a study that suggests that presence of the chloride ion near the Mn_4CaO_5 prevents D2-Lys317 from forming a salt bridge with D1-Asp61 (*108*). This salt bridge would prevent D1-Asp61 from participating in a hydrogen bond network that includes H_2O molecules ligating Mn(4) in the Mn_4CaO_5 cluster (*125*) (Fig. 3.1) in the high resolution crystal structure (*18*) and presumably adversely affect the ability of PSII to evolve oxygen. This was a significant step in defining the role of the chloride ion in the water-oxidation process. However, the D2-Lys317 to D1-Asp61 salt bridge, which is predicted to occur transiently, may play a positive role in the water-oxidation mechanism during some periods of the process. Without a constructive role in the water oxidation process, D2-Lys317 would be selected against and PSII would have evolved without a requirement for chloride. It seems possible that the D2-Lys317 to D1-Asp61 salt bridge

is part of a trapping mechanism that prevents the return of protons to the Mn_4CaO_5. This hypothesis may play a role a future study which will compare the kinetics of O_2 release from the V185N and D61N mutants under various conditions. These two mutants may also play a role in future experiments intended to track the formation of intermediate states during the S-state cycle. The decreased rates of O_2 release and for the lag phase in these mutants may be critical for making observations using experimental instruments with limited time resolution.

A goal in any study of PSII is to find evidence that will support one competing model of the water-oxidation mechanism over the others. The studies described in this dissertation are by no means definitive on this subject, but do provide at least some support for the nucleophilic attack model (Fig 5.1) over the oxo radical model of O-O bond formation. As discussed in chapter 4, the release of O_2 from D61N is exceptionally slow even in comparison to the V185N mutant, which has similar O_2 release characteristics. Chapter 3 shows that the relationship between this slow rate of O_2 release and the pH or pD of the buffering solution are not straight forward and do not match the relationship observed for the lag phase, which is hypothesized to be attributable to a relatively simple proton release step. This is notable because only in the nucleophilic attack model of O_2 formation does the D1-Asp61 residue interact with the substrate H_2O . While in the other widely accepted model the substrate H_2O is intrinsic to the Mn_4CaO_5 cluster. The other piece of evidence that can be interpreted to support the nucleophilic attack model comes from a publication for which I was credited as a co-author and for which a carried out several experiments. This manuscript demonstrated the importance of the residue CP43-Arg357, which had been postulated to act as a catalytic base in order

to facilitate the later S-state transitions, by showing that mutation of CP43-Arg357 resulted in a large miss factor even when replaced by a similar residue (*85*).

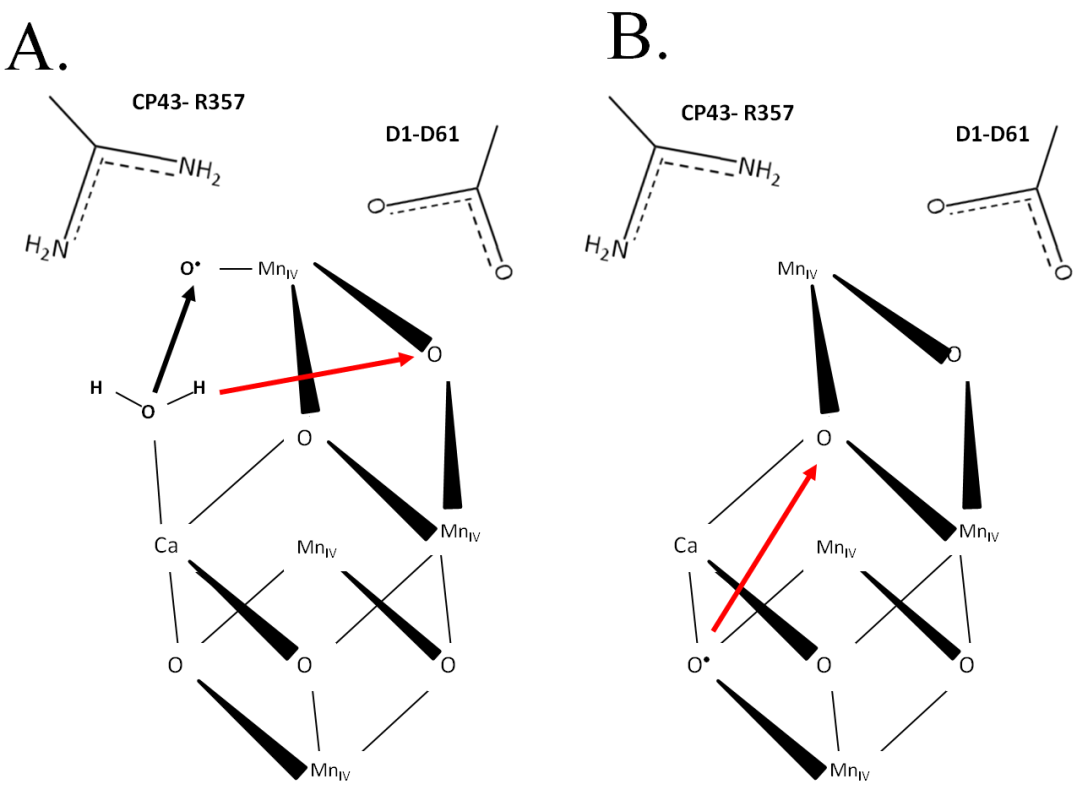

Figure 5.1 Competing models of O-O bond formation. A. One of the more widely accepted models of O_2 formation by the Mn_4CaO_5 cluster is a nucleophilic attach by a calcium bound water onto a deprotonated substrate bound to the dangling manganese ion (Mn4) (*8*, *136*). This basic model has been expanded upon by QM/MM modeling (*73*). B. Another model of O_2 formation involves O-O bond formation between two oxygen atoms that have been incorporated into the structure of the Mn_4CaO_5 cluster as μ-oxo bridges between the manganese and calcium ions in the cluster (*137*). This model, which was developed by DFT calculations, predicts a structure for the S_1 state that is most similar to the most recent and high quality crystallographic studies (*18*).

REFERENCES

1. Nogi, T., and Miki, K. (2001) Structural Basis of Bacterial Photosynthetic Reaction Centers, *Journal of Biochemistry 130*, 319-329.
2. Cogdell, R. J., Isaacs, N. W., Howard, T. D., McLuskey, K., Fraser, N. J., and Prince, S. M. (1999) How Photosynthetic Bacteria Harvest Solar Energy, *Journal of Bacteriology 181*, 3869-3879.
3. Renger, G., and Renger, T. (2008) Photosystem II: The machinery of photosynthetic water splitting, *Photosyn Res 98*, 53-80.
4. Dau, H., and Haumann, M. (2008) The manganese complex of photosystem II in its reaction cycle - Basic framework and possible realization at the atomic level, *Coordination Chem Rev 252*, 273-295.
5. Renger, G., and Kuhn, P. (2007) Reaction pattern and mechanism of light induced oxidative water splitting in photosynthesis, *Biochim Biophys Acta 1767*, 458-471.
6. Kern, J., and Renger, G. (2007) Photosystem II: Structure and mechanism of the water:plastoquinone oxidoreductase, *Photosynth Res 98*, 53-80.
7. Dau, H., and Haumann, M. (2007) Eight steps preceding O-O bond formation in oxygenic photosynthesis--a basic reaction cycle of the Photosystem II manganese complex, *Biochim Biophys Acta 1767*, 472-483.
8. McEvoy, J. P., and Brudvig, G. W. (2006) Water-splitting chemistry of photosystem II, *Chem Rev 106*, 4455-4483.
9. Renger, G. (2004) Coupling of electron and proton transfer in oxidative water cleavage in photosynthesis, *Biochim Biophys Acta 1655*, 195-204.
10. Rutherford, A. W., and Faller, P. (2003) Photosystem II: evolutionary perspectives, *Philos Trans R Soc Lond B Biol Sci 358*, 245-253.
11. Diner, B. A., and Rappaport, F. (2002) Structure, Dynamics, and Energetics of the Primary Photochemistry of Photosystem II of Oxygenic Photosynthesis, *Annu Rev Plant Physiol Plant Mol Biol 53*, 551-580.
12. Vass, I., and Cser, K. (2009) Janus-faced charge recombinations in photosystem II photoinhibition, *Trends Plant Sci 14*, 200-205.
13. Murata, N., Takahashi, S., Nishiyama, Y., and Allakhverdiev, S. I. (2007) Photoinhibition of photosystem II under environmental stress, *Biochim Biophys Acta 1767*, 414-421.
14. Adir, N., Zer, H., Shochat, S., and Ohad, I. (2003) Photoinhibition - A historical perspective, *Photosyn Res 76*, 343-370.
15. Liberton, M., Berg, R. H., Heuser, J., Roth, R., and Pakrasi, H. B. (2006) Ultrastructure of the membrane systems in the unicellular cyanobacterium Synechocystis sp strain PCC 6803, *Protoplasma 227*, 129-138.
16. van de Meene, A. M. L., Hohmann-Marriott, M. F., Vermaas, W. F. J., and Roberson, R. W. (2006) The three-dimensional structure of the cyanobacterium Synechocystis sp PCC 6803, *Archives of Microbiology 184*, 259-270.

17. Rengstl, B., Oster, U., Stengel, A., and Nickelsen, J. (2011) An intermediate membrane subfraction in cyanobacteria is involved in an assembly network for Photosystem II biogenesis, *J Biol Chem 286*, 21944-21951.
18. Umena, Y., Kawakami, K., Shen, J. R., and Kamiya, N. (2011) Crystal structure of oxygen-evolving photosystem II at a resolution of 1.9 Ångstrom, *Nature 473*, 55-U65.
19. Holzwarth, A. R., Muller, M. G., Reus, M., Nowaczyk, M., Sander, J., and Rogner, M. (2006) Kinetics and mechanism of electron transfer in intact photosystem II and in the isolated reaction center: Pheophytin is the primary electron acceptor, *Proc Natl Acad Sci U S A 103*, 6895-6900.
20. Allakhverdiev, S. I., Tomo, T., Shimada, Y., Kindo, H., Nagao, R., Klimov, V. V., and Mimuro, M. (2010) Redox potential of pheophytin a in photosystem II of two cyanobacteria having the different special pair chlorophylls, *Proceedings of the National Academy of Sciences 107*, 3924-3929.
21. Kato, Y., Sugiura, M., Oda, A., and Watanabe, T. (2009) Spectroelectrochemical determination of the redox potential of pheophytin a, the primary electron acceptor in photosystem II, *Proceedings of the National Academy of Sciences 106*, 17365-17370.
22. Allakhverdiev, S. I., Tsuchiya, T., Watabe, K., Kojima, A., Los, D. A., Tomo, T., Klimov, V. V., and Mimuro, M. (2011) Redox potentials of primary electron acceptor quinone molecule (QA)âˆ’ and conserved energetics of photosystem II in cyanobacteria with chlorophyll a and chlorophyll d, *Proceedings of the National Academy of Sciences 108*, 8054-8058.
23. Boussac, A., and Etienne, A. L. (1984) Midpoint potential of singal-II (slow) in Tris-washed photosystem II particles, *Biochim Biophys Acta 766*, 576-581.
24. Babcock, G. T., Barry, B. A., Debus, R. J., Hoganson, C. W., Atamian, M., McIntosh, L., Sitole, I., and Yocum, C. F. (1989) Water oxidation in photosystem II: From radical chemistry to multielectron chemistry., *Biochemistry 28*, 9557-9565.
25. Rutherford, A. W., Mullet, J. E., and Crofts, A. R. (1981) Measurement of the midpoint potential of the pheophytin acceptor of photosystem II, *Febs Letters 123*, 235-237.
26. Rappaport, F., Guergova-Kuras, M., Nixon, P. J., Diner, B. A., and Lavergne, J. (2002) Kinetics and Pathways of Charge Recombination in Photosystem II, *Biochemistry 41*, 8518-8527.
27. Forbush, B., Kok, B., and McGloin, M. P. (1971) Cooperation of charges in photosynthetic O_2 evolution: II Damping of flash yield oscillation, deactivation., *Photochem Photobiol 14*, 307-321.
28. Kok, B., Forbush, B., and McGloin, M. (1970) Cooperation of charges in photosynthetic oxygen evolution: I. A linear four step mechanism., *Photochem Photobiol 11*, 457-475.
29. Joliot, P., Barbieri, G., and Chabaud, R. (1969) Un nouveau modele des centres photochimique du systeme II., *Photochem Photobiol 10*, 309-329.
30. Goussias, C., Boussac, A., and Rutherford, A. W. (2002) Photosystem II and photosynthetic oxidation of water: an overview, *Philos Trans R Soc Lond B Biol Sci 357*, 1369-1381.
31. Hillier, W., and Messinger, J. (2005) Mechanism of photosynthetic oxygen production., in *Photosystem II: The Light-Driven Water:Plastoquinone Oxidoreductase* (Wydrzynski, T., and Satoh, K., Eds.), pp 567-608, Springer, Dordrecht, The Netherlands.
32. Sauer, K., Yano, J., and Yachandra, V. K. (2005) X-ray spectroscopy of the Mn4Ca cluster in the water-oxidation complex of Photosystem II, *Photosynth Res 85*, 73-86.
33. Krishtalik, L. I. (1986) Energetics of Multielectron Reactions - Photosynthetic Oxygen Evolution, *Biochim Biophys Acta 849*, 162-171.

34. Gerencser, L., and Dau, H. (2010) Water oxidation by photosystem II: H_2O-D_2O exchange and the influence of pH support formation of an intermediate by removal of a proton before dioxygen creation, *Biochemistry 49*, 10098-10106.
35. Styring, S., and Rutherford, A. W. (1987) In the oxygen evolving complex of photosystem II the S_0 state is oxidized to the S_1-state by D^+ (Signal II-Slow), *Biochemistry 26*, 2401-2405.
36. Bernat, G., Morvaridi, F., Feyziyev, Y., and Styring, S. (2002) pH dependence of the four individual transitions in the catalytic S- cycle during photosynthetic oxygen evolution, *Biochemistry 41*, 5830-5843.
37. Suzuki, H., Sugiura, M., and Noguchi, T. (2005) pH Dependence of the Flash-Induced S-State Transitions in the Oxygen-Evolving Center of Photosystem II from Thermosynechoccocus elongatus as Revealed by Fourier Transform Infrared Spectroscopyâ€ *Biochemistry 44*, 1708-1718.
38. Styring, S., and Rutherford, A. W. (1988) Deactivation kinetics and temperature dependence of the S-state transition in the oxygen evolving system of Photosystem II measured by electron paramagnetic-res spectroscopy, *Biochim Biophys Acta 933*, 378-387.
39. Messinger, J., and Renger, G. (1994) Analyses of pH induced modifications of the period four oscillation of flash induced oxygen evolution reveal distinct structural changes of the photosystem II donor side at characteristic pH values, *Biochemistry 33*, 10896 10905.
40. Saito, K., Shen, J.-R., Ishida, T., and Ishikita, H. (2011) Short Hydrogen Bond between Redox-Active Tyrosine YZ and D1-His190 in the Photosystem II Crystal Structure, *Biochemistry 50*, 9836-9844.
41. Haumann, M., Hundelt, M., Jahns, P., Chroni, S., Bogershausen, O., Ghanotakis, D., and Junge, W. (1997) Proton release from water oxidation by photosystem II: similar stoichiometries are stabilized in thylakoids and PSII core particles by glycerol, *FEBS Lett 410*, 243-248.
42. Jahns, P., Lavergne, J., Rappaport, F., and Junge, W. (1991) Stoichiometry of proton release during photosynthetic water oxidation a reinterpretation of the responses of neutral red leads to a non-integer pattern, *Biochim Biophys Acta 1057*, 313-319.
43. Schlodder, E., and Witt, H. T. (1999) Stoichiometry of Proton Release from the Catalytic Center in Photosynthetic Water Oxidation, *J Biol Chem 274*, 30387-30392.
44. Rappaport, F., and Lavergne, J. (1991) Proton release during successive oxidation steps of the photosynthetic water oxidation process: Stoichiometries and pH-dependence, *Biochemistry 30*, 10004-10012.
45. Suzuki, H., Sugiura, M., and Noguchi, T. (2009) Monitoring proton release during photosynthetic water oxidation in Photosystem II by means of isotope-edited infrared spectroscopy, *J Amer Chem Soc 131*, 7849-7857.
46. Haumann, M., Muller, C., Liebisch, P., Iuzzolino, L., Dittmer, J., Grabolle, M., Neisius, T., Meyer-Klaucke, W., and Dau, H. (2005) Structural and oxidation state changes of the photosystem II manganese complex in four transitions of the water oxidation cycle (S-0 -> S-1, S-1 -> S-2, S-2 -> S-3, and S-3,S-4 -> S-0) Characterized by X-ray absorption spectroscopy at 20 K and room temperature, *Biochemistry 44*, 1894-1908.
47. Dekker, J. P., Ghanotakis, D. F., Plijter, J. J., Van, G. H. J., and Babcock, G. T. (1984) Kinetics of the oxygen-evolving complex in salt-washed photosystem II preparations., *Biochim Biophys Acta 767*, 515-523.

48. Hundelt, M., Hays, A. M., Debus, R. J., and Junge, W. (1998) Oxygenic photosystem II: the mutation D1-D61N in *Synechocystis* sp. PCC 6803 retards S-state transitions without affecting electron transfer from Y_Z to $P680^+$, *Biochemistry 37*, 14450-14456.
49. Ono, T. A., Noguchi, T., Inoue, Y., Kusunoki, M., Matsushita, T., and Oyanagi, H. (1992) X-ray detection of the period-four cycling of the manganese cluster in photosynthetic water oxidizing enzyme, *Science (Washington D C). 258*, 1335-1337.
50. Dau, H., and Haumann, M. (2007) Time-resolved X-ray spectroscopy leads to an extension of the classical S-state cycle model of photosynthetic oxygen evolution, *Photosynth Res 92*, 327-343.
51. Iuzzolino, L., Dittmer, J., Dorner, W., Meyer-Klaucke, W., and Dau, H. (1998) X-ray absorption spectroscopy on layered photosystem II membrane particles suggests manganese-centered oxidation of the oxygen-evolving complex for the S0-S1, S1-S2, and S2-S3 transitions of the water oxidation cycle [In Process Citation], *Biochemistry 37*, 17112-17119.
52. Dau, H., Liebisch, P., and Haumann, M. (2003) X-ray absorption spectroscopy to analyze nuclear geometry and electronic structure of biological metal centers--potential and questions examined with special focus on the tetra-nuclear manganese complex of oxygenic photosynthesis, *Anal Bioanal Chem 376*, 562-583.
53. Rappaport, F., Lavergne, J., and Blanchard-Desce, M. (1994) Kinetics of electron transfer and electrochromic change during the redox transitions of the photosynthetic oxygen-evolving complex, *Biochim Biophys Acta 1184*, 178-192.
54. Junge, W., Haumann, M., Ahlbrink, R., Mulkidjanian, A., and Clausen, J. r. (2002) Electrostatics and proton transfer in photosynthetic water oxidation, *Philosophical Transactions Of The Royal Society Of London. Series B, Biological Sciences 357*, 1407-1417.
55. Razeghifard, M. R., and Pace, R. J. (1999) EPR kinetic studies of oxygen release in thylakoids and PSII membranes: a kinetic intermediate in the S_3 to S_0 transition, *Biochemistry 38*, 1252-1257.
56. Clausen, J., Debus, R. J., and Junge, W. (2004) Time-resolved oxygen production by PSII: Chasing chemical intermediates, *Biochim Biophys Acta 1655*, 184-194.
57. Haumann, M., Liebisch, P., Muller, C., Barra, M., Grabolle, M., and Dau, H. (2005) Photosynthetic O-2 formation tracked by time-resolved X-ray experiments, *Science 310*, 1019-1021.
58. Hillier, W., and Wydrzynski, T. (2004) Substrate water interactions within the Photosystem II oxygen evolving complex, *Phys Chem Chem Phys 6*, 4882-4889.
59. Haumann, M., Grundmeier, A., Zaharieva, I., and Dau, H. (2008) Photosynthetic water oxidation at elevated dioxygen partial pressure monitored by time-resolved X-ray absorption measurements, *Proceedings of the National Academy of Sciences 105*, 17384-17389.
60. Shevela, D., Beckmann, K., Clausen, J. r., Junge, W., and Messinger, J. (2011) Membrane-inlet mass spectrometry reveals a high driving force for oxygen production by photosystem II, *Proceedings of the National Academy of Sciences 108*, 3602-3607.
61. Ferreira, K. N., Iverson, T. M., Maghlaoui, K., Barber, J., and Iwata, S. (2004) Architecture of the photosynthetic oxygen-evolving center, *Science 303*, 1831-1838.
62. Loll, B., Kern, J., Saenger, W., Zouni, A., and Biesiadka, J. (2005) Towards complete cofactor arrangement in the 3.0 Å resolution structure of photosystem II, *Nature 438*, 1040-1044.

63. Ishikita, H., Saenger, W., Loll, B., Biesiadka, J., and Knapp, E. W. (2006) Energetics of a possible proton exit pathway for water oxidation in photosystem II, *Biochemistry 45*, 2063-2071.
64. Murray, J. W., and Barber, J. (2007) Structural characteristics of channels and pathways in photosystem II including the identification of an oxygen channel, *J Struct Biol 159*, 228-237.
65. Ho, F. M., and Styring, S. (2008) Access channels and methanol binding site to the $CaMn_4$ cluster in Photosystem II based on solvent accessibility simulations, with implications for substrate water access, *Biochim Biophys Acta 1777*, 140-153.
66. Vassiliev, S., Comte, P., Mahboob, A., and Bruce, D. (2010) Tracking the flow of water through photosystem II using molecular dynamics and streamline tracing, *Biochemistry 49*, 1873-1881.
67. Vassiliev, S., Zaraiskaya, T., and Bruce, D. (2012) Exploring the energetics of water permeation in photosystem II by multiple steered molecular dynamics simulations, *Biochim Biophys Acta 1817*, 1671-1678.
68. Service, R. J., Hillier, W., and Debus, R. J. (2010) Evidence from FTIR difference spectroscopy of an extensive network of hydrogen bonds near the oxygen-evolving $Mn_{(4)}Ca$ cluster of photosystem II involving D1-Glu65, D2-Glu312, and D1-Glu329, *Biochemistry 49*, 6655-6669.
69. Haumann, M., and Junge, W. (1994) Extent and rate of proton release by photosynthetic water oxidation in thylakoids - Electrostatic relaxation versus chemical production, *Biochemistry 33*, 864-872.
70. Lubbers, K., Haumann, M., and Junge, W. (1993) Photosynthetic water oxidation under flashing light. Oxygen release, proton release, and absorption transients in the near ultraviolet- a comparison between thylakoids and a reaction center preparation, *Biochim Biophys Acta 1183*, 210-214.
71. Ahlbrink, R., Haumann, M., Cherepanov, D., Bogershausen, O., Mulkidjanian, A., and Junge, W. (1998) Function of tyrosine Z in water oxidation by photosystem II: electrostatical promotor instead of hydrogen abstractor, *Biochemistry 37*, 1131-1142.
72. Ishikita, H., and Knapp, E. W. (2006) Function of redox-active tyrosine in photosystem II, *Biophysical Journal 90*, 3886-3896.
73. Sproviero, E. M., Gascon, J. A., McEvoy, J. P., Brudvig, G. W., and Batista, V. S. (2008) Quantum mechanics/molecular mechanics study of the catalytic cycle of water splitting in photosystem II, *J Am Chem Soc 130*, 3428-3442.
74. Harms, M. J., Schlessman, J. L., Sue, G. R., and GarcÃ-a-Moreno E., B. Arginine residues at internal positions in a protein are always charged, *Proceedings of the National Academy of Sciences 108*, 18954-18959.
75. Hundelt, M., Hays, A. M. A., Debus, R. J., and Junge, W. (1998) The mutation D1-D61N in PS II of *Synechocystis*: Retardation of ET from OEC->Y_z^{ox} and no effect on Y_z->$P680^+$, in *Photosynthesis: Mechanisms and Effects* (Garab, G., Ed.), pp 1387-1390, Kluwer Academic Publishers, Netherlands.
76. Chu, H. A., Nguyen, A. P., and Debus, R. J. (1995) Amino acid residues that influence the binding of manganese or calcium to photosystem II. 1. The lumenal interhelical domains of the D1 polypeptide, *Biochemistry 34*, 5839-5858.
77. Debus, R. J., Campbell, K. A., Gregor, W., Li, Z. L., Burnap, R. L., and Britt, R. D. (2001) Does histidine 332 of the D1 polypeptide ligate the manganese cluster in photosystem II? An electron spin echo envelope modulation study, *Biochemistry 40*, 3690-3699.

78. Williams, J. G. K. (1988) Construction of specific mutations in Photosystem II photosynthetic reaction center by genetic engineering methods in *Synechocystis* 6803., *Methods in Enzymology 167*, 766-778.
79. Burnap, R. L., Qian, M., and Pierce, C. (1996) The manganese-stabilizing protein (MSP) of photosystem II modifies the in vivo deactivation and photoactivation kinetics of the H2O-oxidation complex in Synechocystis sp. PCC6803, *Biochemistry 35*, 874-882.
80. Meunier, P. C., Burnap, R. L., and Sherman, L. A. (1995) Modelling of the S-state mechanism and Photosystem II manganese photoactivation in cyanobacteria, *Photosyn Res 47*, 61-76.
81. Qian, M., Dao, L., Debus, R. J., and Burnap, R. L. (1999) Impact of mutations within the putative Ca^{2+}-binding lumenal interhelical a-b loop of the photosystem II D1 protein on the kinetics of photoactivation and H_2O-oxidation in *Synechocystis* sp. PCC6803, *Biochemistry 38*, 6070-6081.
82. Nixon, P. J., and Diner, B. A. (1992) Aspartate 170 of the photosystem II reaction center polypeptide D1 is involved in the assembly of the oxygen evolving manganese cluster, *Biochemistry 31*, 942 948.
83. Lavorel, J. (1976) Matrix analysis of the oxygen evolving system of photosynthesis., *J. Theor. Biol 57*, 171-185.
84. Bouges-Bocquet, B. (1973) Limiting steps in photosystem II and water decomposition in Chlorella and spinach chloroplasts, *Biochim Biophys Acta 292*, 772-785.
85. Hwang, H. J., Dilbeck, P., Debus, R. J., and Burnap, R. L. (2007) Mutation of arginine 357 of the CP43 protein of photosystem II severely impairs the catalytic S-state cycle of the H2O oxidation complex, *Biochemistry 46*, 11987-11997.
86. Allahverdiyeva, Y., Deak, Z., Szilard, A., Diner, B. A., Nixon, P. J., and Vass, I. (2004) The function of D1-H332 in Photosystem II electron transport studied by thermoluminescence and chlorophyll fluorescence in site-directed mutants of Synechocystis 6803, *Eur J Biochem 271*, 3523-3532.
87. Chu, H.-A., Nguyen, A. P., and Debus, R. A. (1994) Site-directed mutagenesis of photosynthetic oxygen evolution: Instability or inefficient assembly of the manganese cluster in vivo., *Biochemistry 33*, 6137-6149.
88. Diner, B. A., and Nixon, P. J. (1992) The rate of reduction of oxidized redox-active tyrosine, Z^+, by exogenous Mn^{2+} Is slowed in a site-directed mutant, at aspartate 170 of polypeptide D1 of photosystem II, inactive for photosynthetic oxygen evolution, *Biochim Biophys Acta 1101*, 134-138.
89. McEvoy, J. P., and Brudvig, G. W. (2004) Structure-based mechanism of photosynthetic water oxidation, *Phys Chem Chem Phys 6*, 4754-4763.
90. Meunier, P. C. (1993) Oxygen evolution by photosystem II: The contribution of backward transitions to the anomalous behaviour of double-hits revealed by a new analysis method., *Photosyn Res 36*, 111-118.
91. Tu, C. K., Silverman, D. N., Forsman, C., Jonsson, B. H., and Lindskog, S. (1989) Role of histidine 64 in the catalytic mechanism of human carbonic anhydrase II studied with a site-specific mutant, *Biochemistry 28*, 7913-7918.
92. Jackman, J. E., Merz, K. M., Jr., and Fierke, C. A. (1996) Disruption of the active site solvent network in carbonic anhydrase II decreases the efficiency of proton transfer, *Biochemistry 35*, 16421-16428.
93. Christen, G., and Renger, G. (1999) The role of hydrogen bonds for the multiphasic $P680^{+*}$ reduction by Y_Z in photosystem II with intact oxyen evolution capacity. Analysis of kinetic H/D isotope exchange effects, *Biochemistry 38*, 2068-2077.

94. Hyman, H. H., Kaganove, A., and Katz, J. J. (1960) The basicity of amino acids in D_2O, *The Journal of Physical Chemistry 64*, 1653-1655.
95. Bell, R. P. (1973) *The Proton in Chemistry*, 2d ed., Chapman and Hall, London,.
96. Burnap, R., Koike, H., Sotiropoulou, G., Sherman, L. A., and Inoue, Y. (1989) Oxygen evolving membranes and particles from the transformable cyanobacterium *Synechocystis* sp. PCC6803., *Photosynth. Res. 22*, 123-130.
97. Burnap, R., Shen, J. R., Jursinic, P. A., Inoue, Y., and Sherman, L. A. (1992) Oxygen yield and thermoluminescence characteristics of a cyanobacterium lacking the manganese-stabilizing protein of photosystem II, *Biochemistry 31*, 7404-7410.
98. Joliot, P. (1966) L'émission d'oxygène par des algues soumises à un eclairement, *Journal De Chimie Physique 63*, 1423-1441.
99. Meunier, P. C., and Popovic, R. (1991) The time for oxygen release in photosynthesis: Reconciliation of flash polarography with other measurement techniques., *Photosyth. Res. 28*, 33-39.
100. Sinclair, J., and Arnason, T. (1974) Studies on a thermal reaction associated with photosynthetic oxygen evolution, *Biochim Biophys Acta 368*, 393-400.
101. Lavorel, J. (1992) Determination of the photosynthetic oxygen release time by amperometry, *Biochim Biophys Acta 1101*, 33-40.
102. Plijter, J. J., Aalbers, S. E., Barends, J. P. F., Vos, M. H., and Vangorkom, H. J. (1988) Oxygen Release May Limit the Rate of Photosynthetic Electron-Transport - the Use of a Weakly Polarized Oxygen Cathode, *Biochim Biophys Acta 935*, 299-311.
103. Christen, G., Seeliger, A., and Renger, G. (1999) P680(+)* reduction kinetics and redox transition probability of the water oxidizing complex as a function of pH and H/D isotope exchange in spinach thylakoids, *Biochemistry 38*, 6082-6092.
104. Haumann, M., Bogershausen, O., Cherepanov, D., Ahlbrink, R., and Junge, W. (1997) Photosynthetic oxygen evolution: H/D isotope effects and the coupling between electron and proton transfer during the redox reactions at the oxidizing side of Photosystem II, *Photosyn Res 51*, 193-208.
105. Babcock, G. T., Blankenship, R. E., and Sauer, K. (1975) The rapid component of electron paramagnetic resonance signal II: A candidate for the physiological donor to photosystem II in spinach chloroplasts., *Biochim Biophys Acta 376*, 329-344.
106. Razeghifard, M. R., Wydrzynski, T., Pace, R. J., and Burnap, R. L. (1997) $Yz^{\cdot}$ reduction kinetics in the absence of the manganese-stabilizing protein of photosystem II, *Biochemistry 36*, 14474-14478.
107. Diner, B. (1973) The turnover times of photosynthesis and redox properties of the pool of electron carriers between the photosystems., *Biochim Biophys Acta 305*, 353-363.
108. Rivalta, I., Amin, M., Luber, S., Vassiliev, S., Pokhrel, R., Umena, Y., Kawakami, K., Shen, J. R., Kamiya, N., Bruce, D., Brudvig, G. W., Gunner, M. R., and Batista, V. S. (2011) Structural-functional role of chloride in photosystem II, *Biochemistry 50*, 6312-6315.
109. Koike, H., Hanssum, B., Inoue, Y., and Renger, G. (1987) Temperature dependence of the S-state transitions in a thermophilic cyanobacterium, *Synechococcus vulcanus* Copeland measured by absorption changes in the ultraviolet region., *Biochim Biophys Acta 893*, 524.
110. Rivalta, I., Amin, M., Luber, S., Vassiliev, S., Pokhrel, R., Umena, Y., Kawakami, K., Shen, J. R., Kamiya, N., Bruce, D., Brudvig, G. W., Gunner, M. R., and Batista, V. S. Structural-Functional Role of Chloride in Photosystem II, *Biochemistry 50*, 6312-6315.

111. Harms, M. J., Schlessman, J. L., Sue, G. R., and García-Moreno E., B. (2011) Arginine residues at internal positions in a protein are always charged, *Proceedings of the National Academy of Sciences 108*, 18954-18959.
112. Garczarek, F., Brown, L. S., Lanyi, J. K., and Gerwert, K. (2005) Proton binding within a membrane protein by a protonated water cluster, *Proc Natl Acad Sci U S A 102*, 3633-3638.
113. Freier, E., Wolf, S., and Gerwert, K. (2011) Proton transfer via a transient linear water-molecule chain in a membrane protein, *Proceedings of the National Academy of Sciences 108*, 11435-11439.
114. Hays, A. M., Vassiliev, I. R., Golbeck, J. H., and Debus, R. J. (1998) Role of D1-His190 in proton-coupled electron transfer reactions in photosystem II: a chemical complementation study, *Biochemistry 37*, 11352-11365.
115. Hays, A. M., Vassiliev, I. R., Golbeck, J. H., and Debus, R. J. (1999) Role of D1-His190 in the proton-coupled oxidation of tyrosine Y_Z in manganese-depleted photosystem II, *Biochemistry 38*, 11851-11865.
116. Rappaport, F., and Lavergne, J. (1997) Charge recombination and proton transfer in manganese depleted photosystem II, *Biochemistry 36*, 15294 15302.
117. Kamiya, N., and Shen, J. R. (2003) Crystal structure of oxygen-evolving photosystem II from Thermosynechococcus vulcanus at 3.7-Å resolution, *Proc Natl Acad Sci U S A 100*, 98-103.
118. Zouni, A., Witt, H. T., Kern, J., Fromme, P., Krauss, N., Saenger, W., and Orth, P. (2001) Crystal structure of photosystem II from *Synechococcus elongatus* at 3.8 Å resolution, *Nature 409*, 739-743.
119. Petrek, M., Otyepka, M., Banas, P., Kosinova, P., Koca, J., and Damborsky, J. (2006) CAVER: a new tool to explore routes from protein clefts, pockets and cavities, *Bmc Bioinformatics 7*.
120. Chu, H.-A., Nguyen, A. P., and Debus, R. A. (1994) Site-directed mutagenesis of photosynthetic oxygen evolution: Increased binding or photooxidation of manganese in the absence of the extrinsic 33-kDa polypeptide in vivo., *Biochemistry 33*, 6150-6157.
121. Chu, H. A., Nguyen, A. P., and Debus, R. J. (1995) Amino acid residues that influence the binding of manganese or calcium to photosystem II. 2. The carboxy terminal domain of the D1 polypeptide, *Biochemistry 3496*, 5859-5882.
122. Dilbeck, P. L., Hwang, H. J., Zaharieva, I., Gerencser, L., Dau, H., and Burnap, R. L. (2012) The D1-D61N Mutation in *Synechocystis* sp PCC 6803 Allows the Observation of pH-Sensitive Intermediates in the Formation and Release of O-2 from Photosystem II, *Biochemistry 51*, 1079-1091.
123. Jursinic, P. A., and Dennenberg, R. J. (1990) Oxygen release time in leaf discs and thylakoids of peas and Photosystem II membrane fragments of Spinach., *Biochim Biophys Acta 1020*, 195-206.
124. Boussac, A., Ishida, N., Sugiura, M., and Rappaport, F. (2012) Probing the role of chloride in Photosystem II from *Thermosynechococcus elongatus* by exchanging chloride for iodide, *Biochimica et Biophysica Acta (BBA) - Bioenergetics 1817*, 802-810.
125. Kawakami, K., Umena, Y., Kamiya, N., and Shen, J. R. (2011) Structure of the catalytic, inorganic core of oxygen-evolving photosystem II at 1.9 A resolution, *Journal of photochemistry and photobiology. B, Biology 104*, 9-18.
126. Wincencjusz, H., Yocum, C. F., and van Gorkom, H. J. (1999) Activating anions that replace Cl- in the O2-evolving complex of photosystem II slow the kinetics of the

terminal step in water oxidation and destabilize the S2 and S3 states, *Biochemistry 38*, 3719-3725.

127. Siegbahn, P. E. M. (2012) Mechanisms for proton release during water oxidation in the S_{-2} to S_{-3} and S_{-3} to S_{-4} transitions in photosystem II, *Phys Chem Chem Phys 14*, 4849-4856.
128. Han, G., Mamedov, F., and Styring, S. r. (2012) Misses during Water Oxidation in Photosystem II Are S State-dependent, *J Biol Chem 287*, 13422-13429.
129. Rapatskiy, L., Cox, N., Savitsky, A., Ames, W. M., Sander, J., Nowaczyk, M. M., RÃ¶gner, M., Boussac, A., Neese, F., Messinger, J., and Lubitz, W. (2012) Detection of the Water-Binding Sites of the Oxygen-Evolving Complex of Photosystem II Using W-Band 17O Electronâ€“Electron Double Resonance-Detected NMR Spectroscopy, *J Amer Chem Soc 134*, 16619-16634.
130. Pantazis, D. A., Ames, W., Cox, N., Lubitz, W., and Neese, F. Two Interconvertible Structures that Explain the Spectroscopic Properties of the Oxygen-Evolving Complex of Photosystem II in the S2 State, *Angewandte Chemie International Edition 51*, 9935-9940.
131. Boussac, A., Kuhl, H., Un, S., Rogner, M., and Rutherford, A. W. (1998) Effect of near-infrared light on the S2-state of the manganese complex of photosystem II from Synechococcus elongatus, *Biochemistry 37*, 8995-9000.
132. Peloquin, J. M., and Britt, R. D. (2001) EPR/ENDOR characterization of the physical and electronic structure of the OEC Mn cluster, *Biochim Biophys Acta 1503*, 96-111.
133. Tagore, R., Chen, H., Zhang, H., Crabtree, R. H., and Brudvig, G. W. (2007) Homogeneous water oxidation by a di-Î¼-oxo dimanganese complex in the presence of Ce4+, *Inorganica Chimica Acta 360*, 2983-2989.
134. Hillier, W., Messinger, J., and Wydrzynski, T. (1998) Kinetic determination of the fast exchanging substrate water molecule in the S3 state of photosystem II, *Biochemistry 37*, 16908-16914.
135. Noguchi, T., Suzuki, H., Tsuno, M., Sugiura, M., and Kato, C. (2012) Time-resolved infrared detection of the proton and protein dynamics during photosynthetic oxygen evolution, *Biochemistry 51*, 3205-3214.
136. Dau, H., Iuzzolino, L., and Dittmer, J. (2001) The tetra-manganese complex of photosystem II during its redox cycle - X-ray absorption results and mechanistic implications, *Biochim Biophys Acta 1503*, 24-39.
137. Siegbahn, P. E. M., and Blomberg, M. R. A. (2009) A combined picture from theory and experiments on water oxidation, oxygen reduction and proton pumping, *Dalton Transactions*, 5832-5840.

APPPENDICES

Appendix A.1 Mathematical model of the O_2 electrode signal.

The model used for fitting the O_2 release curves divides the volume of the deposited PSII sample and the buffer above it into layers (Δx, layer thickness) and calculates the concentration of O_2 in each layer. Three processes are considered by the model:

1. O_2 diffusion – in the whole volume (all layers)
2. O_2 production from PSII – only in the layers containing PSII
3. O_2 consumption from the electrode – only in the lowest PSII-containing layer, which is in contact with the electrode surface.

The three processes are described by a mathematical model and the differential equations are solved by numerical integration. The physical basis of the model is the (one-dimensional) diffusion equation (for O_2 diffusion) with source and sink terms describing O_2 production by PSII and O_2 consumption by the electrode, respectively.

The magnitude of the O_2 signal is proportional to the oxygen consumption by the electrode, that is:

$$\Delta[O_2]_x^t = -R_{el} \cdot [O_2]_x^{t-\Delta t} \cdot \Delta x$$

(Equation A1)

The O_2 concentration at the electrode surface is obtained using the following equation (D represents the value of the O_2 diffusion constant; the meaning of other parameters is explained in the main manuscript):

$$[\mathbf{O_2}]_{x=0}^{t} = [\mathbf{O_2}]_{x=0}^{t-\Delta t} + \left[\left([\mathbf{O_2}]_{x=1}^{t-\Delta t} - [\mathbf{O_2}]_{x=0}^{t-\Delta t}\right)\right] \cdot \left(\frac{\boldsymbol{D}}{\Delta \boldsymbol{x}}\right)^2$$

$$\cdot \Delta \boldsymbol{t} + \frac{\boldsymbol{k_1 \cdot k_2}}{\boldsymbol{k_1 - k_2}} \cdot \left[\boldsymbol{S_3^0}\right] \cdot \left(\boldsymbol{e}^{-\boldsymbol{k_2}(\boldsymbol{t}-\boldsymbol{t_{lag}})} - \boldsymbol{e}^{-\boldsymbol{k_1}(\boldsymbol{t}-\boldsymbol{t_{lag}})}\right)$$

$$\cdot \Delta \boldsymbol{t} - \boldsymbol{R_{el}} \cdot [\mathbf{O_2}]_{x=0}^{t-\Delta t} \cdot \Delta \boldsymbol{x}$$

(Equation A2)

For simulation of the diffusion within the sample compartment, the sink term is dropped and the diffusion between the (virtual) layers is simulated according to:

$$[O_2]_x^t = [O_2]_x^{t-\Delta t} + \left[\left([O_2]_{x-\Delta x}^{t-\Delta t} - [O_2]_x^{t-\Delta t}\right) + \left([O_2]_{x+\Delta x}^{t-\Delta t} - [O_2]_x^{t-\Delta t}\right)\right] \cdot \left(\frac{D}{\Delta x}\right)^2 \cdot \Delta t$$

(Equation A3)

Equation A3 is applicable directly to the buffer space, that is the volume containg the aequeous buffer but no photosystems. In the PSII-containing volume, Equ. A3 is complemented by a source term that is identical to the one given in the second line of Equ. A2.

The numercial integration starts a $t = 0$ with $[O_2]_x$ being zero in all layers (for all values of x). Discrete values of t are used with the step width being equal to Δt. Typical parameter values are given in Table A1.1.

A.1.1 Determination of error in O_2 release fits.

To determine the error present in each of $t_{1/2}$'s derived from the mathematical model described above, the fit for each O_2 release trace was repeated multiple times using an automated version of the same program used to perform the original fits. For these fits the value for either $1/k_1$ or $1/k_2$ was incrementally modified through a range of values above and below the originally determined value. The other parameters of the model were allowed to vary for each fit, with the exceptions of the lag corresponding to the flash artifact which was set at 400 μsec and the thickness of the thylakoid membrane layer, which should fit within a narrow range of realistic values (these three parameters were fixed to the valued originally obtained for each O_2 release trace). The fixed values for $1/k_1$ or $1/k_2$ were plotted against a sum of squares deviation between the experimental trace and the fit. This results in a parabola with the original value at the minimum. These parabolas were used to determine what deviation from the original value is required to double the sum of squares deviation of the fit. The resulting values were reported as the error bars (after multiplying by ln2) in Figure 3.7, and were found to be commensurate with the values of standard deviations obtained from the subset of the measurements for which measurements from three

individual samples were available and three corresponding independent fits were made to the separate samples (not shown).

	Parameter	wild-type PSII	D61N mutant
Electrode system	R_{Elec} [ms^{-1}]	7.2	7.2*
Electrode system	d_{PSII} [µm]	10.8	9.5
PSII	τ_{lag} [ms]	0.55	.65
PSII	τ_1 [ms]	0.66	0.7
PSII	$\tau_1+\tau_{lag}$ [ms]	1.2	1.35
PSII, estimated delay in O_2 evolution	$\tau_1+\tau_{lag}-\tau_{elec}$ [#] [ms]	0.25[#]	0.40[#]
PSII, time constant of O_2 evolution	$\tau_2 = \tau_{ox}$ [ms]	1.6	30.9

Table A.1.1 Simulation parameters of the O_2 transients shown in Fig. 3.6

*Values obtained by curve-fitting for the WT and kept constant in the simulation of the O_2 transients of the D61N mutant.

[#]Based on the results of time-resolved X-ray absorption experiments on PSII particles of spinach, we assume that in PSII, the onset of oxygen formation is delayed by about 250 µs. Consequently we estimate that the electrode response contributes by about 0.95 ms to the delay in the rise of the O_2-signal. The given values are obtained by correcting for the electrode delay of 0.95 ms.

Further parameters were used in the simulations of both time courses. Their value is largely uncritical with respect to determination of the time constants.

O_2 diffusion coefficient: D = 2.2 $\mu m^2/ms$

Integration-time interval, dt = 40 µs

Thickness of sample layer on the electrode surface: d_{PSII}, estimated during the numberical fitting along with the other fit parameters such as R_{Elec} and τ_1.

Layer-width: dx = 0.5 µm

Data range for calculation of the error sum: 1.5-55 ms (WT) and 1.5-170 ms (D61N). We note that variation of the lower or upper limit of the respective time range by +/-30% hardly affects the values of the resulting time constants.

Appendix A.2 Additional UV absorption and double flash polarography figures.

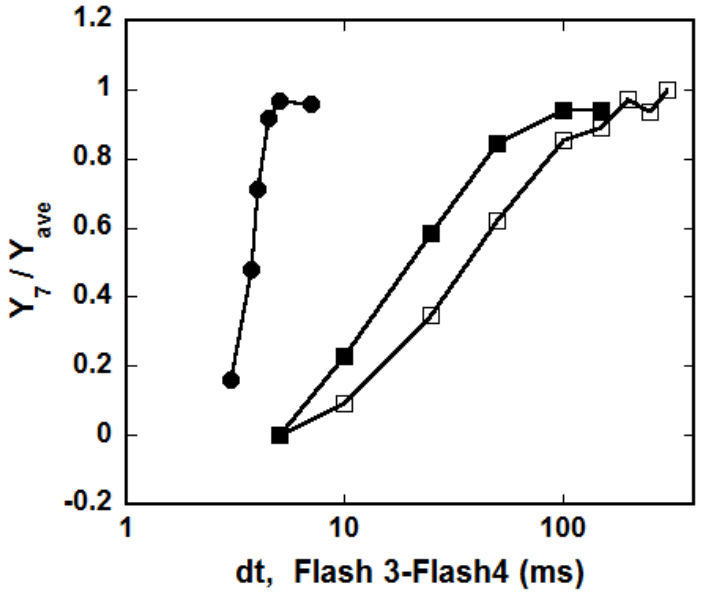

Figure A.2.1 **Double flash polarography**. D1-D61N and wild type thylakoid membranes (2 µg) were exposed to a series of flashes from a red LED. The time interval between third and fourth flashes was adjusted from 1 to 350 ms and the relative yield of the seventh flash from each measurement was recorded in order to estimate the rate of the S_3-S_0 transition which takes place after the third flash. The $t_{1/2}$ of PSII turnover in the S_3-S_0 transition of the D1-D61N membranes is 31 ms in 10 mM NaCl (open square) and 22 ms in 200 mM NaCl (closed square). The $t_{1/2}$ of PSII turnover in the S_3-S_0 transition of the wild type membranes was 3.7 ms in 200 mM NaCl.

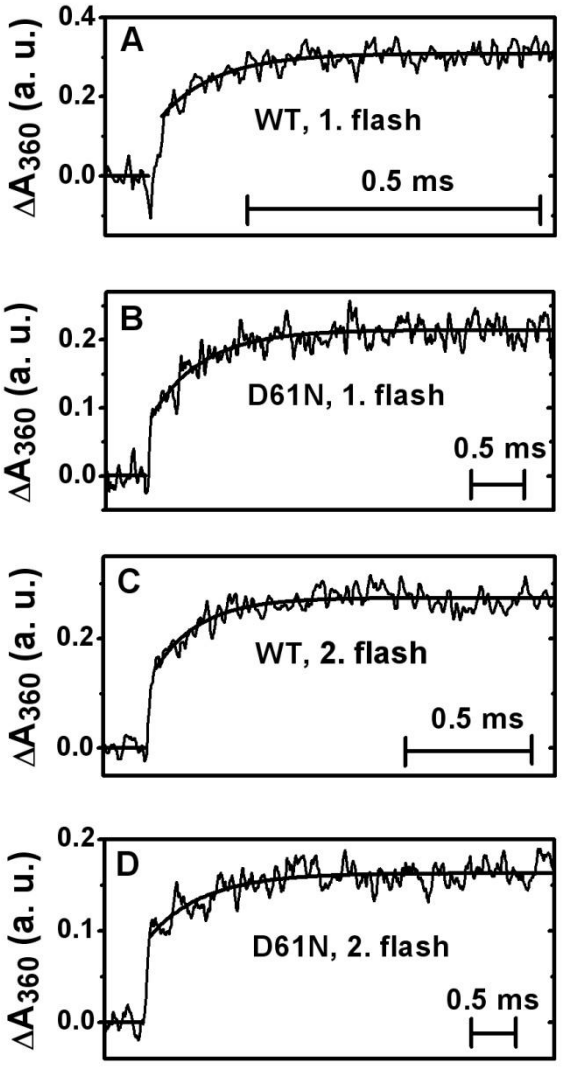

Figure A.2.2 Flash-induced absorption change transients of PSII core particles of the wild type (WT) and D61N mutant strain were monitored at 360 nm. The laser excitation initiates a fast absorption change due to the Q_A^- formation followed by slow rise due to the Mn oxidation in the S state transitions. The mutation causes significant deceleration of the slow rise both after the 1st and 2nd flash (note the different length of the 0.5 ms bar). Fit by monoexponential functions provides the following time constants: WT, 1st flash (τ = 95±10 μs, A); D61N, 1st flash (τ = 505±30 μs, B); WT, 2nd flash (τ = 165±12 μs, C) and D61N, 2nd flash (τ = 645±80 μs, D).

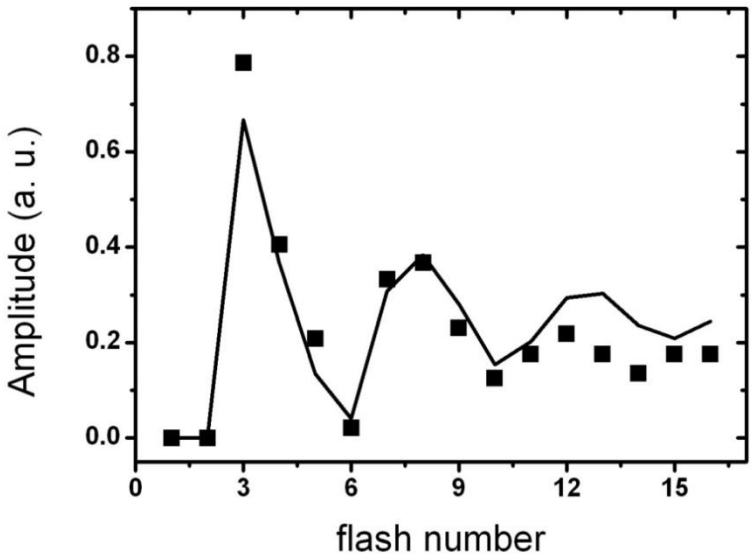

Figure A.2.3 The amplitude of the ms component in the near-UV data for core particle of the D61N mutant. The amplitude of this ms component indicates the extent of Mn reduction and concomitant O_2-formation; a characteristic period of four oscillation is oberserved not only in the WT, but also for PSII core particles of the D1-D61N mutant (■). The oscillation pattern was fitted using the classical Kok model (α=0.174, β=0) (solid line).

Appendix A.3 Basic characterization of additional water cavity mutants.

D1-Ile60. D1-Ile60 comes into contact with the portion of the broad channel (*65*) that extends away from the Mn_4CaO_5. This residue is also in close to D1-D61 and several other residues in the proton exit pathway (*63*). The substitution of D1-Ile60 with phenylalanine could lead to the disruption of waters in the hydrogen bond network that removes protons from the vicinity of the Mn_4CaO_5. The D1-I60F mutant has not yet been characterized.

D1-Gly166. D1-Gly166 is located approximately 9 angstroms from the Mn_4CaO_5 on a loop that comes into contact with the channel previously labeled as the back channel (*65*). This channel has also been identified as a possible O_2 exit channel (*64*). Other authors have concluded that the back channel is impermeable to water (*66*, *67*). Substitution of D1-Gly166 with leucine was intended to introduce a hydrophobic residue into this channel. While the steady state rate of O_2 production by the D1-G166L mutant is reduced to 34% of wild type the concentration of PSII is also decreased to 52% of wild type (Table S1). This indicates that the D1-G166L mutation introduces significant structural defects into PSII and the defect in O_2 production cannot be attributed solely to changes in the enzymatic activity of the mutant protein. The D1-G166A mutant has not been characterized.

D1-Ser169. The residue D1-Ser169 faces the channel labeled the narrow channel by Ho and Styring (*65*) and channel iii by Murray and Barber (*64*) at the point where the channel passes between D1-Asp61 and CP43-Arg357. The residues surrounding this channel have been identified as a possible proton exit pathway (*63*). This channel may also provide access to water for one of the substrate binding sites (*67*).

D1-Pro173. D1-Pro173 is a residue that is part of a loop that comes into contact with the broad channel (*65*) that is located a greater distance from the Mn_4CaO_5 (8.5 Å) than the Ile60 (6.0 Å) or Val185 (5.5 Å) residues. Substitution of Pro173 with a glycine residue causes a reduction in oxygen evolving capacity to 62% of wild type *Synechocystis* (Table 1) while still allowing the mutant to accumulate 96% of the PSII content of the wild type strain.

strain	photoautotrophic growth	relative PSII content (% of wt) [a]	Variable Fluorescence (% of wt) [b]	oxygen evolution (% of wt) [c]
I60F	-	Not determined	Not determined	43
G166A	+	Not determined	Not determined	49
G166L	+	54	47	34
S169A	+	71	37	36
S169C	+	94	91	53
S169T	+	73	55	36
P173G	+	96	54	62

Table A.3.1 Characterization of additional water pathway mutants. [a]The relative PSII content of each strain was estimated from the yield of variable chlorophyll *a* fluorescence (Fmax - F_0)/F_0 after 40 flashes. Measurements were taken by in the presence of 20 mM hydroxylamine and 20 μM DCMU, according to previously described methods (*82*, *87*). [b]The ability of each strain to undergo a stable charge separation was assessed by recording the the yield of variable fluorescence (F_{max} - F_0)/F_0 after a single actinic flash in the presence of 20 μM DCMU. [c]Steady state rates of oxygen evolution were measured with a Clark type electrode using a chlorophyll concentration of 6.35 μg in HN buffer [10 mM Hepes-NaOH and 30 mM NaCl (pH 6.5)] with the addition of 750 μM DCBQ and 2 mM K_3Fe(CN).

ACKNOWLEDGEMENTS

The authors are especially indebted to Prof. Richard Debus for many useful discussions and for supplying the D1-D61N *Synechocystis* mutant. Funding by the National Science Foundation MCB 0818371 (to RLB) and the Edward R. & Mary M. Grula Distinguished Graduate Fellowship (to PLD) is gratefully acknowledged.

VITA

Preston L. Dilbeck

Candidate for the Degree of

Doctor of Philosophy/Education

Thesis: SECOND SPHERE LIGANDS OF THE MANGANESE CLUSTER

MODULATE THE WATER OXIDATION MECHANISM OF PHOTOSYSTEM II

Major Field: Microbiology, Cell and Molecular Biology

Biographical:

Education:

Completed the requirements for the Doctor of Philosophy in your Microbiology, Cell and Molecular Biology at Oklahoma State University, Stillwater, Oklahoma in December, 2012

Completed the requirements for the Bachelor of Science in Molecular Biology at Oklahoma State University, Stillwater, Oklahoma May, 2006.

Peer-Reviewed Publications:

Hong Jin Hwang, Preston Dilbeck, Richard J. Debus, and Robert L. Burnap (2007) Mutation of arginine 357 of the CP43 protein of photosystem II severely impairs the catalytic S-state cycle of the H_2O oxidation complex. Biochemistry 46:11987-97 (Accelerated Publication)

Fiona Bentley, Hao Luo, Preston Dilbeck, Robert L. Burnap, and Julian J. Eaton-Rye. (2008) Effects of Inactivating *psbM* and *psbT* on Photodamage and Assembly of Photosystem II in *Synechocystis* sp PCC 6803, Biochemistry 47:11637-11646.

Preston Dilbeck, Hong Jin Hwang, Ivelina Zaharieva, Laszlo Gerencser, Holger Dau, and Robert L. Burnap. (2011) The mutation D1-D61N in *Synechocystis* sp. PCC 6803 allows the observation of intermediates in the formation and release of O_2 from Photosystem II. Biochemistry, 51:1079–1091

Preston Dilbeck, Han Bao, Curtis Neveu, Robert L. Burnap. (2012) Mutations perturbing the water cavity surrounding the Mn_4CaO_5 cluster have a profound effect on the water oxidation mechanism of Photosystem II. (In preparation)

Name: Preston L. Dilbeck Date of Degree: December, 2012

Institution: Oklahoma State University Location: Stillwater, Oklahoma

Title of Study: PROTON TRANSFER REACTIONS IN PHOTOSYNTHETIC WATER OXIDATION: SECOND SPHERE LIGANDS OF THE MANGANESE CLUSTER MODULATE THE WATER OXIDATION MECHANISM OF PHOTOSYSTEM II

Pages in Study: 112 Candidate for the Degree of Doctor of Philosophy

Major Field: Microbiology, Cell and Molecular Biology

Scope and Method of Study: Physiological and Biophysical characterization of point mutations in the D1 subunit of PSII

Findings and Conclusions:

In the D1-D61N mutant, it was possible to resolve a clear lag phase prior to the appearance of O_2, indicating formation of an intermediate before onset of O_2 formation. The lag phase and the photochemical miss factor were more sensitive to isotope substitution in the mutant indicating that proton efflux in the mutant proceeds via an alternative pathway. The results are discussed in comparison with earlier results obtained from the substitution of CP43-Arg357 with lysine and in regards to hypotheses concerning the nature of the final steps in photosynthetic water oxidation. These considerations lead to the conclusion that proton expulsion during the initial phase of the S_3-S_0 transition starts with the deprotonation of primary catalytic base, probably CP43-Arg357, followed by efficient proton egress involving the carboxyl group of D1-D61 in a process that constitutes the lag phase immediately prior to O_2 formation chemistry. The asparagine, phenylalanine and threonine substitutions to D1-V185 were able to accumulate significant levels of charge separating PSII. Of the three substitutions the phenylalanine substitution was the most severe with a complete inability to evolve oxygen, despite being able to accumulate Photosystem II and to undergo stable charge separations. The threonine substitution had no apparent effect on oxygen evolution other than a 40% reduction in the steady state rate of O_2 production compared to type *Synechocystis*, which can be attributed to that mutants reduced ability to accumulate PSII. The asparagine substitution produced the most complex phenotype. While still able to evolve oxygen, it does so less efficiently than wild type PSII, with a miss factor 4% higher than wild type *Synechocystis*. The substitution on D1-Val185 with asparagine also decreased the $t_{1/2}$ of O_2 release from thylakoid membranes from 1.2 ms to 10.0 ms and decreased the $t_{1/2}$ lag phase prior to the onset of O_2 release to 2.8 ms. The combination of a long lag period and a decreased rate of O_2 release can also be observed in the D1-D61N mutant strains of *Synechocystis* and in PSII centers in which chloride has been replaced by iodide.